FINAL REPORT

POROSITY AND PERMEABILITY STUDIES OF VIRGINIA AGGREGATES

by

W. Cullen Sherwood
Faculty Consultant

Jinn-Huie Huang
Former Highway Research Engineer

Joseph J. Dudash
Graduate Assistant

and

Kenneth H. McGhee
Highway Research Engineer

(The opinions, findings, and conclusions expressed in this report are those of the authors and not necessarily those of the sponsoring agencies.)

Virginia Highway Research Council
(A Cooperative Organization Sponsored Jointly by the Virginia Department of Highways and the University of Virginia)

In Cooperation with the U. S. Department of Transportation
Federal Highway Administration

June 1972
VHRC 71-R39

PREFACE

The working plan for this project titled "Porosity and Permeability Studies of Virginia Aggregates" was prepared and submitted in November 1963. At that time large-scale construction of the interstate system was getting under way and the solving of materials problems and materials research were among the most pressing highway needs. Some of the more difficult highway materials problems have defied solutions even to this day while many others have been alleviated tremendously by the research undertaken in the decade of the sixties.

Certainly, one of the most perplexing materials problems has been, and continues to be, the formulation of rapid laboratory tests which will accurately predict the long-term field durability of such materials as aggregates and aggregate-containing concrete.

It was within this context that the research presented in this final report was undertaken. The purpose of the study as delineated in the Working Plan was "... to study the porosity and permeability characteristics of the major rock types used for aggregate in Virginia." The Working Plan pointed out the logical future use of the findings of this research in the statement, "A most logical extension and utilization of this initial fundamental work will be that of relating freeze-thaw durability of aggregate in concrete to the three properties: (a) total porosity, (b) pore size distribution, and (c) permeability."

It was found convenient to divide the anticipated research into several fairly well defined phases or stages. The final report reflects these stages. Part 1 of the final report is devoted strictly to porosity studies, Part 2 to permeability, and Part 3 to a mathematical treatment attempting to relate porosity and permeability.

During the later stages of the research, conferences with the project coordinators from the Federal Highway Administration resulted in an agreement that if rapid mercury injection porosimetry could predict the long-term water absorption of aggregates then a rapid test method might be possible. Part 4 describes the extensive efforts to relate mercury determined porosity to long-term water absorption. Unfortunately, it must be stated that this research did not establish such a correlation, even after numerous careful experiments and the use of several additional parameters such as (1) absorption rate, (2) aggregate texture, and (3) pore size, interjected in efforts to improve the correlation.

Consequently it would appear that the major value of the research presented here will be rather in line with the original purpose of the project — that of providing fundamental information and understanding of the complex properties of aggregate porosity and permeability. The authors are hopeful that this work, along with the efforts of others, will serve to provide further insights into the difficult problems involving aggregate durability.

SUMMARY

It is generally recognized that the volume and geometry of included pores within a mineral aggregate have a significant effect on the physical and chemical behavior of the aggregate when used as a structural material. However due to the technicial difficulties involved in measuring pore parameters, accurate correlation of field behavior with pore characteristics has not readily evolved. This study was proposed to provide accurate data on pore characteristics for a variety of Virginia aggregates with the expectation that future durability studies would attempt to correlate these findings with field performance.

All of the aggregates studied showed relatively low porosities ranging from a high of 3.66% to a low of 0.19% with most values being less than 1%. Pore size distributions showed carbonate aggregates to have pores of nearly all one size while igneous and metamorphic rocks contain several sizes. Permeabilities of all rocks fell in the range of 10^{-1} to 10^{-5} millidarcys. A set of equations was developed to relate porosity and permeability values. Finally in order to investigate the feasibility of a rapid test method to predict aggregate water absorption, a correlation between porosity determined by high pressure mercury injection and porosity determined by long-term water absorption was attempted. The results ranged from poor to fair. Incorporation of other parameters such as rate of water uptake, pore size, and rock grain size served to make only modest improvements in the correlation. In view of this lack of strong correlation no recommendation concerning a rapid test method is offered at this time.

FINAL REPORT

POROSITY AND PERMEABILITY STUDIES OF VIRGINIA AGGREGATES

by

W. Cullen Sherwood
Faculty Consultant

Jinn-Huie Huang
Former Highway Research Engineer

Joseph J. Dudash
Graduate Assistant

and

Kenneth H. McGhee
Highway Research Engineer

INTRODUCTION

In reviewing the literature on the subject of highway materials it becomes increasingly apparent that the characteristics and behavior of aggregates are now recognized as fundamental factors in the durability of pavements and structures. In previous decades the prevailing philosophy was to consider the aggregate as an inert part of the material system, and many specifications contained statements to this effect. The recognition of deleterious chemical reactions by Stanton (1940) and others has done much to dispel this myth of inertness.

Aggregate pore structure is generally conceded to be of importance with regard to both the chemical and physical durability of aggregates and aggregate-containing structural materials. Despite this widespread recognition, detailed studies of pore structure and related tests have been slow to evolve.

A quote from the classical paper by Lewis, Dolch, and Woods (1953) focuses sharply on this problem.

> With a property as important as pore space, it is surprising that more emphasis has not been given to this subject — not only by research workers in the field of aggregate and concrete technology but also by those interested in specifications and in the development of methods of tests. It would be difficult to prove that any other physical property is of greater importance than the porosity characteristics (amount, size, and continuity of the pores) in either natural or artificial aggregates. The pore characteristics of a coarse aggregate not only influence the physical durability properties

of concrete but also any potential chemical reaction. It is apparent from the information collected in this paper that research in this area should be extremely fruitful. Immediate attention should be given to methods of test, particularly with respect to methods used in related fields for determining pore characteristics of porous materials. It is probable that specification writers will be seeking material of this character in an attempt to obtain the best quality of aggregate for use in various types of construction.

A logical reason for this lack of published work on what was recognized as a crucial property of aggregates was the practical difficulties involved in attaining accurate measurements of porosity and permeability. The advent of commercially available instrumentation in mercury porosimetry and other techniques has facilitated measurements of these properties and accelerated interest in this aspect of materials research.

Due to the scope of the research presented here, its various aspects are considered as separate parts and specific experiments were designed and performed for each. The format of this final report will reflect this division of effort, containing specific parts on the following: (1) Aggregate Porosity — including total porosity and pore size distributions; (2) Aggregate Permeability — considering both gas and water flow; (3) Some fundamental relationships between porosity and permeability, and (4) Some relationships between porosity and water absorption.

VIRGINIA AGGREGATES

Due to its geographic position astride four major physiographic provinces, Virginia contains a wide range of rock types from which aggregates are commonly produced (see Figure 1). The physiographic provinces are, from east to west, (1) The Atlantic Coastal Plain; (2) The Piedmont, (3) The Valley and Ridge; and (4) The Appalachian Plateau.

Briefly, the Coastal Plain yields a variety of unconsolidated sands and gravels, mainly composed of quartz. The Piedmont is underlain by a very complex mix of igneous and metamorphic rocks. Aggregates produced in this area include granite, diabase, and a variety of metamorphosed limestones, sandstones, and intrusive and extrusive igneous rocks. Aggregates produced in the Valley and Ridge portion of the state are primarily limestones and dolomites with some siliceous gravel and quartzite coming from the vicinity of the west slope of the Blue Ridge Mountains. Aggregate production in the Appalachian Plateau of Virginia is limited to limestone and small quantities of crushed sandstone.

The majority of the rocks studied for this project were from the Piedmont and the Valley and Ridge Provinces.

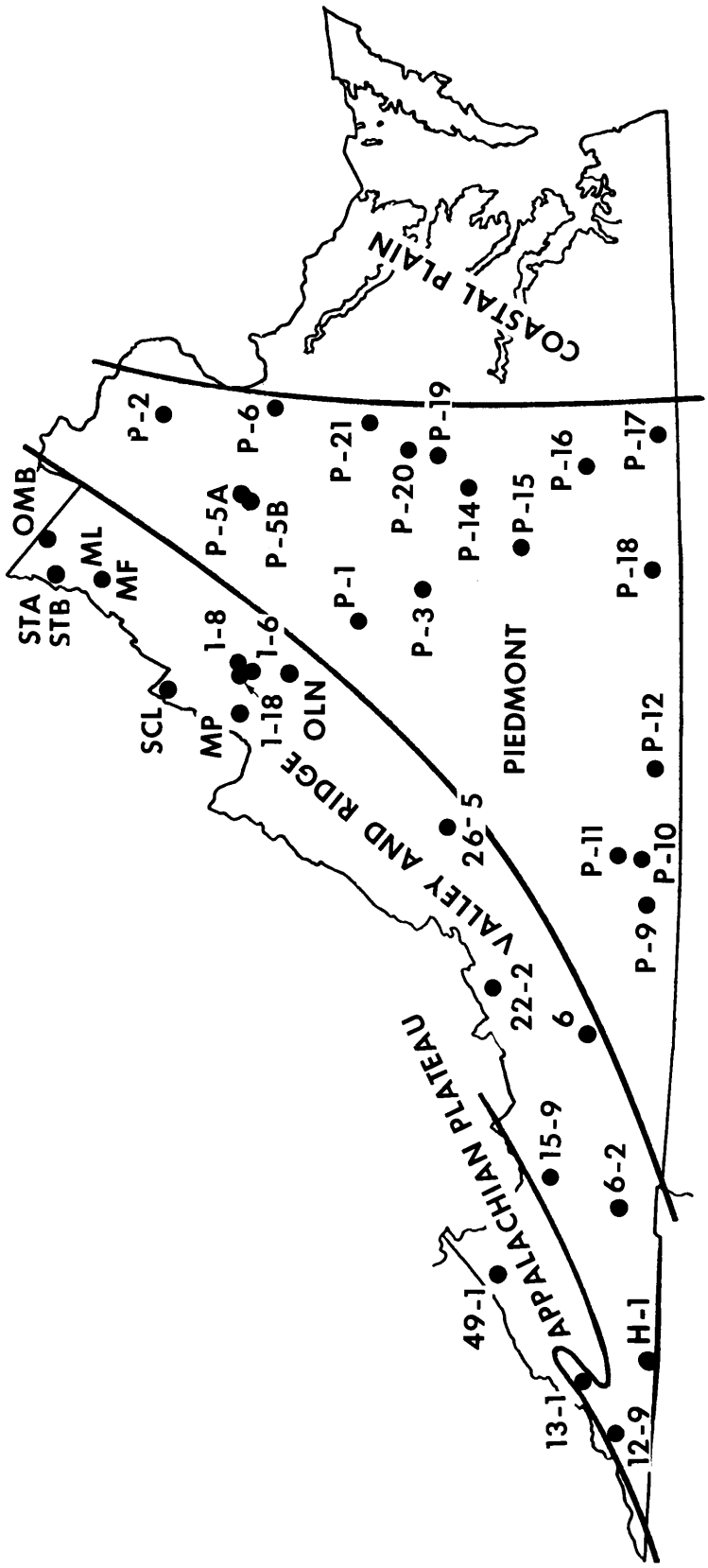

Figure 1. Outline map of Virginia with sample localities and physiographic provinces.

PART 1

AGGREGATE POROSITY

Background

The three characteristics generally considered of maximum importance for pore systems in porous solids are the following: (1) total porosity; (2) pore size distribution; and (3) permeability. Only the first two of these will be considered in this section. The total porosity of a solid may be defined as the fluid capacity of a given bulk volume of the solid. This property of aggregates has long been recognized as important to durability and this recognition has resulted in the adoption of a 24-hour immersion test to determine water absorption (ASTM Test C-128). Pore size distribution, or the volume of pores of various sizes in a solid, while being recognized by some research workers as critically important in aggregate durability (Lewis et al. 1953, Verbeck and Landgren 1960; etc.) has not been adapted to a simple or widely used test procedure.

Pore data on naturally occurring rock materials have come largely from studies of petroleum reservoirs and of aggregate durability. Many of the techniques used have been developed in such diverse disciplines as ceramic engineering, chemical engineering, concrete technology, and surface chemistry and physics. One of the earliest systematic studies of the porosity of petroleum reservoirs was done by Carll (1880) for the western Pennsylvania oil fields. Later Slichter (1898) and King (1898) studied pore volumes and the movement of fluids in rocks. Since the turn of the century several techniques have been developed and used to measure pore volume, size, and geometry. Lewis et al. (1953) divided the various techniques applicable to rock-pore systems into three classes: (1) those that measure porosity, such as the specific gravity, absorption, and gas displacement methods; (2) those that give a simple indication of pore size, such as the microscopic, capillary rise, and permeability methods; and (3) those that determine the pore size frequency distribution, such as the gas adsorption, mercury porosimetry, capillary diaphragm, and low angle X-ray methods. The details of the various techniques are described in the works of Fancher (1950), Hassler and Brunner (1945), Lewis et al. (1953), Melcher (1921), Ritter and Drake (1945), Ritter and Erich (1948), Sweet (1948), Waldschmidt et al. (1956), and Washburn and Bunting (1922).

From the large accumulation of pore data derived from petroleum reservoir studies, it appears that the porosity of oil producing sandstone generally ranges between 10 and 30 percent (Russell and Dickey 1950). Pore sizes of interest generally range from a minimum of 0.1 μ (Purcell 1949) to large macroscopic openings. The research reported here has demonstrated that much of the information on pores gained from Mid-Continent reservoir studies is very different from that for the dense, highly indurated Appalachian rocks.

Pore studies of various rock types have been carried out in the areas of mineral aggregate and concrete technology. Studies by Blanks (1949), Rhoades and Mielenz (1946), Schaffer (1932), and Sweet (1948) involved rock pore measurements. Lemish et al. (1958) published several pore size distribution curves for Iowa aggregates. Most of the rocks studied in these works, however, were Mid-Continent carbonate rocks that might be expected to have a considerably greater porosity than their Virginia equivalents.

Experimental Procedure

Mercury Porosimetry

The theory involved in mercury porosimetry is well-known. In practice the method consists of immersing an evacuated sample in liquid mercury and observing the reduction of mercury volume as a function of pressure. The method is particularly applicable to the measurement of pores with diameters of more than 0.01 μ. E. W. Washburn (1921) was the first to suggest the use of mercury under pressure to determine the pore size distribution in porous solids. The relation he developed may be stated in the conventional form

$$d = \frac{-4\sigma \cos\theta}{p} \quad \left(\text{or } r = \frac{-2\sigma \cos\theta}{p}\right) \qquad (1\text{-}1)$$

where d is the diameter of the pore just enterable by mercury at pressure p, σ is the surface tension of mercury, and θ is the contact angle. The value for σ used in this work was obtained from the American Instrument Company as 473 dynes/cm, and the contact angle of 130° is considered the most acceptable value for a wide range of materials. The equation for equivalent cylindrical pores reduces to the empirical approximation

$$d = \frac{175}{p} \qquad (1\text{-}2)$$

where d is the pore diameter in microns and p is the pressure in psi. Equation 1-2 was used to convert pressures into pore diameters in all the work reported herein.

Apparatus

An Aminco-Winslow 15,000-psi mercury porosimeter was used for measuring the porosity and pore size distribution (see Figures 2 and 3). The instrument is designed to measure the size of pores ranging from 200 μ to 0.01 μ in diameter, with a volume precision of 0.0005 ml.

Technique

A small piece, approximately 0.5-1.5 g, of sample was soaked in acetone solution for several hours, then dried and placed in a penetrometer (a glass reservoir with a graduated capillary stem). The penetrometer was placed in a filling device. The device was evacuated to a vacuum of less than 100 μ of mercury. After a small release of vacuum had allowed mercury to flow into the penetrometer and surround the sample, the larger pores (from 200 to 12 μ diameter) were measured by further releasing the vacuum in the filling device by suitable increments and taking penetrometer and gage readings until the system reached atmospheric pressure (14.7 psi). The penetrometer then was transferred to a pressure chamber in which pressure from 14.7 to 15,000 psi can be applied to the mercury through a hydraulic medium. This

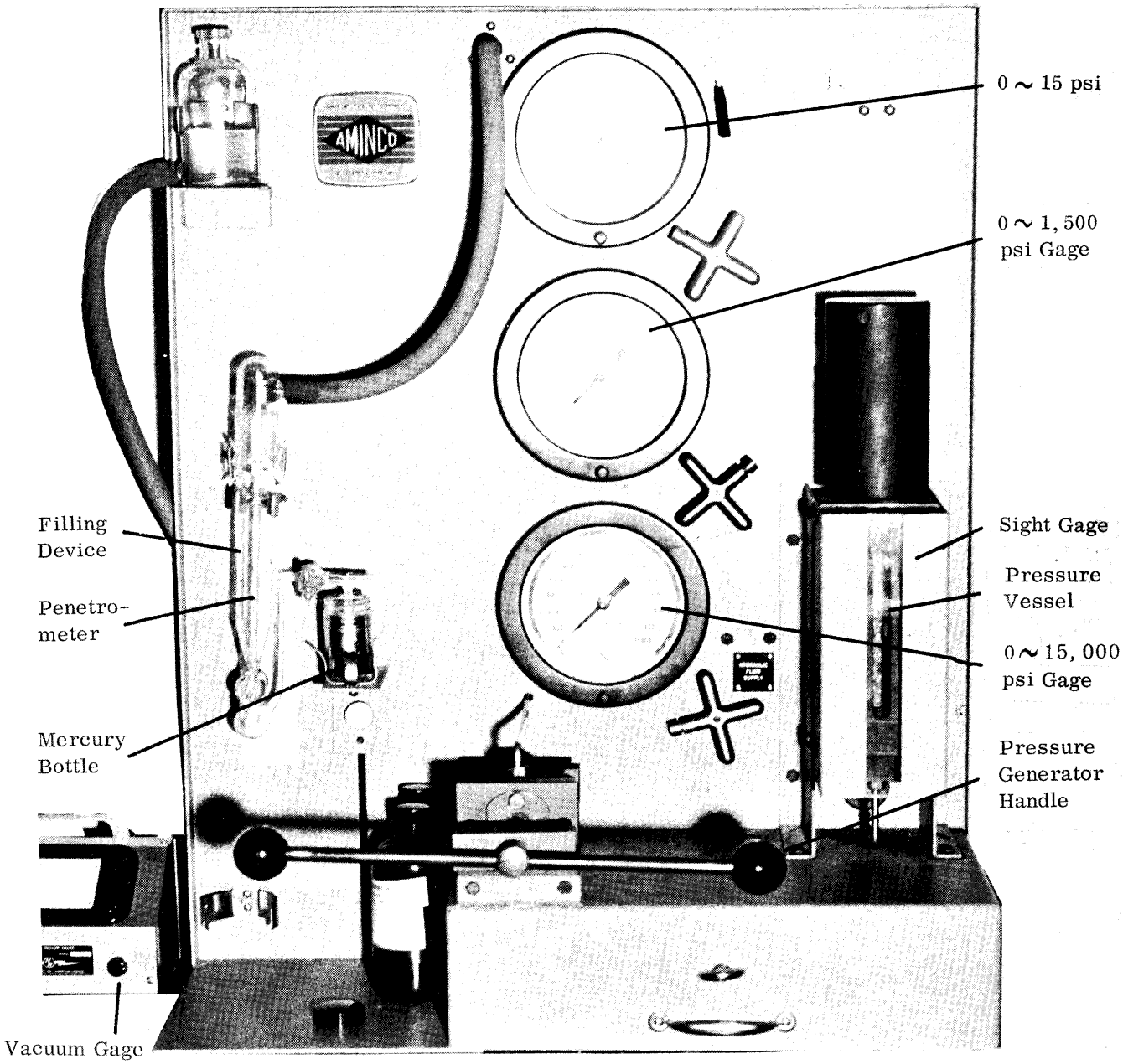

Figure 2. Mercury porosimeter (front view).

pressure range allows the measurement of pore sizes down to 0.01 μ. Bulk specific gravity measurements were made with a Jolly balance in accordance with ASTM Method C 127-59. Three samples of each rock were measured and the average of the three values was used. The specific gravity and weight for the sample under test, in conjunction with porosimeter values, allow computations of porosity as a percent of the bulk volume and of the percentages of the bulk volume represented by the various pore sizes.

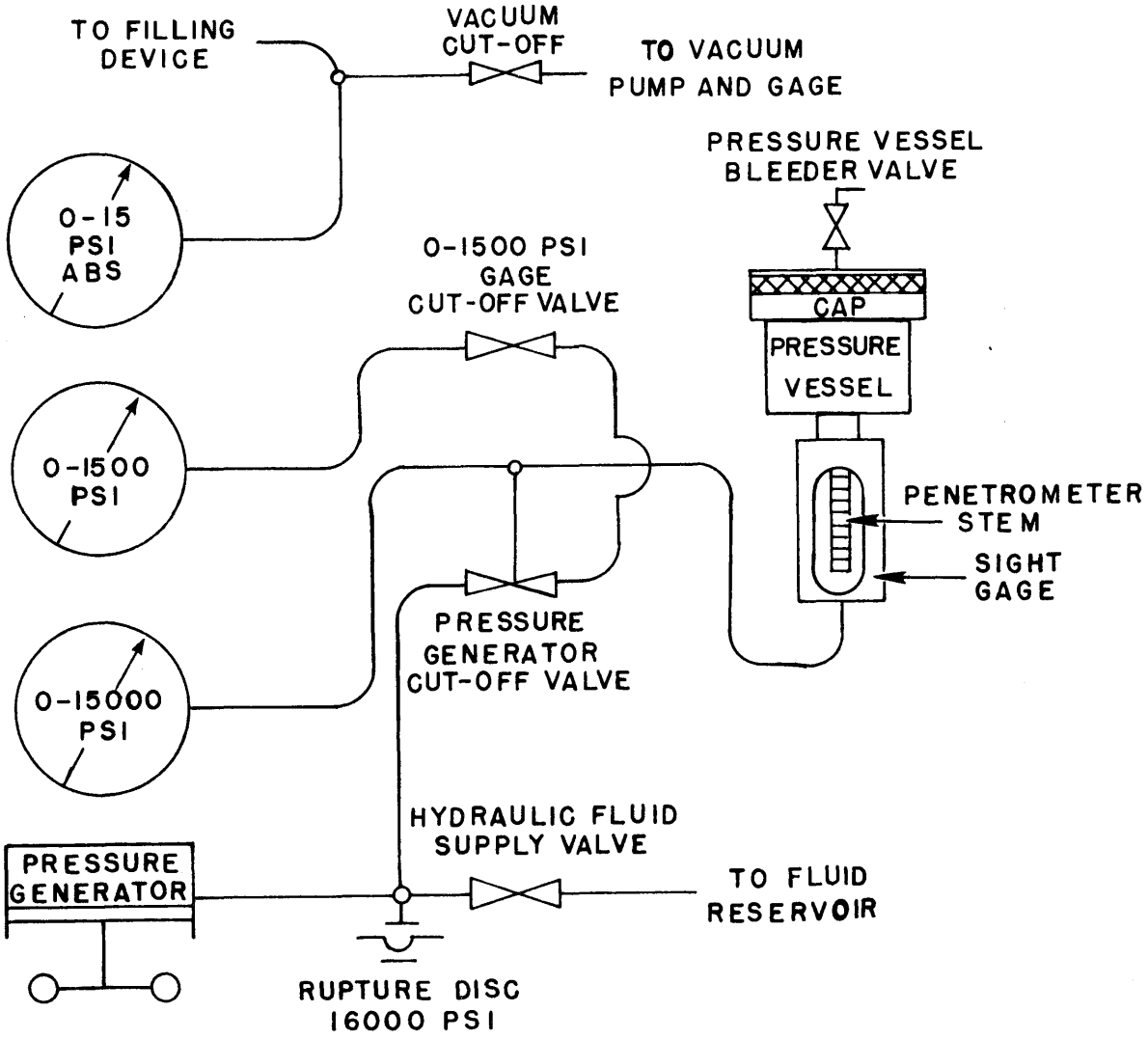

Figure 3. Schematic piping diagram for mercury porosimeter.

Data Treatment

Pore-Size Distribution

Data obtained by mercury porosimetry measurements were plotted in two forms. First, the pore volume occupied by mercury was plotted against the pore diameter on semilog graphs. The data were adjusted for differences in sample size by basing the curves on a 1 g original sample. Figure 4 shows a typical curve of this type. Second, pore size distribution curves were produced by differentiation (plotting the slope value of the pore volume-pore size curves). Figure 5 shows the pore size distribution curve constructed from the data plotted in Figure 4.

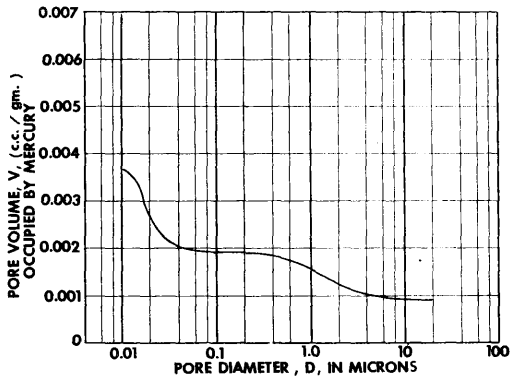

Figure 4. Pore volume-pore size curve for sample P-7, a granitized sediment.

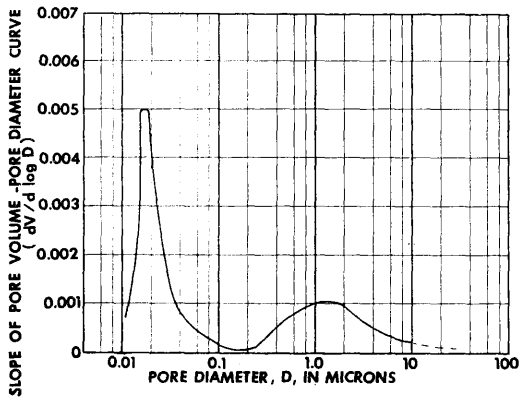

Figure 5. Pore size distribution curve constructed by differentiating the pore volume-pore size curve in Figure 4.

Mean Pore Diameter

The geometric quantities commonly used to describe the structures of porous materials are the total pore volume, V_t, the surface area, S_t, and the pore size distribution. It is customary to express the average radius of the pores in porous materials as

$$\bar{r} = \frac{2V_t}{S_t} \tag{1-3}$$

where all pores are assumed to be cylindrical and to have a radius of r. The total length of capillaries with radii between r and r + dr is represented by n (r) dr. The pore size distribution then can be described by the function f(r) + π r^2n (r), which gives the volumes of capillaries associated with the various radii. The pore volume per unit mass of sample is given by the equation

$$V_t = \int_{r_1}^{r_2} n(r)\pi r^2 dr = \int_0^{V_t} dV \tag{1-4}$$

where dV is the volume of pores between r and r + dr, per unit mass of sample, and r_2 and r_1 are the upper and the lower limits of pore radii. The surface area per unit mass of sample is

$$S_t = \int_{r_1}^{r_2} n(r)2\pi r dr. \tag{1-5}$$

By substituting equations 1-4 and 1-5 into equation (1-3) an equation for the mean pore radius can be derived.

$$\bar{r} = \frac{2V_t}{S_t} = \frac{\int_{r_1}^{r_2} n(r)\pi r^2 dr}{\int_{r_1}^{r_2} n(r)\pi r dr}. \tag{1-6}$$

In the absence of internal surface measurements, equation 1-6 can be multiplied by r in the numerator and denominator, and the result can be written in terms of the known pore volume per unit mass of the sample as

$$\bar{r} = \frac{2V_t \times r}{S_t \times r} = \frac{\int_{r_1}^{r_2} r \times n(r)\pi r^2 dr}{\int_{r_1}^{r_2} n(r)\pi r^2 dr} = \frac{\int_0^{V_t} r dV}{\int_0^{V_t} dV} = \frac{\int_0^{V_t} V r d}{V_t} \tag{1-7}$$

where dV is the volume of pores between r and r + dr, per unit mass of sample. The calculated mean pore diameters for all the samples tested are shown in Tables 1 and 2.

Table 1

Pore Data for Carbonate Rocks Studied

Sample	*Description*	*Formation Age*	*Mean Pore Diameter (μ)*	*Porosity (%)*	*Pore-Size-Dist. Type*[1]
MF-1	Very fine-grained, high-calcium limestone	New Market, Ordovician	0.0113	0.643	1
1-8	Fine-grained, argillaceous calcitic dolomite	Beekmantown, Ordovician	0.0133	0.191	1
ML-1	Very fine-grained, high-calcium limestone	New Market, Ordovician	0.0139	0.398	1
15-9	Fine-grained, argillaceous limestone	Ward Cove, Ordovician	0.0154	0.454	1
1-6	Fine-grained, dolomitic limestone	Beekmantown, Ordovician	0.0158	0.686	1
6-2	Dense, fine-grained dolomite	Beekmantown, Ordovician	0.0218	0.798	1
1-18	Dense, medium-grained dolomite	Beekmantown, Ordovician	0.0228	0.295	2
12-9	Fine-grained, laminated dolomitic limestone	Lowville, Ordovician	0.0262	0.319	2
26-5	Dense, medium-grained dolomite	Shady, Cambrian	0.0466	3.26	2
22-2	Dense, medium-grained dolomite	Beekmantown, Ordovician	0.0264	1.22	3
13-1	Medium-grained, argillaceous dolomite	Newman Seam, Mississippian	0.0318	3.66	3
H-1	Medium-grained, high-calcium limestone	Holston, Ordovician	0.088	0.739	3

[1] Explanation and discussion of this classification method are given in the section, "Pore-Size Distribution."

Table 2

Pore Data for Crystalline Rocks Studied

Sample	*Description*	*Formation, Age*	*Mean Pore Diameter (μ)*	*Porosity (%)*	*Pore-Size Dist. Type*[1]
P-18	Medium-grained, light-colored granite	Red Oak Granite, Precambrian-Paleozoic	0.021	0.664	1
P-3	Slate	Arvonia, undif., Paleozoic	0.0352	0.710	1
P-9	Mica, quartz schist	Metasediments, uncertain age	0.484	1.93	1
P-17	Medium-grained biotite granite gneiss	Petersburg Gran., Precambrian-Paleozoic	0.0129	0.674	2
P-19	Fine-grained muscovite granite gneiss	Undif. granite gneiss, uncertain age	0.015	0.624	2
P-16	Medium-grained biotite granite gneiss	Petersburg Gran., Precambrian-Paleozoic	0.0435	1.71	2
P-14A	Porphyritic biotite gneiss	Metasediments, uncertain age	0.0743	1.66	2
P-2	Medium-grained diabase	Intrusion, Triassic	0.0104	0.654	3
P-6	Fine-grained biotite granite	Petersburg Gran., Precambrian-Paleozoic	0.0247	0.544	3
P-15	Fine-grained biotite granite	Granite, uncertain age	0.0274	0.616	3
P-20	Quartz, mica, feldspar schist	Metasediments, uncertain age	0.0774	0.550	3
P-10	Coarse-grained biotite granite gneiss	Leatherwood Gran., Precambrian-Paleozoic	0.055	1.45	4
P-12	Medium-grained granite gneiss	Granite gneiss, uncertain age	0.126	0.965	4
P-11	Medium-grained granite gneiss	Leatherwood Gran., Precambrian-Paleozoic	0.272	1.32	4
P-21A	Coarse-grained granite gneiss	Granite gneiss, uncertain age	0.292	0.390	4
P-1	Coarse-grained granite gneiss	Lovingston, Precambrian	0.866	1.86	4

[1] Explanation and discussion of this classification method are given in the section, "Pore-Size Distribution."

Porosity

The porosity of any rock can be calculated by the following formula if the volume of pores V_t, expressed as cc/g, is known. The volume, measured by mercury porosimetry, includes pores with diameters greater than 0.01 μ. Designating ϵ as porosity,

$$\epsilon = V_t \times \text{bulk density} \times 100. \qquad (1\text{-}8)$$

The calculated porosity values for the rocks studied are shown in Tables 1 and 2, which also contain a column that classifies the pore size distribution of each sample by a method discussed subsequently in this section.

Results and Discussion

Pore Size Distribution

The most striking characteristic of the pore size distribution curves plotted for the rocks in this study is the fundamental difference in the shapes of the curves for the limestones and dolomites or carbonate rocks and the 19 igneous and metamorphic or crystalline rocks. The carbonate rocks almost invariably show a unimodal distribution of pores, with the peak generally in the lower size range. The crystalline rocks generally are characterized by two to four peaks, which are indicative of several pore size concentrations within the same rock.

Carbonate Rocks

Table 1 shows the results of measurements of the mean pore diameter and porosity, together with brief sample descriptions and types of pore size distributions, for each of the carbonate rocks studied. Table 1 also contains a column indicating the classes of pore size distributions suggested by this work. Figures 6-8 show examples of pore size distribution curves from each of these classes. The size of pores represented by the well developed principal peak or peaks have been chosen as the basis of the ensuing classifications of the 12 carbonate rocks investigated.

Class 1. Single peak below 0.02 μ. — Peaks of this type are characteristically sharp and narrow (Figure 6) and occur between 0.01 and 0.02 μ.

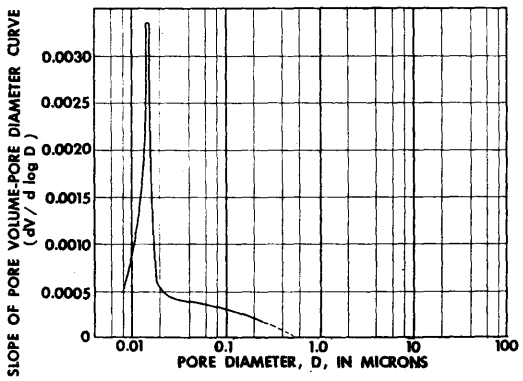

Figure 6. Pore size distribution for sample ML-1, representative of class 1 carbonate rock distribution.

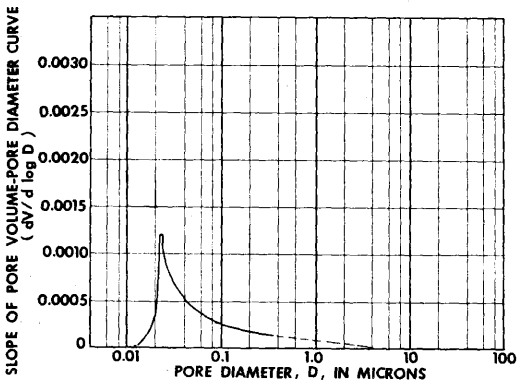

Figure 7. Pore size distribution for sample 1-18, representative of class 2 carbonate rock distribution.

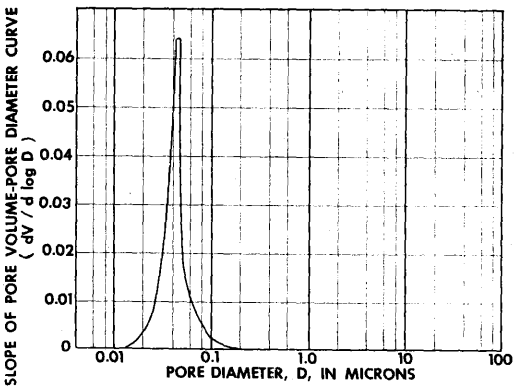

Figure 8. Pore size distribution for sample 13-1, representative of class 3 carbonate rock distribution.

The six rocks showing this type of curve, as seen in Table 1, are characteristically of fine to very fine texture. Thin sections taken beside the porosimetry samples show sample MF-1 to be very fine, dense micrite, with well interlocked grains ranging in diameter from 7 to 28 μ. Sample 1-8 is partly dolomitized clayey micrite with well developed dolomite rhombs that are unattached in the fine groundmass. Sample ML-1 is pelsparite with well developed pellets up to 140 μ in diameter and clear sparry cement. Samples 15-9 and 1-6 resemble 1-8; 15-9 has stylolite controlled dolomitization and stylolite like concentrations of impurities that mark an obvious structural cleavage. Sample 6-2 is fine, dense, relatively pure dolomite with individual grains averaging about 20 μ.

Class 2. Single peak between 0.02 and 0.03 μ. — The peak representative of this distribution type (Figure 7) is somewhat less sharp than that shown in Figure 6,

and it has a sweeping tail to the right caused by the presence of larger pores. Three of the samples listed in Table 1 belong to this class. Samples 1-18 and 26-5 are homogeneous, equigrained dolomite devoid of primary structures. Sample 1-18 has an average grain size of 40 μ; 26-5 is coarser and has an average grain size of about 200 μ. Sample 12-9 is composed of partly recrystallized dense micrite with small dolomite rhombs, averaging 25 μ, scattered throughout.

Class 3. Single peak greater than 0.03 μ. — Figure 8 shows a typical example of this type distribution, which is characterized by a well developed, somewhat narrow peak at approximately 0.045 μ. As noted in Table 1, three of the samples studied fall into this class. Thin sections show samples 13-1 and 22-2 to be coarsely crystalline dolomite with significant argillaceous material. Sample H-1 is composed of coarse (800μ) fossil and angular grains with oriented overgrowths.

On the basis of these descriptions of the samples making up each of the proposed classes, two points appear worthy of further discussion: (1) the pore size distribution is related directly to grain size, and (2) the pore size distribution appears to be independent of the carbonate rock mineralogy. The first observation is not unexpected, because fine particles in any solid generally are accompanied by correspondingly small interconnecting pores.

The second observation is somewhat surprising because dolomitization commonly is assumed to require a reduction in volume and an increase in pore space (Weyl 1960). This is obviously not the case for the samples studied, for dolomite is present in each of the three recognized classes of pore size distribution. Either of two explanations may account for this observation. First, several of the dolomites appear to represent Chilingar's (1956) primary dolomites, which are described as "lacking primary porosity and caverns." Second, Hobbs (1957) studied many of these formations and concluded that dolomitization was penecontemporaneous with deposition, taking place at, or just below, the water-sediment interface. In either case the formation of dolomite would have preceded the strong compactive forces of Appalachian folding, which must have affected greatly any pores present.

Crystalline Rocks

The 16 samples of igneous and metamorphic rocks collected from the Virginia Piedmont represent a wide variety of both textural and compositional types. Also, the degree of foliation (parallel orientation of platey grains) and alteration by metamorphic processes ranges from essentially zero in the Triassic diabase (P-2) to moderately severe in the slate, schist, and gneiss (see Table 2).

The crystalline rocks, in all but isolated examples, contain concentrations of pores of two to four different sizes rather than a single size as was found in the carbonate rocks. Consequently, the crystalline rocks are not amenable to classification on the basis of peak pore size alone, as are the carbonate rocks. A logical classification of the crystalline rocks is on the basis of the number and shape of the peaks in the pore size range, and that method has been adopted.

Four types of pore size distribution have been recognized.

Class 1. Quadrimodal distribution. — Distribution curves of this type show four well developed peaks in the interval 0.01 — 10 μ (Figure 9). Three of the samples listed in Table 2 show this characteristic pattern. Surprisingly, each rock type is different. P-18 is slightly foliated, coarse-grained granite (mean grain size, 1,100 μ) composed dominantly of feldspar with minor quartz and mica; P-9 is medium-grained, strongly foliated quartz-mica schist; and P-3 is very strongly foliated quartz-muscovite-chlorite-bearing commercial slate.

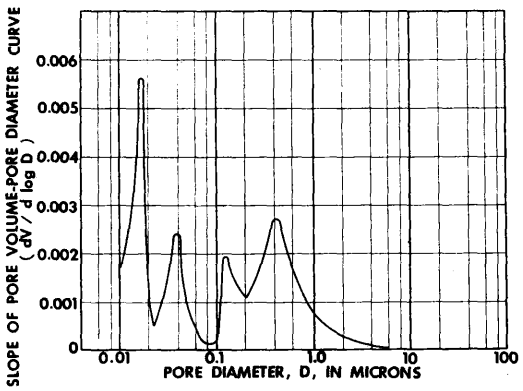

Figure 9. Pore size distribution for sample P-18, representative of class 1 crystalline rock distribution.

Class 2. Trimodal distribution. — Three of the four curves in this class show distributions characterized by a sharp, dominant peak at the lower limit of the measured pore size interval and two smaller, more diffuse peaks in the larger size range (Figure 10). The other curve, from sample P-14A, differs only in that the two peaks indicative of the larger pores are both narrow and well defined. All the rocks classified as this type are granite gneiss with fine to medium mean grain size (200-2,100 μ). Samples P-16 and P-17 contain coarse feldspar showing considerable alteration, and quartz that is finer grained than the feldspar. The mica content is small. Samples P-19 and P-14A show a strong foliation and fine texture (200-400 μ), with strained quartz and feldspar in about equal amounts. The mica content is small. P-14A contains angular and rounded garnets up to 1 mm in size.

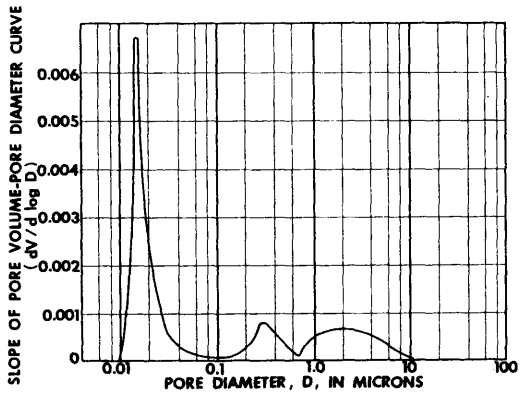

Figure 10. Pore size distribution for sample P-17, representative of class 2 crystalline rock distribution.

Class 3. Bimodal distribution, narrow and well defined. — These distributions, as shown in Figure 11, are composed of a sharp, well defined peak at a diameter of about 0.01 μ and a secondary, slightly broader peak at a larger size. The four samples with this type of distribution are varied in composition but show a generally fine texture in thin section. P-2, Triassic diabase with a typical ophitic texture, and P-6, fine-grained biotite granite (average grain diameter approximately 200 μ), are dense, equigrained rocks. P-15 is slightly coarser (500-700 μ) granite, dominantly quartz and orthoclase. P-20 is foliated, quartz-rich rock in which elongate sutured quartz with interlaced mica surrounds coarser feldspar grains.

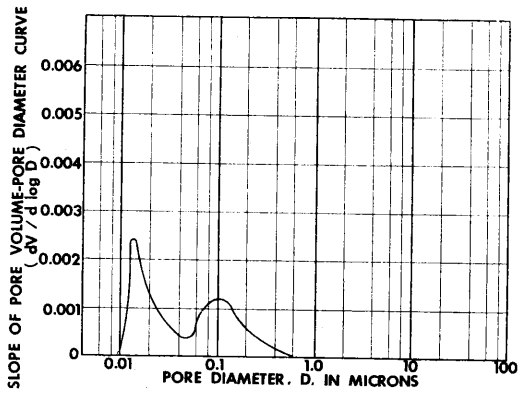

Figure 11. Pore size distribution for sample P-2, representative of class 3 crystalline rock distribution.

Class 4. Bimodal distribution, broad and diffuse. — Curves of this type are characterized by two broad peaks. The peaks may be approximately equal, as shown in Figure 12, or one peak may be larger than the other. All, however, indicate sizable volumes of pores over a broad size range. The five samples (P-10, P-12, P-11, P-21A, and P-1) which show this type of distribution are strikingly similar. Each is medium-to coarse-grained granite gneiss with well developed foliation. Much of the quartz and feldspar forms elongate pods with some fractures. Mica is present between the quartz and feldspar grains and as relatively pure bands.

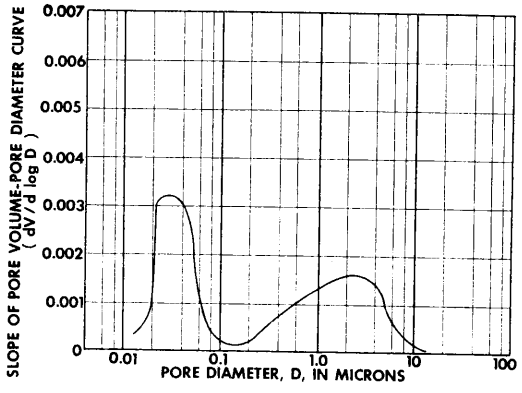

Figure 12. Pore-size distribution for sample P-10, representative of class 4 crystalline rock distribution.

Interpretation of the data for the samples of crystalline rocks is more complex than that for the carbonate rocks. The diverse mineral compositions and textures of igneous and metamorphic rocks give rise to a more complex system of pores than that in the carbonate rocks. Several reasons for differences within the crystalline rock group can be proposed. The most logical explanation, however, concerns the complexity and variation of the constituent mineral grains. Rocks of complex mineralogy, such as highly metamorphosed samples P-3 and P-9, contain a wide range of mineral grain shapes and sizes. This causes a comparable variation in the interconnecting pores. Sample P-2 (diabase) and samples P-15 and P-6 (fine- to medium-grained granite) are each composed essentially of only two mineral species, and thus would be expected to have a simpler pore structure, which in turn would be reflected in fewer peaks in the pore size distribution. The pore size distribution curve for an altered basalt or greenstone provides further evidence of this relation. This very fine-grained and equigrained rock gave a single-peaked distribution similar to that for the carbonate rocks.

Multiple-peaked pore size distributions also may be related to such factors as variations in the contact angle of different minerals with mercury or the effect of possible voids within the constituent mineral grains. More investigation will be required to ascertain the complete answer to this complex problem.

Mean Pore Diameter

Figure 13 shows the distribution of mean pore sizes for all of the rocks in Tables 1 and 2. Two points of interest brought out by this distribution are: (1) most samples tested, regardless of rock type, have mean pore diameters of less than 0.4 μ; and (2) the mean pore diameters of the crystalline rocks are generally larger and have a greater range than those of the carbonate rocks.

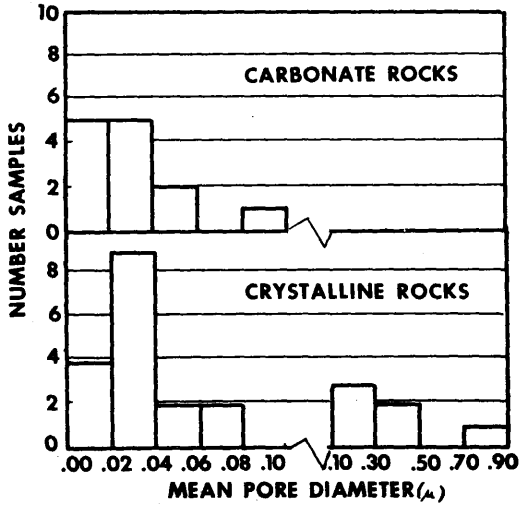

Figure 13. Mean pore diameters, carbonate and crystalline rocks.

The sample descriptions in the preceding section indicate that mean pore size is related to texture or grain size, just as is pore size distribution. This is particularly true of carbonate rocks, in which very small pore diameters generally are associated with the micrite or dolomitized micrite, the mean pore sizes of medium range are associated with the dense equigrained dolomite, and the larger pore sizes are calculated for the rocks with coarser detrital and fossil grains.

The same relation applies in a general way to the crystalline rocks. The mean pore diameters of the diabase, slate, and fine granite are small in contrast with those of the coarse granite gneiss.

Porosity

Cumulative frequency distributions of porosity for all the carbonate and crystalline rocks were constructed from the porosity data shown in Tables 1 and 2 (Figure 14). The range in porosity is much greater for the carbonate rocks tested than for the crystalline rocks. Whereas no crystalline rock had more than 2 percent porosity, 19 percent of the carbonate rocks had more than that value. These porosity values appear to be particularly significant in comparison with the mean pore diameters plotted in Figure 13. In the case of the mean pore diameter, the range for the crystalline rocks is greater and the average pore size is larger. This implies that for all the rocks tested, carbonate rocks have smaller and more uniform pores but greater pore volume than the crystalline rocks.

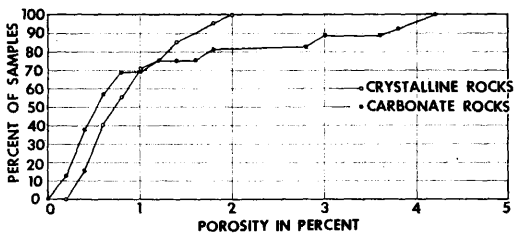

Figure 14. Cumulative porosity curves for samples of carbonate and crystalline rocks.

Plots were constructed for pore diameter versus percent porosity for each of the rock groups. As would be expected from the data presented in Tables 1 and 2, no systematic relation between these properties was observed.

Conclusions

1. Comparison of the results presented here with data published in the literature suggests that carbonate rocks from the folded Appalachians have considerably less porosity and smaller pores than rocks from the Mid-Continent area.

2. Pore size distributions determined for the pore size range 0.01 — 200μ indicate that pores in carbonate rocks generally are concentrated at a single size, whereas most igneous and metamorphic rocks contain pores concentrated at two to four different sizes.

3. The mean pore diameters of carbonate rocks are generally smaller and show a lesser range in size among different rocks than those of igneous and metamorphic rocks.

4. In general the mean pore size appears to vary with the grain size or texture of the rock, regardless of the mineral composition.

5. The porosity of the carbonate rocks generally is higher and shows greater variation among samples than that of the crystalline rocks.

PART 2

AGGREGATE PERMEABILITY

Background

The study of the physics of flow of water and gases through porous media has become of basic importance for porous structural materials such as concrete, where the flow of absorbed water must be sufficient to alleviate the destructive forces of freezing and thawing. Since mineral aggregates compose the bulk of the volume of such materials it is important to investigate the flow of gas and water through rocks which make up these aggregates.

The concept of permeability is a simple one and is recognized here as the measure of the flow rate versus the pressure drop between the inlet of the fluid and the outlet of the fluid in a given sample. When Darcy's law is applicable the relationship between flow rate and pressure drop is linear and the coefficient of permeability is constant. The dimension of this constant (or permeability) is length square, which in the c.g.s. system should be cm^2. The proportionality constant varies for each sample depending on the direction of flow and the pore size and porosity of the media. These phenomena have been observed by Sullivan (1941), Pressler (1947), Johnson and Breston (1951), Griffiths (1950), and many others.

The present work attempts to present two aspects of this overall study: (1) the flow of gas, and (2) the flow of water through selected Virginia aggregates. The samples to be measured were selected from a typical cross section of the aggregates commonly used in Virginia highway construction. Preliminary results showed that the relationship between flow rate and pressure drop is not linear. Therefore, a direct method for calculating the permeability constant by Darcy's law is not possible, so a modification of Darcy's law for the calculation of the permeability constant is presented.

As a second object of this section of the report, permeability data on some very fine-grained aggregates are presented. The rates of a gas flow for these aggregates appeared to be either nonexistent or too small to be measured by usual methods. Consequently the techniques of determining gas permeabilities of porous aggregates are presented along with an attempt to develop a procedure so that very low gas flow rates could be measured routinely.

Later in this section, a comparison of water and gas permeability for selected rocks is presented. Baptist (1966) has compared the permeability of gas with that of water in some clay minerals. His results show that even when normal viscosity differences are considered water permeability is lower than gas permeability. Likewise, this work shows that results obtained

for permeability of water through Virginia rocks is lower than for the permeability of gas. This phenomenon is probably due to the capillary structure's having random fine pores, which cause the coefficient of viscosity of water to rapidly increase due to the surface tension at the wall of the pores. In this matter, Bondarenko and Nerpin (1965) have assumed that real water is a viscous plastic liquid and is characterized as a Bingham's body by two coefficients, plastic viscosity $\bar{h}$ and yield stress τ_y. Based on this assumption the permeability constant can be computed from water permeability measurements. This report attempts to describe this approach.

Flow of Gas Through Rock Samples

The apparatus used for permeability measurements in this work is shown in Figure 15. This system utilized nitrogen flowing through a carefully dried disc sample of porous rock having parallel ends, a cross-sectional area A = 5.06 cm^2, and a length L = 0.2 ~ 0.8 cm. The sample was mounted in a tube, the wall of which was tightly bonded to the sample with epoxy resin to prevent leakage. A layer of coarse-grained anhydrous $CaSO_4$ was placed in contact with the sample to prevent moisture from collecting in the pores during the experiment. The details of the experimental apparatus are shown in Figures 15 and 16. Nitrogen from a cylinder was supplied to the end of the sample and the other end was connected to the soap-film meter by which a small flow rate at steady state could be measured. The outlet pressure, p_2, was one atmosphere and the inlet pressure, p_1, varied from 1 to 11 atm. The temperature was kept at 24°C during all runs.

Most of the gas permeabilities presented here were determined using the equipment shown in Figures 15 and 16. However, it was found that certain very fine-grained rocks produced flow rates too small to be measured in this manner. This led to efforts aimed at determining very low flow rates for low permeability sample.

Six fine-grained aggregates were utilized in this portion of the study. Five were limestone and one a granite. Permeability data had been collected previously for the granite, hence this aggregate was used as a basis from which to develop a test method suitable for the fine-grained limestones.

Muskat (1937) discusses the determination of both gas and water permeabilities of porous rocks. From his discussion, it is apparent that sample preparation must be given adequate consideration if consistent and meaningful permeability results are to be obtained. One precaution advanced concerns the capillary absorption of foreign material into a rock sample while the sample is being shaped on cutting or grinding wheels. Muskat found that this effect could be prevented by working with saturated samples in which the pores were filled with water and could not easily absorb foreign matter.

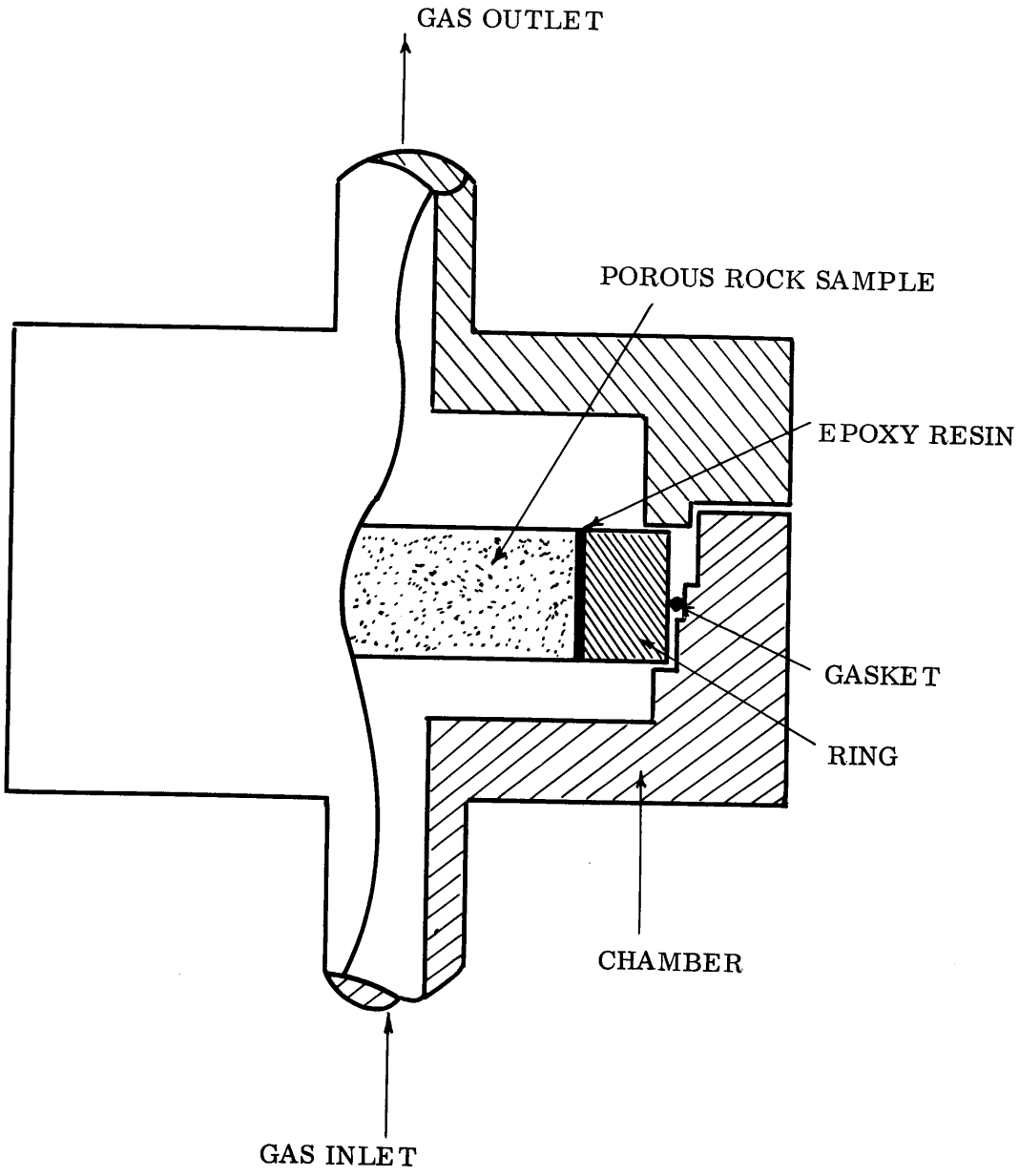

Figure 15. Test chamber for permeability measurements.

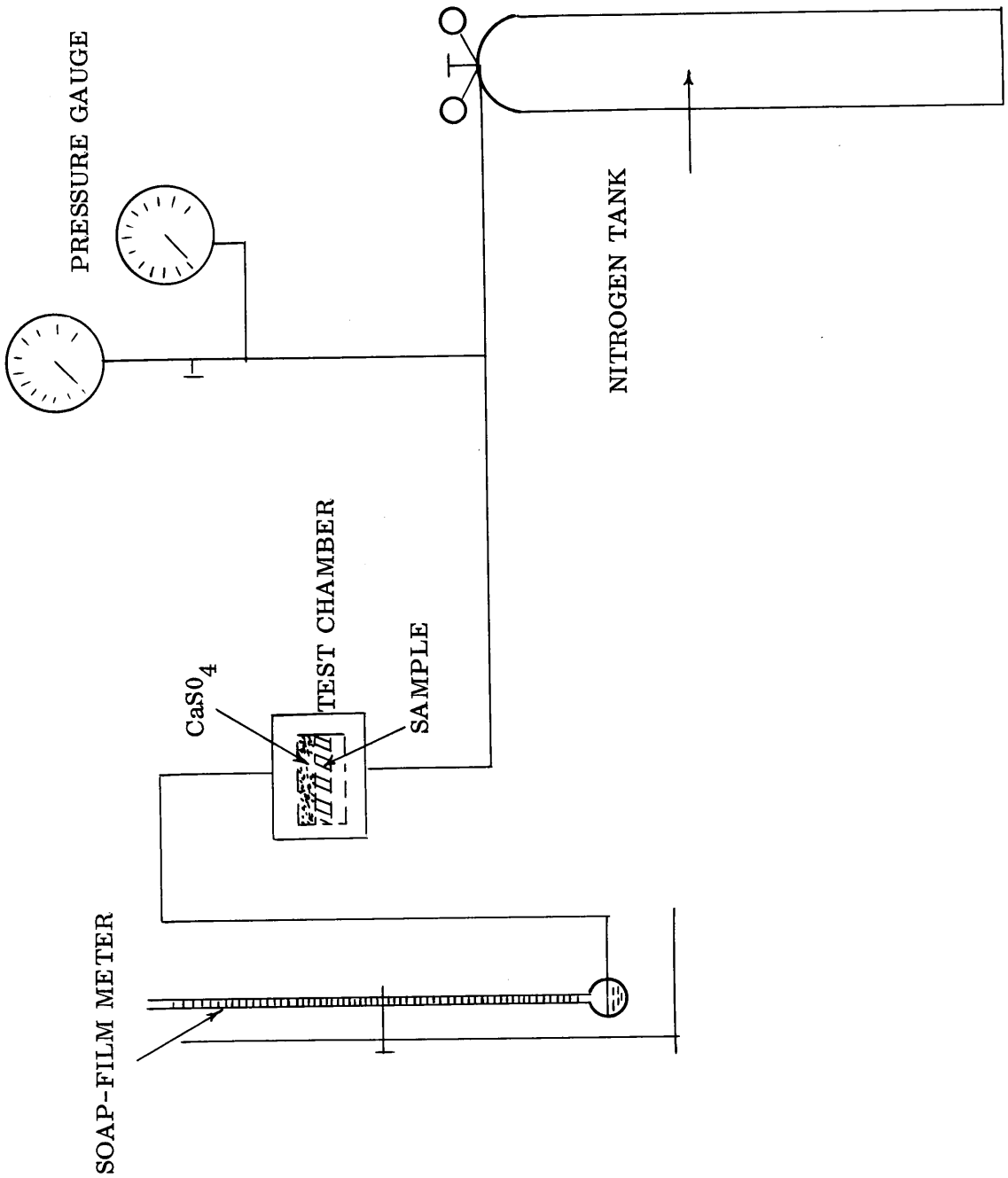

Figure 16. Diagram of permeability apparatus.

Unfortunately, pore water, while necessary when samples are being shaped, is not desirable when a gas permeability test is being conducted. Carman (1956) shows that for a consolidated sand, no gas permeability can be observed if 80 to 85 percent of the available pore space is occupied by water and also that permeability is very significantly reduced when the sample is more than 10 percent water saturated. Apparently, gas may enter a sample and displace water from relatively large pores, but in very small pores water is held so tightly by capillary forces that the pores are blocked and gas can not flow.

Experimental Work

Measurement of Low Flow Rates

The measurement of gas flow through most rock is relatively simple. However, for the special case of flow through some very fine-grained aggregates the following adaptation of the normal apparatus and procedure was used.

(1). Aggregate samples were soaked for several days to permit the pores to become filled with water.

(2). Permeability specimens were shaped with the saw and grinding wheel.

(3). Specimens were surface dried, then mounted in the test rings with epoxy resin.

(4). The mounted specimens were dried at 100°C to constant weight. It was found to be helpful after several hours of drying to rinse the specimens in acetone. This rinse removed any oils accumulated on the specimen and appeared to aid in removing water from the very fine pores after the less tightly held water had been removed by drying; this permitted better acetone penetration. The sample was placed in a dessicator to cool before weighing. Otherwise, specimens were observed to gain water rapidly when the temperature of the specimen fell below the dew point for the prevailing relative humidity.

(5). For measurement of the flow rate for the very low permeability specimens, a water displacement method was devised. In this method, a nominal 4 mm inside diameter glass tube partially filled with water was connected to a hose from the sample chamber. Reproducible results were obtained by calibrating the tube so that counting the number of drops of water displaced in a given time yielded the flow rate in cubic centimeters per second. For the tube used each drop of water represented 0.1 cc of flow. Figure 17 shows the apparatus for flow measurement used in this method.

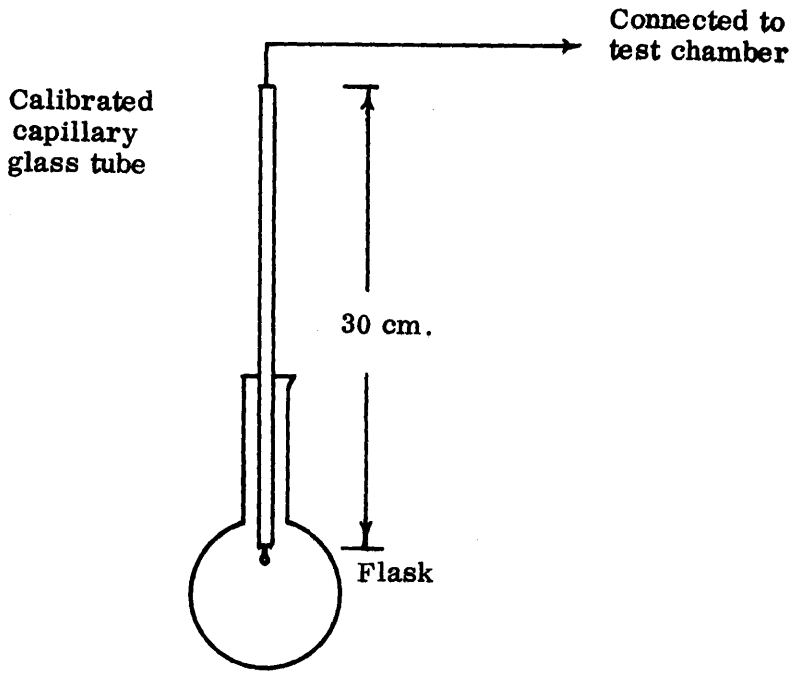

Figure 17. Flow measurement for fine pore materials.

Note that in this method of flow measurement the gas outlet pressure, due to the weight of the column of water, is a vacuum of about 0.4 psi. Consequently, any gas flow through the sample is detectable because the vacuum is lowered and water is permitted to drop from the tube. Obviously, reproducible water flow rates require that the column of water remain at an approximately constant height. Hence, before measuring the flow rate at a given pressure the gas flow through the sample is permitted to reach a steady state, as indicated by a constant reading on the pressure gauge, then the water tube is filled to around a 30 cm height and the flow rate determined by timing several drops of water. The resultant head loss is negligible compared to the height of the water column. Then because the difference between the gas outlet pressure and the water outlet pressure is approximately only 0.4 psi, the gas and water flow rates are essentially equal. When the gas pressure is increased to the next desired level, the system is again permitted to reach a steady state condition and the water column returned to the 30 cm height before the flow measurement is attempted.

Flow rates down to 10^{-5} cc per second were successfully measured, usually with complete reproducibility. When the reproducibility was in question, a series of four or

five water drops with a time coefficient of variation of less than 5% between drops was taken as an acceptable reading. In either event, a steady state gas flow condition was absolutely essential. Six aggregates were tested by means of these procedures.

Studies on Effects of Pore Moisture on Permeability

In order to examine the effect of pore moisture on gas permeability, several fine-grained rocks were chosen. Most of the samples had extremely small mean pore radii. Consequently, as indicated previously, it was necessary to drive off all pore water before gas permeability tests could be run. Thus, one mounted sample, P-6, was dried to a constant weight at 100°C. However, when a permeability test was attempted, it was found that at constant pressure the permeability decreased with time. The obvious indication was that the oven dry sample had begun to pick up atmospheric moisture and to show reduced permeability. Subsequently, the sample was again oven dried and with the sample surrounded by granular anhydrous $CaSO_4$ another permeability test was attempted and the permeability at constant pressure now remained constant with time. The results of these two tests are shown in Figure 18.

Further studies of the effects of atmospheric moisture were conducted on sample P-6, the fine-grained granite. The mounted sample was soaked for 24 hours, weighed and gradually dried, first in air, then in the oven. The relative permeability and the degree of saturation were periodically determined during this drying period. Figure 19 shows the results of this test. Note that at 12.5 percent saturation the effective permability is significantly reduced, while at 75 percent saturation the gas permeability is essentially zero. Carman (1956) found similar results in his studies of consolidated sands.

In order to evaluate the actual degree of dryness reached by an "air dried" sample, several samples were oven dried, then left in the laboratory to equilibrate with the atmospheric moisture. Several equilibrium weights were determined for each sample. Depending on the relative humidity in the laboratory, the equilibrium weights showed a considerable amount of variation. Finally, the 24-hour absorption was determined for each sample. Table 3 shows the absorption and the maximum degree of saturation attained in air for each sample. The relative humidity of the laboratory during the test period ranged from 45 to 70 percent.

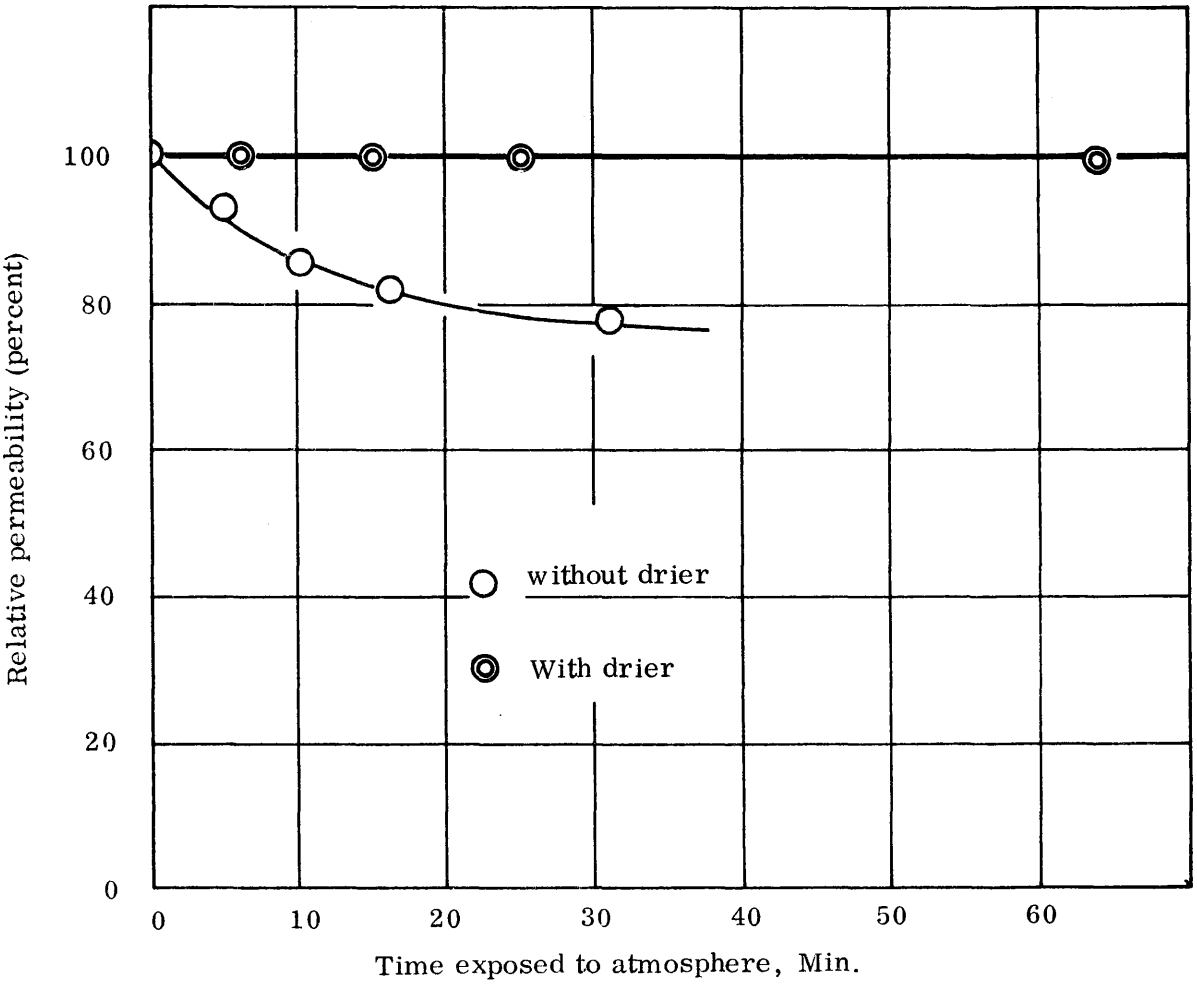

Figure 18. Sample P-6 — Relative permeability (expressed as percentage of absolute permeability vs. time exposed to atmosphere) with pressure constant at 50 psi and relative humidity 50 percent.

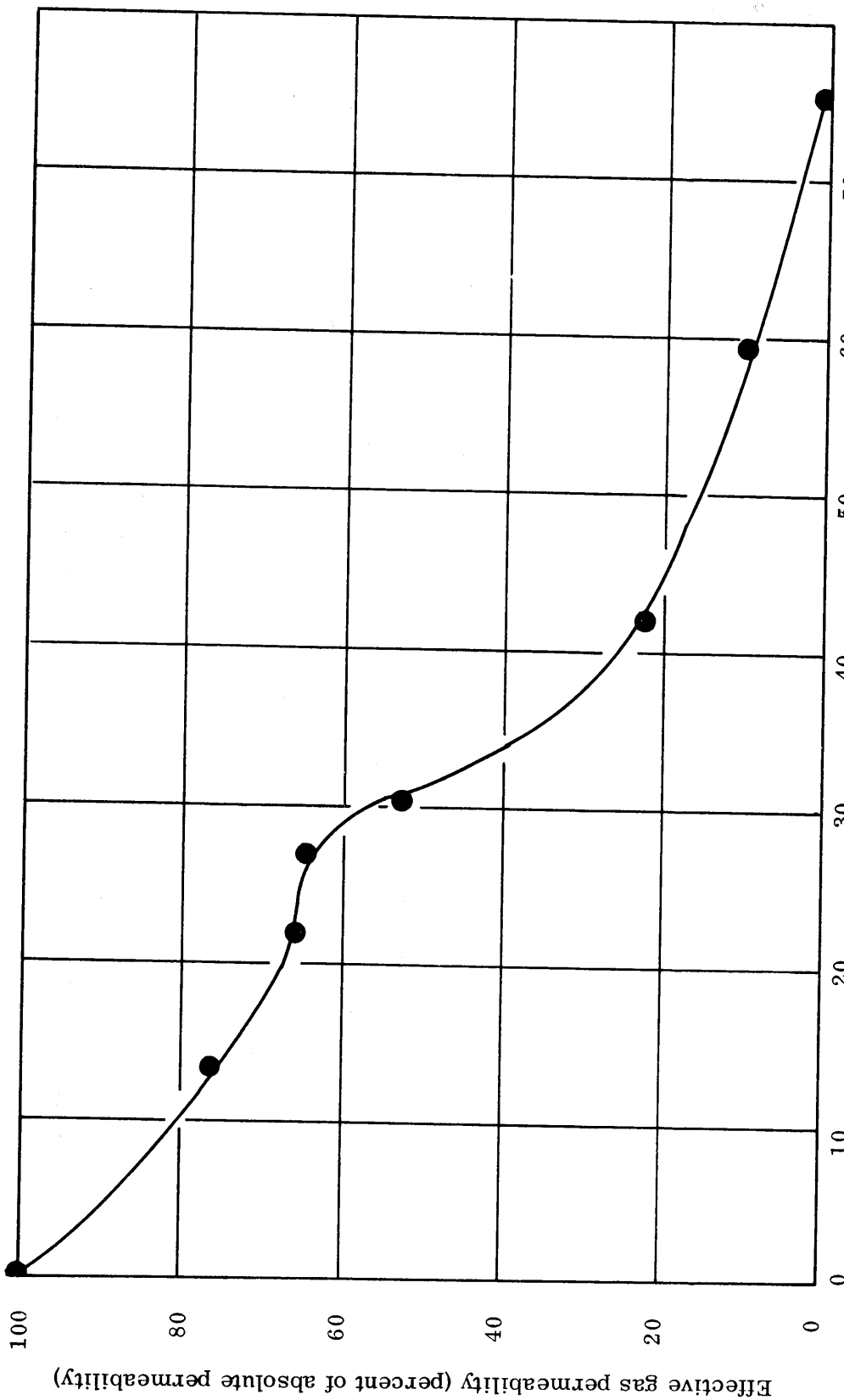

Figure 19. Sample P-6 — Effective gas permeability vs. percent of H_2O saturation.

TABLE 3

DEGREE OF SATURATION OF FINE-GRAINED AGGREGATES IN LABORATORY ENVIRONMENT

Rock Type	Sample No.	24-Hour Absorption (%)	Percent of 24-Hour Saturation Attained In Laboratory Environment
Limestone	1-8-A	0.476	32.8
Limestone	1-8-A	0.425	36.9
Dolomite	1-18	0.169	46.7
Limestone	12-9	0.445	38.2
Limestone	MF	0.0255	55.7
Granite	P-6	0.298	20.8

An examination of Table 3 and Figure 19 shows that due to the high degree of saturation attained by fine-grained aggregates under room conditions, the effective gas permeability will be significantly less than the absolute permeability. The assumption that "air dried" and "oven dried" are essentially equal is not justified for fine-grained aggregates. Verbeck and Langren (1960) found a similar relationship between the degree of saturation and relative humidity.

Permeability Constant

As mentioned previously, the relationship between flow rates and pressure change for Virginia aggregates is not linear. Consequently, only limited usage can be made of the wellknown expression of Darcy's Law,

$$Q = K \frac{A}{\mu} \frac{\Delta p}{L} \qquad (2\text{-}1)$$

where Q is the fluid flow rate in volume per unit time, with the viscosity, μ, under the applied pressure difference Δp across the cross-sectional area A and length L of porous material. Here K is the permeability constant expression in terms of cm^2. For the dense rocks commonly used for aggregate in Virginia, K is best expressed in millidarcys.

In order to explain the many observed deviations from simple flow as envisioned by Darcy's law, a number of workers have introduced more complex concepts with attendant mathematical expressions.

Kozeny (1927) treated porous media as a bundle of capillary tubes of equal length through which laminar flow was assumed to occur, thereby obtaining the expression for the permeability of porous media. Numerous modifications of the Kozeny type equation have been published. A modification proposed by Carman (1956) accounts for the slip flow at the capillary wall, as well as the Poiseuille flow.

In Part 3 of this report, a theoretical equation is developed for gas flow through capillaries where diffusion, slip flow and Poiseuille flow are taken into account. This equation has been proved experimentally to hold for flow through small capillaries. It allows the determination of not only the permeability constant but also the effective area fraction and mean pore radius. In its simplest form this theoretical treatment results in graphs where an increase in the pressure, $\Delta P/P_0$, is plotted against the flow parameter, $Q_0 L \quad / \left(A \frac{P}{P_0}\right)$, to yield straight line results.

Figure 20 shows the results of permeability tests on sample P-6 at three levels of water saturation reached at room equilibrium. The three lines shown are the results of tests on a single specimen conducted on different days and reflecting different prevailing relative humidities in the laboratory. The curve designated 0% saturated was plotted from data collected for the oven dry sample surrounded by anhydrous $CaSO_4$.

In Figure 20 it can be seen that the slope and intercept are both strongly influenced by the degree of saturation. Obviously, if the slope and intercept are affected by saturation, Equations (3-15) and (3-16) in Part 3 show that the mean pore radius and effective area fraction also must be influenced. The calculated effective area and mean pore radius for the three states of saturation are listed in Table 4.

Taking the $\bar{a}$ and f values found for the dry sample as absolute or true values, note that at 13.6% saturation the mean effective pore radius has increased by a factor of 6 while the effective area fraction has been decreased by about 90%. Similarly, at 13.6% saturation the effective permeability was 76.5% of the absolute permeability. The obvious implication of these results is that at relatively low saturation many very small pores which do not contribute greatly to the gas flow are plugged with water, causing the indicated or effective mean pore radius to appear much larger. This tendency toward the small pores being the first to be filled with water is best understood through analogy with the capillarity concept, where the affinity of a tube for water is found to increase inversely with the tube diameter. Comparison of the coarser-grained aggregates with the finer-grained shows that the $\bar{a}$ values found for both are of the same order of magnitude. On the other hand, the f values are significantly lower for the finer-grained aggregates.

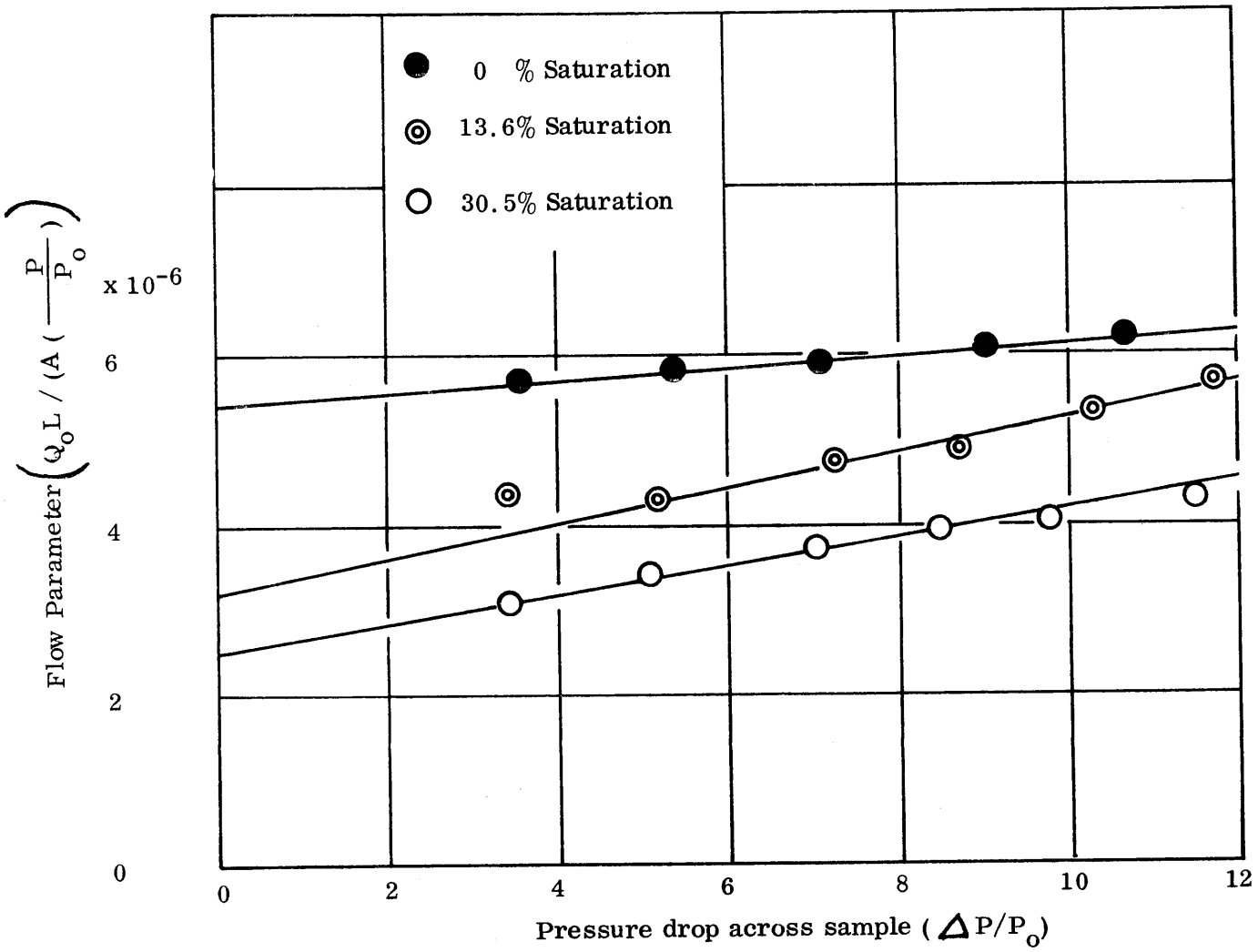

Figure 20. Aggregate P-6 — Influence of degree of saturation on gas flow characteristics.

TABLE 4

EFFECTIVE FLOW PROPERTIES AT THREE LEVELS OF SATURATION
SAMPLE P-6

Level of Saturation (%)	Mean Pore Radius, $\bar{a}$	Effective Area Fraction, f	Effective Permeability, %
0	0.0081	2.93×10^{-4}	100
13.6	0.0481	2.57×10^{-5}	76.5
36.5	0.0555	1.62×10^{-5}	53.1

Therefore, it appears that in some cases due to partial saturation a fine-grained aggregate may show a mean pore size which is as large as that of a coarse-grained aggregate, but the pores are significantly less in number for the fine-grained material.

The distribution of permeabilities of the Virginia aggregates under test can be seen in Figures 21, 22, and 23 and Tables 5 through 7. Figure 21 shows the sandstone rocks with random flow direction through the beds. The permeability range is from 3.2×10^{-4} to 3200×10^{-4} md as listed in Table 5. Figure 22 shows the carbonate rocks (limestones and dolomites) with random, perpendicular and parallel flow, and their permeability ranges are divided into the following classifications: Very low permeability is less than 0.1×10^{-4} md; low permeability is between 0.1×10^{-4} and 1.0×10^{-4} md; medium permeability is between 1.0×10^{-4} and 10×10^{-4} md; high permeability is between 10×10^{-4} and 100×10^{-4} md; and very high permeability is all values over 100×10^{-4} md. These data are listed in Table 5 for sandstones and Table 6 for carbonates. Table 7 and Figure 23 show the data for igneous and metamorphic (crystalline) rock samples. The overall permeability ranges are from 0.18×10^{-4} to 282×10^{-4} md for carbonate rocks and 0.08×10^{-4} to 3720×10^{-4} md. for crystalline rocks.

The cumulative curves shown in Figure 22 represent the permeabilities measured parallel, perpendicular, and random to the bedding for the carbonate rocks under study. As would be expected the general shapes of the curves would indicate that the flow perpendicular to the bedding is lowest and the flow parallel to the bedding is highest. The flow in directions random to the bedding appears to be somewhat intermediate between the two. Despite this difference it was surprising to the investigators that the variation was no greater. This finding might indicate that the carbonate rocks under consideration are generally massive, highly lithified materials which show little variation in pore structure with direction.

This same general behavior was noted for the crystalline rocks shown in Figure 23. In many cases random flow resulted in a lower permeability than flow perpendicular to foliation. This might be due to the fact that random flow measurements were made on massive, non-foliated rocks where planes of weakness had not been developed, whereas measurements perpendicular and parallel to foliation might be affected by planes of weakness in the rock.

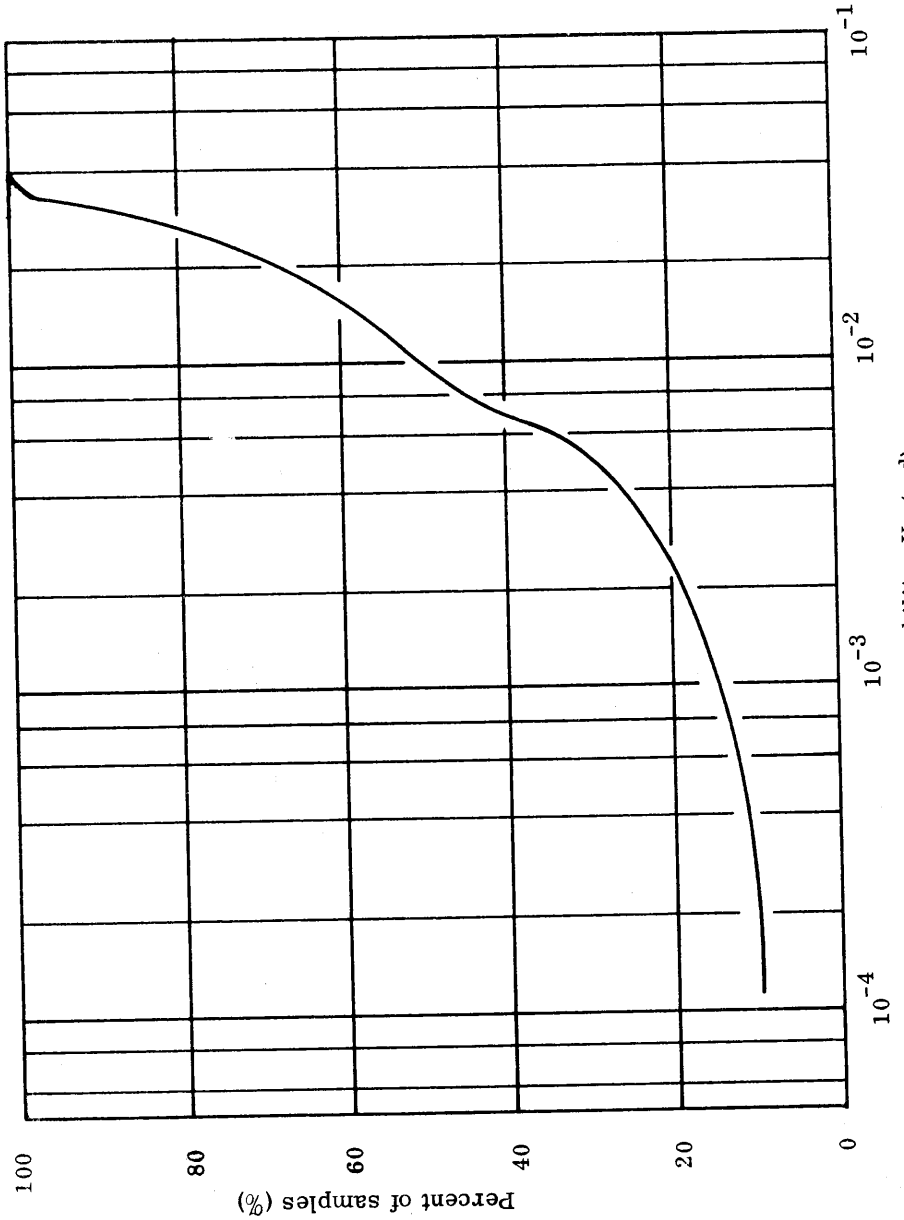

Figure 21. Cumulative distribution of permeabilities of sandstone rocks.

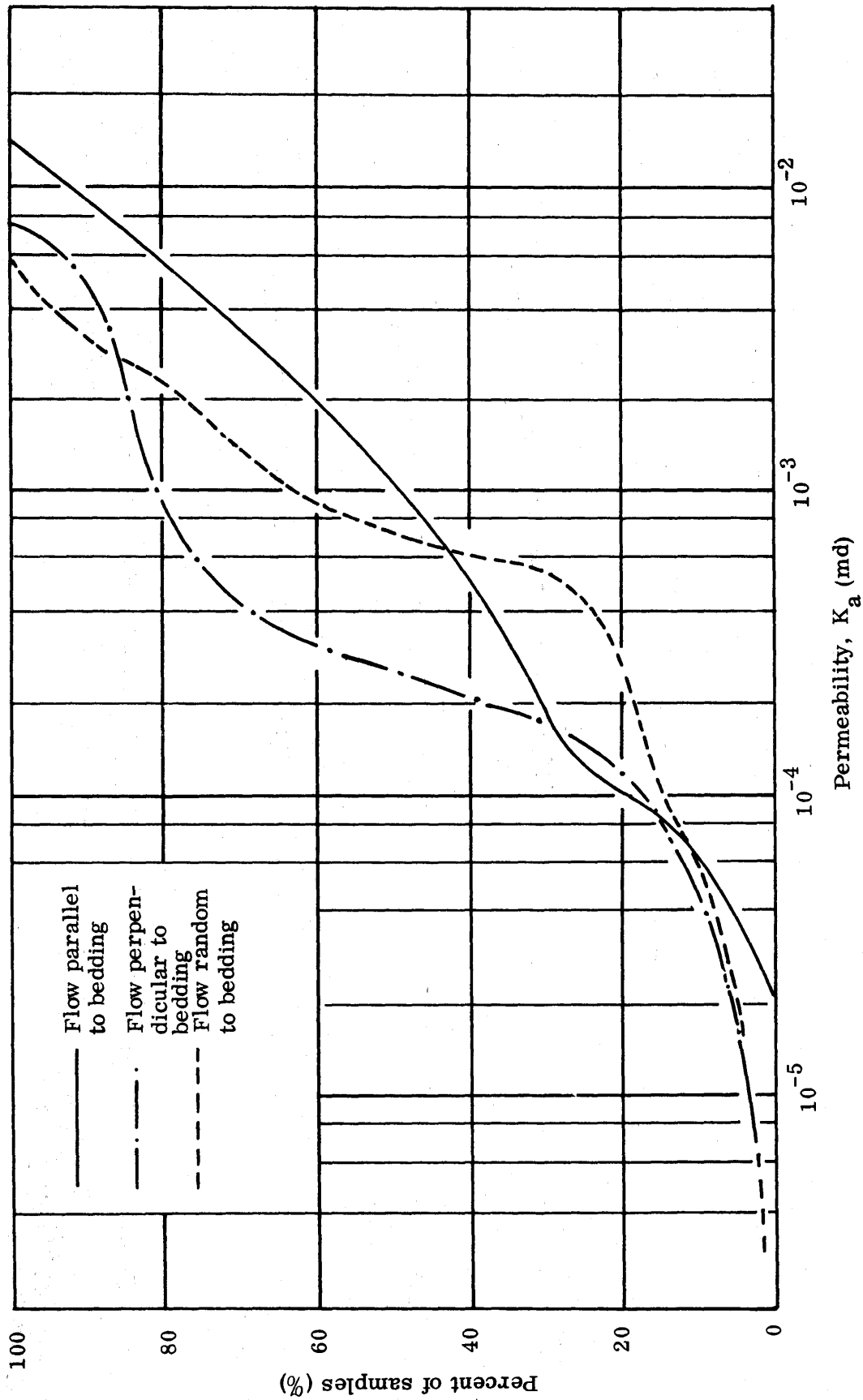

Figure 22. Cumulative distribution of permeabilities of carbonate rocks.

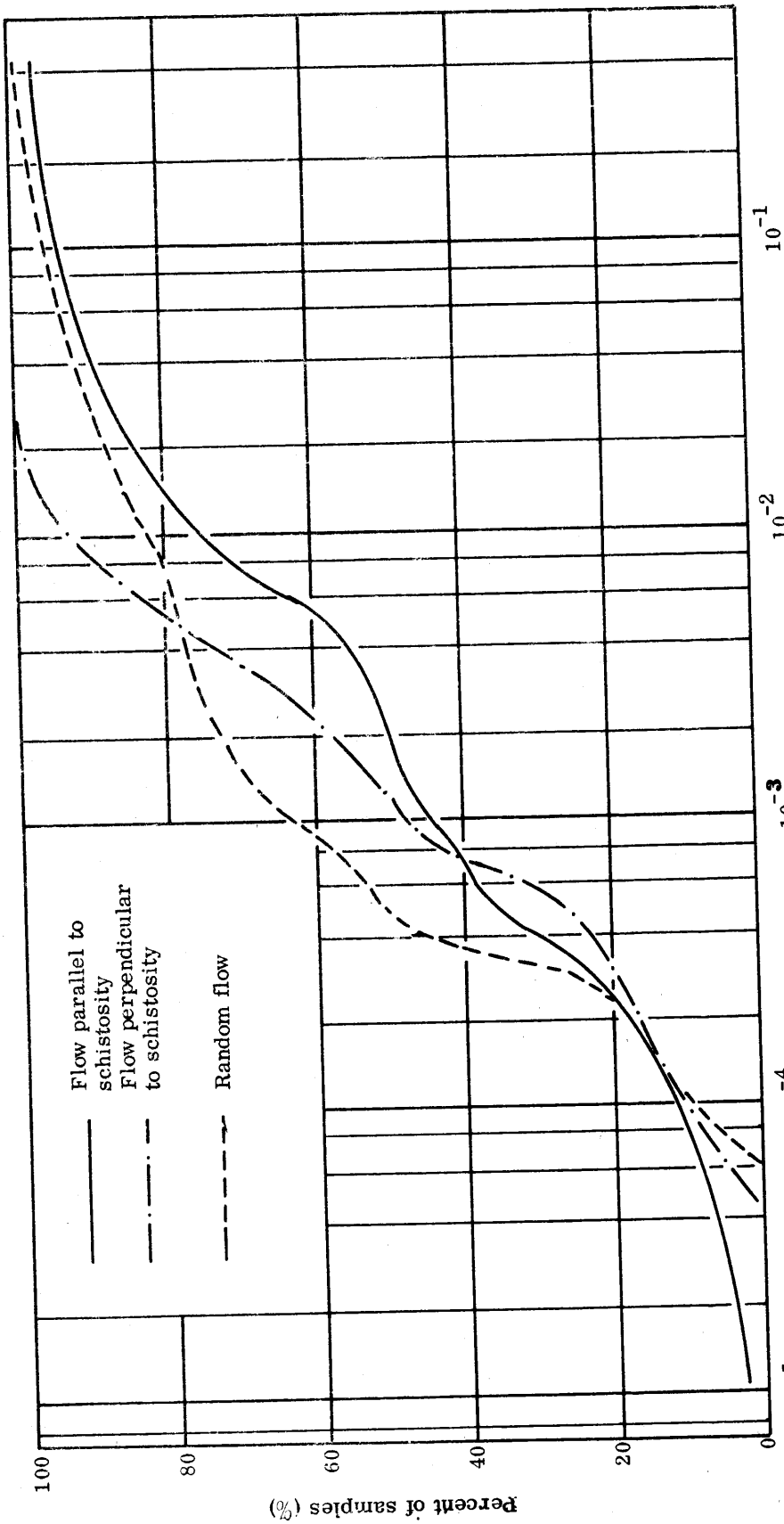

Figure 23. Cumulative distribution of permeabilities of igneous and metamorphic (crystalline) rocks.

TABLE 5

PERMEABILITIES OF SANDSTONE ROCKS

Permeability, $K_a \times 10^4$ (md)

Sample	Description	Random Flow	Flow Parallel To Bedding	Flow Perpendicular To Bedding	Range
(1) P - 5C	Triassic Siltstone		0.0642	0.665	Low
(2) P - 5B	Triassic Siltstone	3.2			Medium
(3) 49 - 1	Medium Grained Sandstone	360 - 512			Very High
(4) 6	Coarse Grained Quartz Sandstone	890 - 3200			Very High

TABLE 6

PERMEABILITIES OF CARBONATE ROCKS

Permeability, $K_a \times 10^{-4}$ (md)

Sample	Description	Random Flow	Flow Parallel To Bedding	Flow Perpendicular To Bedding	Range
ML	Very Fine Grained High Calcium Limestone	0.297			Low
12 - 9	Very Fine Grained Laminated Dolomitic Limestone		0.694	0.183	Low
MF	Very Fine Grained High Calcium Limestone	0.419			Low
P - 23	Medium Grained, Metamorphosed Argillaceous Limestone			1.71	Medium
1 - 18	Dense, Medium Grained Dolomite	1.9 - 2.45			Medium
6 - 2	Dense, Fine Grained Dolomite		1.29 - 2.54	2.38 - 7.25	Medium
26 - 5	Dense, Medium Grained Dolomite	1.51 - 770			Medium
H - 1	Medium Grained High Calcium Limestone	5.4 - 18.5			High
22 - 2	Dense, Medium Grained Dolomite	5.4 - 24.9			High
15 - 9	Fine Grained Argillaceous Limestone			0.71 - 71	High
Mo - C	Medium Grained Soft Dolomite Argillaceous Limestone from Missouri	15.8 - 20.2			High
S - 1	Coarse Grained Limestone	26.2 - 34.5			High
13 - 1	Medium Grained, Argillaceous Dolomite	32.6 - 50.0			High
P - 13	Medium Grained, Micaceous, Metamorphic Limestone		7.4 - 1310	1.40	Very High
P - 23B	Fine to Medium Grained, Foliated, Metamorphic Limestone		17.9	282.0	Very High

TABLE 7

PERMEABILITIES OF IGNEOUS AND METAMORPHIC ROCKS

Permeability $K_a \times 10^{-4}$ (md)

Sample	Description	Random Flow	Flow Parallel To Bedding	Flow Perpendicular To Bedding	Range
P - 20	Chlorite Feldspar Schist		0.085 - 0.206	1.32	Low
P - 7	Coarse Grained, Fledspar Rich Granite Gneiss		.306 - 2.02	0.680 - 0.735	Low
P - 17	Medium Grained, Biotite Granite Gneiss	0.612 - 3.2			Medium
P - 6	Fine Grained, Biotite Granite	2.78 - 3.28			Medium
P - 2	Triassic Diabase	3.4 - 4.65			Medium
P - 8	Greenstone (Altered Basalt)		3.83 - 4.24		Medium
P - 19	Fine Grained, Muscovite, Granite Gneiss		1.78 - 2.64	6.3 - 7.2	Medium
P - 16	Medium Grained, Biotite Granite		1.76 - 7.89	3.16 - 7.8	Medium
P - 15	Fine Grained, Biotite Granite	8.2 - 12.5			High
P - 1	Coarse Grained Granite Gneiss		54.5 - 86.5	0.486 - 70.3	High
P - 3	Slate		79.3	1.28 - 1.41	High
P - 10	Coarse Grained, Biotite, Granite Gneiss		19.5 - 39.4	5.9 - 60.6	High
P -14B			29.2 - 33.4	15.9 - 21.2	High
P - 21A	Coarse Grained, Granite Gneiss		70.5	12.0 - 32.6	High
P - 9	Mica, Quartz Schist		965 - 3720	6.48 - 10.7	Very High
P - 14	Garnetiferous, Quartz, Biotite Gneiss		17.5 - 951	63.5 - 290	Very High
P - 11	Medium Grained, Granite Gneiss		59.5 - 545	37.7 - 57.1	Very High
P - 12	Medium Grained, Granite Gneiss		115 - 148	21.1 - 28.3	Very High
P - 20B	Chlorite Schist		3.56 - 4.30	8.0	Medium
P - 15A	Fine Grained, Garnetiferous, Biotite Granite	3.14 - 651			Very High
p - 18A	Medium Grained, even Textured, Light Granite	260 - 282			Very High

Flow of Water Through Rock Samples

Experimental Work

The apparatus for the measurement of water flow through rock (Figure 24) is similar to that used for glas flow shown in Figure 15. The sample has parallel ends, a cross-sectional area A = 5.06 cm^2, and a thickness of 0.2 cm. The sample was mounted in a ring, and the wall of the ring was tightly bonded to the sample with epoxy resin to prevent leakage.

The experimental procedure was first to saturate the sample and then surround it by filling both the inlet and outlet sides of the apparatus with distilled water. A capillary tube (1/10 in. = 1/100 ml) was connected to the outlet side and partially filled with distilled water (see Figure 24). With pressure on the inlet side, a small flow rate at steady state could be measured by observing the increase in the volume of water in the capillary tube. Gaseous nitrogen was used as the driving medium. The solubility of nitrogen in water is quite small and its effect on the pressure drop can be neglected. The range of pressure supplied was from 10 to 100 psi. In order to prevent the evaporation of the water from the capillary tube, the outlet of the tube was connected by plastic tubing to wetted particles in a beaker (see Figure 24). All runs were at room temperature (the average being about 24.5°C); the water pressure and flow rate were recorded.

Results and Discussion

The experimental data for water flow were plotted as flow rate versus pressure drop across the sample. The results shown in Figure 25 for sample H-1 show that the plot is not a straight line corresponding to Darcy's law but is at a distance ΔP_o from the origin and parallel to the "Darcy" line.

Several investigators have suggested that the simple relationship expressed by Darcy's law may not always be valid for fine-grained samples, particularly under conditions of low hydraulic gradient. Mitchell and Younger (1966) in their work on "Abnormalities in Hydraulic Flow Through Fine-Grained Soils" have discussed this non-Darcy's flow phenomenon.

Bondarenko and Nerpin (1965) have shown that this phenomenon of water flow through fine porous media is similar to viscous plastic flow. They assumed that real water is a viscous plastic liquid and is characterized as Bingham's body by the two coefficients, plastic viscosity and yield stress.

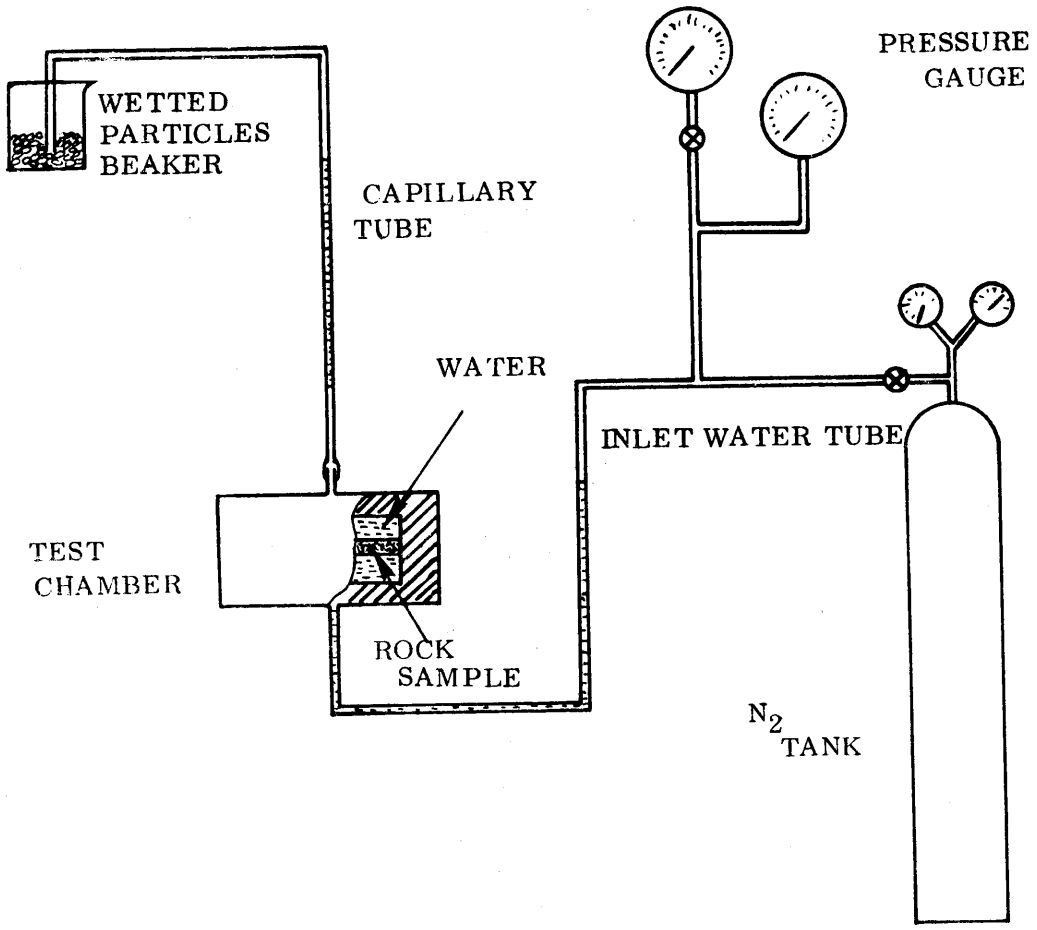

Figure 24. Water permeability apparatus.

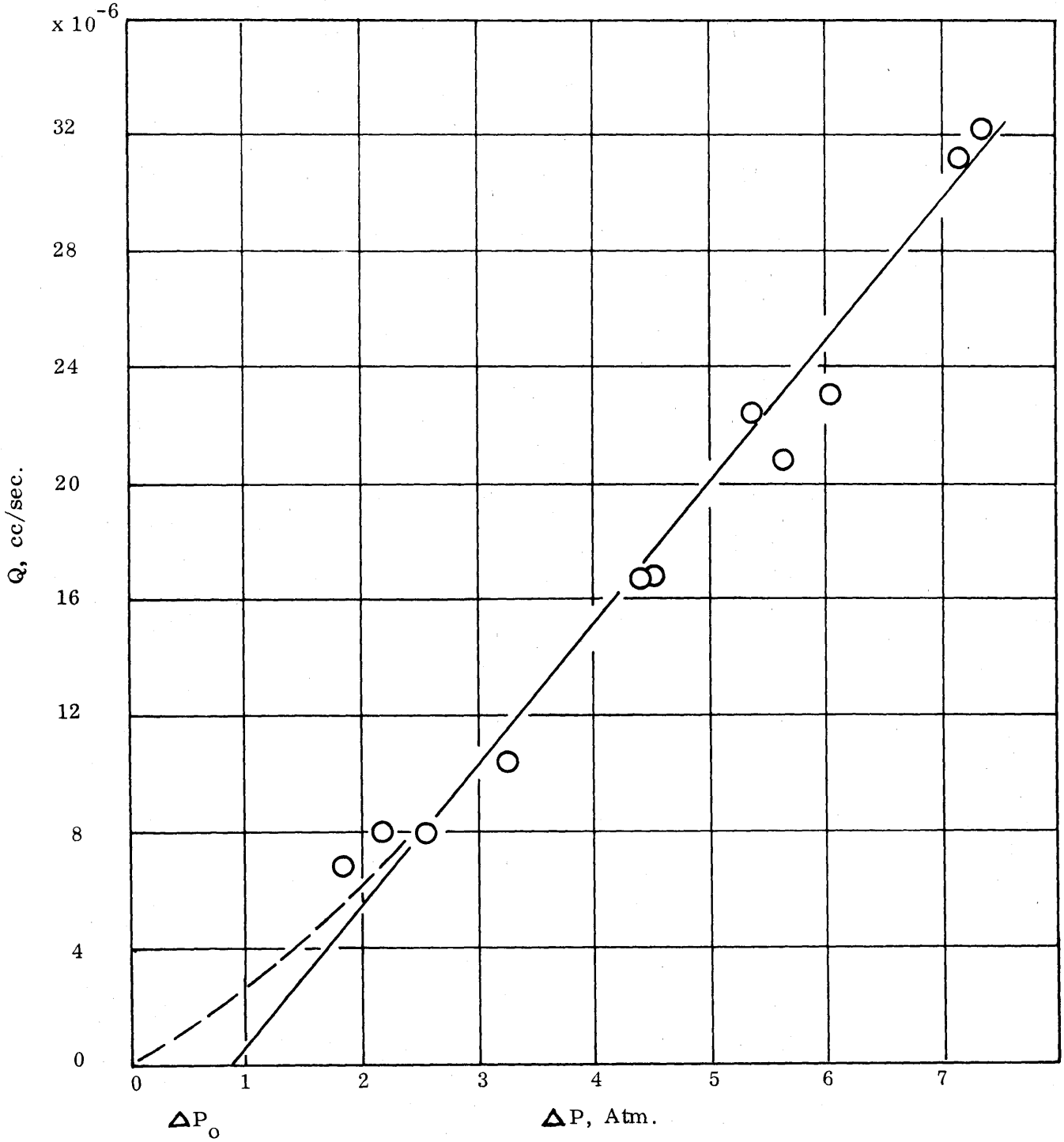

Figure 25. Water flow rate versus pressure for Sample H-1.

According to the Poisseulle's equation for the Bingham body the flow per capillary is

$$Q = \frac{\pi \bar{a}^4}{8 L \eta} \Delta P \left[1 - \frac{4}{3} \left(\frac{2L \tau_y}{\bar{a} \Delta P} \right) + \frac{1}{3} \left(\frac{2L \tau_y}{\bar{a} P} \right)^4 \right] \quad (2\text{-}2)$$

where η is the coefficient of viscous water, τ_y is shear stress, $\bar{a}$ is the mean pore radius, L is the length of sample and Q is the volume flow rate. If there are n such capillaries of cross section of the model, the total flow then is:

$$Q = \frac{n \pi \bar{a}^4}{8 L \eta} \Delta P \left[1 - \frac{4}{3} \left(\frac{2L \tau_y}{\bar{a} \Delta P} \right) + \frac{1}{3} \left(\frac{2L \tau_y}{\bar{a} \Delta P} \right)^4 \right] \quad (2\text{-}3)$$

Darcy's law is written:

$$Q = \frac{K_w A \Delta P}{L \mu_o} \quad (2\text{-}4)$$

where μ_o is the apparent viscosity of water and K_w is the permeability constant of porous media. Using Equations (2-3) and (2-4), the permeability of water, K_w, can be obtained as follows,

$$K_w = \frac{n \pi \bar{a}^4 \mu_o}{8 A \eta} \left[1 - \frac{4}{3} \left(\frac{2L \tau_y}{\bar{a} \Delta P} \right) + \frac{1}{3} \left(\frac{2L \tau_y}{\bar{a} \Delta P} \right)^4 \right] \quad (2\text{-}5)$$

According to Equation (2-3) the last term can be omitted with little error ($\tau_y / \tau_p = 0.5$ is 5.0% of error and $\tau_y / \tau_p = 0.4$ is 1.8% of error, where $\tau_p = \bar{a} \Delta P / L$). Therefore, Equation (2-3) can be written as

$$Q = M \Delta P - N \quad (2\text{-}6)$$

where

$$M = n \pi \bar{a}^4 / (8L \eta) \qquad \eta = n \pi \bar{a}^4 / (8LM)$$
$$N = n \pi \bar{a}^4 \tau_y / (3 \bar{a} \eta) \qquad \tau_y = 3 \bar{a} N / (8LM) \qquad (2\text{-}7)$$

Substituting Equation (2-7) into Equation (2-5) the water permeability, K_w, is

$$K_w = \frac{L \mu_o M}{A} \left(1 + \frac{N}{M \Delta P}\right) \qquad (2\text{-}8)$$

where M is the slope of Equation (2-6) and N is the intercept.

By plotting the results of flow rate versus pressure drop as shown in Figure 25 for sample H-1, M and N can be obtained experimentally as 5.7×10^{-6} and -4.2×10^{-6} respectively. The water permeability constant, K_w, can be calculated from Equation (2-8). Similar results for all samples studied are shown in Table 8 (these are also based on a P of one atmosphere). The pore size distribution of sample H-1 as determined by mercury porosimetry is shown in Figure 26.

It should be pointed out also at this point that water flow through porous media is more complex than gas flow, due to the movement of the liquid phase and vapor phase together by diffusion, sorption, and ion exchange.

Geologic Interpretation

In the section on porosity it was noted that in many cases rocks of similar type and texture exhibited similar pore size distribution curves. Also it was found that fundamental differences in pore structure existed between carbonate and crystalline rocks. A close look at the data reproduced in Tables 5, 6, and 7 indicates that the relationship between intrinsic rock properties and permeability are not nearly so well defined. On the other hand certain interesting trends appear worthy of mention.

In the case of the four sandstones listed in Table 5 a simple relationship appears to exist between grain size and permeability. This relationship would be expected to hold except in cases where the material was highly cemented or highly lithified or both. The logical analogy would be to sand beds with different sizes of particles and consequently different pore sizes and permeabilities.

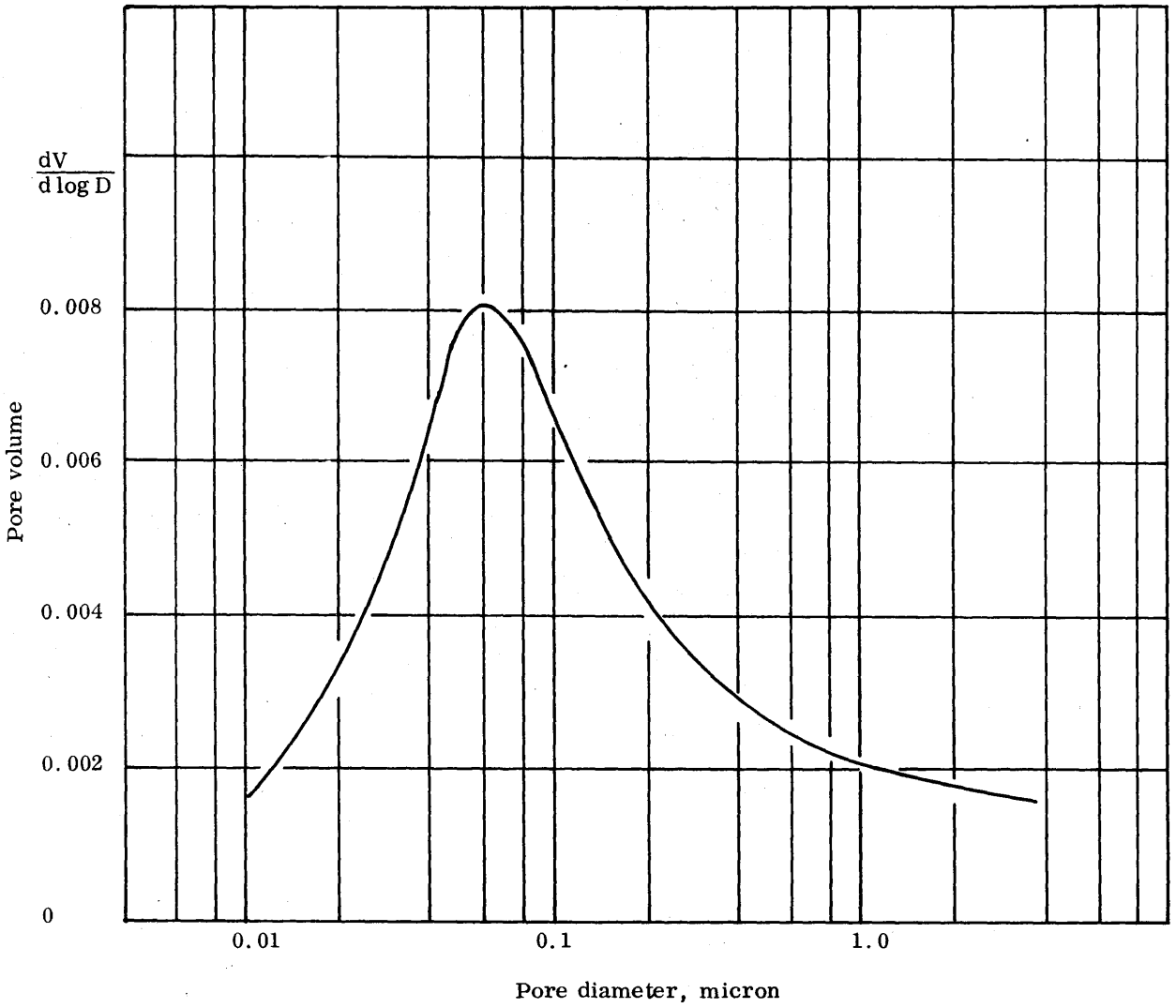

Figure 26. Pore size distribution curve for Sample H-1.

TABLE 8

WATER AND AIR PERMEABILITIES

Sample*	N cc/Sec.	M cc/Sec. at m	L (cm)	K_w, md	K_a, md
6	0	1.88×10^{-3}	0.35	1.33×10^{-1}	2.36×10^{-1}
49-1a	0	3.30×10^{-5}	0.20	1.33×10^{-3}	1.6×10^{-2}
b	0	3.90×10^{-5}	0.22	1.72×10^{-3}	3.29×10^{-2}
c	0	2.9×10^{-5}	0.20	1.30×10^{-3}	1.73×10^{-2}
H-1	-4.2×10^{-6}	5.7×10^{-6}	0.20	6.10×10^{-5}	8.57×10^{-4}
13-1	-0.65×10^{-6}	0.81×10^{-6}	0.20	6.43×10^{-6}	3.31×10^{-3}
P-2	0	0.53×10^{-5}	0.20	2.13×10^{-4}	3.46×10^{-3}
P-18A	0	0.50×10^{-4}	0.20	2.0×10^{-3}	1.05×10^{-2}
P-11	0	1.74×10^{-5}	0.20	7.0×10^{-4}	6.76×10^{-3}
22-2	-0.7×10^{-6}	1.0×10^{-6}	0.20	1.20×10^{-5}	1.81×10^{-3}
P-14	0	0.45×10^{-4}	0.20	1.92×10^{-3}	1.38×10^{-2}
P-13V	-0.2×10^{-6}	0.40×10^{-6}	0.20	8.05×10^{-6}	9.07×10^{-4}
H	0	1.0×10^{-6}	0.20	4.03×10^{-5}	2.52×10^{-3}
P-11 aH	0	0.80×10^{-4}	0.20	3.22×10^{-3}	2.20×10^{-2}
bH	0	0.32×10^{-4}	0.20	1.29×10^{-3}	5.45×10^{-2}
P-12 aH	0	3.90×10^{-5}	0.18	1.57×10^{-3}	1.25×10^{-2}
bH	0	2.80×10^{-5}	0.21	1.12×10^{-3}	1.48×10^{-2}
P-10 aV	0	1.35×10^{-5}	0.20	4.00×10^{-4}	6.06×10^{-3}
bV	0	0.75×10^{-5}	0.20	3.02×10^{-4}	5.79×10^{-3}
aH	0	1.35×10^{-5}	0.20	5.42×10^{-4}	1.95×10^{-3}

* Description, see Tables 5, 6 & 7

Table 6 shows the permeabilities measured for the sixteen different carbonate rocks included in this study. These rocks had the lowest permeabilities of any rocks studied. Also evident is the general relationship between texture and permeability. All of the samples falling under the designations of very low and low permeability are either fine-or very fine-grained materials. Only one other rock (sample 15-9) was fine-grained, and the spread in data indicates that one of the permeability disks used may have been cracked. This presence of fine cracks, whether from quarry blasting, laboratory preparation, or original rock fracture, was found in many samples and made them unacceptable for permeability work.

Included under the medium and high permeability designations were a series of predominantly medium-grained dolomitic and argillaceous carbonates with no clear-cut distinctions between the lithologies of the groups. Finally, the two samples designated very high permeability were found to be the only two metamorphic or schistose carbonates under study. These were collected from Piedmont sources whereas all other carbonate samples were from the Valley and Ridge area.

Of the three groups under consideration in this report the igneous and metamorphic rocks showed the least tendency to correlate texture or lithology with permeability. Each permeability level appears to contain a variety of rock types. A possible reason for this apparent lack of any clear-cut relationship between rock type and permeability might be in the nature of the sample disks used for permeability measurements. To permit the measurement of the permeability of the specimens in a reasonable amount of time the disks were cut only 2 mm thick. This is the order of magnitude of the individual grains in many of the silicate rocks studied. In such cases it is not difficult to visualize a single grain boundary extending entirely through the disk. If such a boundary contained imperfections of a type which could yield a flow disproportionate to that in the remainder of the rock it is clear that an abnormal permeability could result.

Studies have shown that water permeabilities are somewhat lower than gas permeabilities (see Figure 27). Baptist (1966) has studied water permeability and gas permeability in several reservoir sands in Wyoming. The results of measurements for Virginia rocks seem to compare somewhat favorably to Baptist's results for the Tensleep sandstone. The difference between the water and gas permeabilities increases when the permeabilities of the rock decrease. This phenomenon is probably due to the capillary structure of the rock having random fine pores. These pores could cause a rapid increase in the coefficient of viscosity of the water due to the surface tension of water at the pore walls.

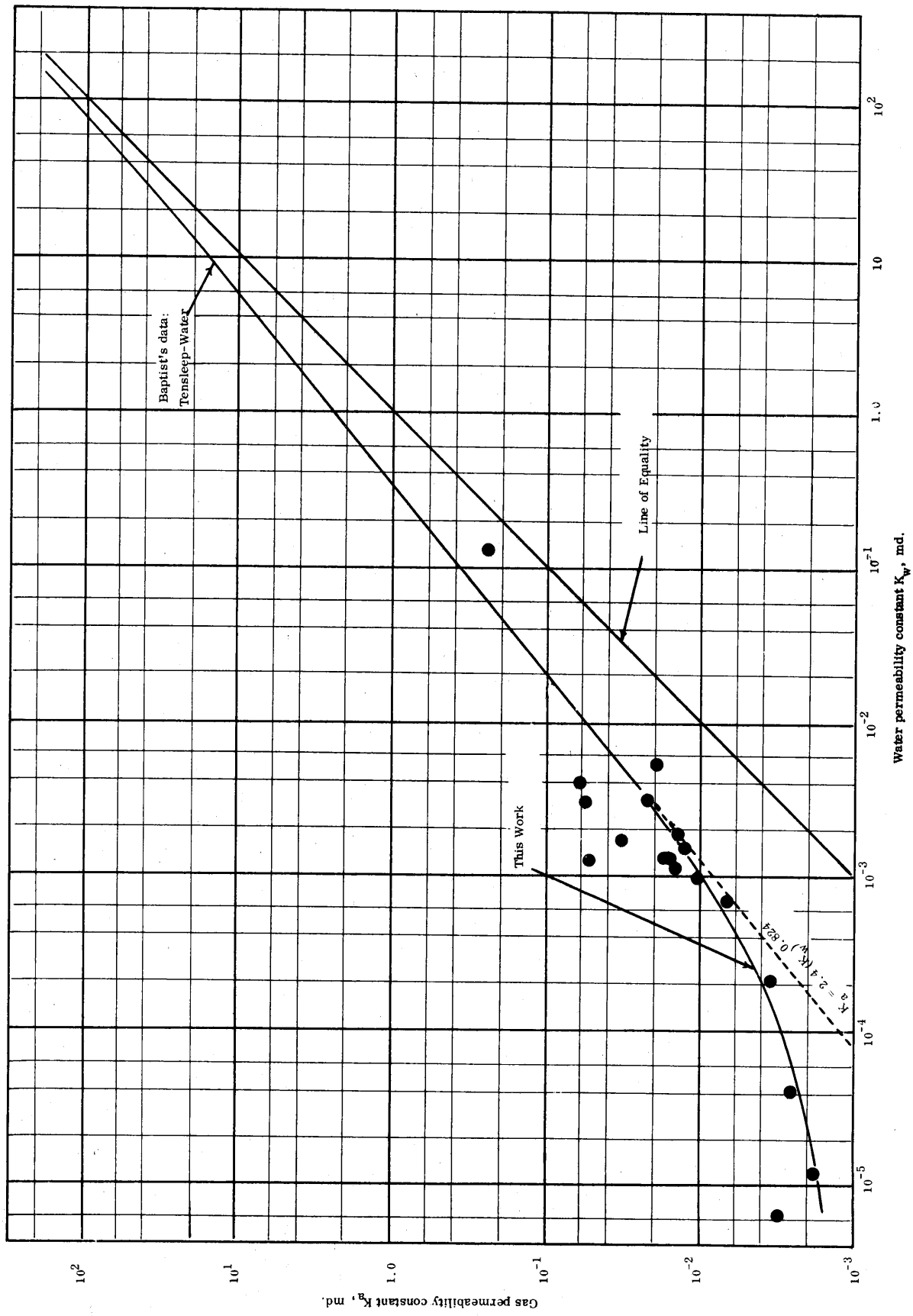

Figure 27. Relation of air permeability to water permeability for Virginia rocks.

Baptist has explained that the occurrence of this phenomenon in clay-rich rocks probably can be due to the following properties of clay minerals.

(1) Type of clay mineral.
(2) Amount of clay-size material.
(3) Type of exchangeable ions held by the clays.
(4) Ions in the water.
(5) Total salinity of the water and the absolute permeability.

While the effects of clay and other mineral constituents have not been investigated here, it appears that the following relationship may be valid when the line is drawn to Baptist's line for Tensleep materials:

$$K_a = 2.4\ (K_w)^{0.824}$$

Conclusions

The conclusions resulting from this portion of the study are as follows:

(1) The techniques developed here for measuring gas and water permeabilities are satisfactory for fine-grained mineral aggregates. Gas flow rates down to 10^{-5} cc/sec and water flow rates down to 10^{-7} cc/sec were successfully measured with good reproducibility.

(2) The permeability of rock to gas is a function of porosity and pore size as suggested by the Kozeny-Carman relation. However, some modification of this relation is necessary to develop more accurate relationships in rock samples.

(3) The permeability of rock to gas ranges from about 0.05×10^{-4} to 282×10^{-4}md for carbonate rocks, 0.08×10^{-4} to 3720×10^{-4} md for igneous and metamorphic rocks and 3.20×10^{-4} to 3200×10^{-4} md for sandstone rocks.

(4) Gas permeability appears to be related to rock texture. In the cases of sandstone and limestones, as grain size decreases permeability decreases. This relationship is less evident in the igneous and metamorphic rocks studied.

(5) Gas flow measurements perpendicular, parallel, and random to the bedding or foliation were carried out. In general the permeability increased from perpendicular to random to parallel. However, the differences were considerably smaller than expected and probably reflect the massive, homogeneous, highly lithified nature of the common Virginia rock types.

(6) Gas permeability is considerably higher than water permeability. The difference between K_a and K_w decreases when the permeability increases. For Virginia rocks the relationship can be expressed approximately as $K_a = 2.4\ (K_w)^{0.824}$ if a straight line can be drawn following Baptist's line.

(7) Water flow measurement in porous media is a more complicated problem than gas flow, due to the movement of the water phase and vapor phase together by diffusion, sorption, and ion exchange. Detailed studies of this phenomenon in the future could prove fruitful in understanding the destructive mechanisms of water movement and pressures during freeze-thaw cycles.

PART 3

SOME FUNDAMENTAL RELATIONSHIPS BETWEEN POROSITY AND PERMEABILITY

Background

The purpose of this portion of the project was to further the understanding of the fundamental relationships between porosity and permeability in porous aggregates. A mathematical model is offered which will allow prediction of the mean pore radius and effective pore area by gas permeability measurements. The mean pore radius thus determined is compared to that obtained by mercury porosimetry. This model, of necessity, utilizes gas transfer because the kinetic theory of gases is further advanced and mathematically more workable than the comparable theory of liquids.

NOTATION

a = capillary radius, cm;
$\bar{a}$ = mean pore radius, cm;
A = cross-sectional area, cm^2;
C = coefficient defined by Eq. 3 , cm^2/sec;
D = pore diameter, cm;
D_{AA} = molecular diffusivity = $\bar{v}\ \lambda/3$, cm^2/sec;
D_{KA} = Knudsen diffusivity = $\bar{v}a/3$, cm^2/sec;
f = effective area fraction;
K = permeability, cm^2;
L = length, cm;
M = molecular weight, g/g-mole;
N = fluid flow rate in moles per unit time, g-mole/sec;
p = pressure, $dyne/cm^2$;
Δp = pressure difference $p_1 - p_2$, $dyne/cm^2$;
Q = fluid flow rate in volumes per unit time, cm^3/sec;
R = gas constant, (dyne) (cm)/(g-mole) (deg K);
S = surface area per unit mass of sample, cm^2/g;
T = temperature, deg K;
$\bar{v}$ = mean molecular velocity, cm/sec;
V = pore volume per unit mass of sample, cm^3/g;
x = distance variable, cm;
λ = mean free path, cm;
μ = viscosity, g/cm/sec;
ϵ = void fraction; and
τ = tortuosity.

Wakao et al. (1965) have developed a theoretical equation for gas flow through capillaries where diffusion, slip flow, and Poiseuille flow are taken into account. This equation has been proved experimentally to hold for flow through small capillaries. In this section, this flow equation is applied to porous mineral aggregates, and the manner whereby the mean pore radius and the effective pore area for flow are calculated from permeability experiments is described. Considerable difference in permeability due to the flow direction suggests inhomogeniety of pores in many rocks. The mean pore radii obtained from permeability experiments are compared with those estimated from pore size distribution curves for typical samples.

Theoretical Developments

The flow rate of a gas through a capillary of radius "a" in centimeters is expressed in moles per sec (Wakao et al. 1965) as

$$N = (\pi a^2)\left(\frac{C}{RT}\right)\frac{dp}{dx} \tag{3-1}$$

where C is the coefficient of permeability
R is the gas constant, dyne-cm/g-mole (deg K),
T is temperature in deg K, and
$\frac{dp}{dx}$ is the pressure gradient in dyne/cm^3.

also

$$C = D_{KA}\frac{1+\left(\frac{\pi}{4}\right)\left(\frac{2a}{\lambda}\right)}{1+\left(\frac{2a}{\lambda}\right)} + \frac{\frac{a^2 p}{8\mu}}{1+\left(\frac{\lambda}{2a}\right)} \tag{3-2}$$

where λ represents the mean free path in cm and μ is the viscosity in g/cm/sec (Wakao et al. 1965) D_{ka} is the Knudsen diffusivity in cm^2/sec:

$$D_{KA} = \frac{2\bar{v}a}{3} \tag{3-3}$$

Equation 3-2 shows that C reduces to $a^2p/8\mu$ (the Poiseuille flow) as the capillary radius becomes large, and that the first term (diffusion and slip flow) tends to be dominant as the capillary radius and/or the pressure decreases.

For flow through porous media, Equation 3-1 is modified as follows:

$$N = -f\left(\frac{AC}{RT}\right)\frac{dp}{dx} \tag{3-4}$$

where f represents the area fraction effective for fluid flow. A comparison of Equations 2-1 and 3-4 indicates that

$$K = \frac{C\mu}{p}f \tag{3-5}$$

According to the kinetic theory of gases the viscosity, μ, is independent of pressure and the mean free path is inversely proportional to the pressure, thus

$$\lambda p = \lambda_o p_o \tag{3-6}$$

where λ_o is the mean free path at the reference pressure p_o. In subsequent treatment, the reference pressure is taken as one atmosphere.

When mean pore radius, $\bar{a}$, is substituted for a in Equation 3-2 and Equation 3-2 is substituted into Equation 3-4, integration between p_1 at x = 0 and p_2 at x = L yields

$$\frac{NRT}{p_o} = \frac{fA}{L}\left\{\left[\frac{\left(1-\frac{\pi}{4}\right)\bar{D}_{KA}}{\frac{2\bar{a}}{\lambda_o}} + \frac{\bar{a}^2 p_o}{8\mu\left(\frac{2\bar{a}}{\lambda_o}\right)^2}\right] \ln\left[\frac{1+\left(\frac{2\bar{a}}{\lambda_o}\right)\left(\frac{p_1}{p_o}\right)}{1+\left(\frac{2\bar{a}}{\lambda_o}\right)\left(\frac{p_2}{p_o}\right)}\right]\right.$$

$$\left. + \left\{\frac{\pi\,\bar{D}_{KA}}{4p_o} + \frac{\bar{a}^2\left[\left(\frac{2\bar{a}}{\lambda_o}\right)\left(\frac{\bar{p}}{p_o}\right)-1\right]}{8\mu\left(\frac{2\bar{a}}{\lambda_o}\right)}\right\}\Delta p\right\} \qquad (3\text{-}7)$$

Gas kinetics indicate that Knudsen diffusivity is expressed as

$$\bar{D}_{KA} = \frac{2\bar{v}\bar{a}}{3}$$

and the viscosity, μ, as

$$\mu = \frac{pM\bar{v}}{2RT}\lambda \qquad (3\text{-}8)$$

where M is the molecular weight, g/g-mole, and the mean molecular velocity, $\bar{v}$, is

$$\bar{v} = \sqrt{\frac{8RT}{\pi M}} \qquad (3\text{-}9)$$

Using Equations 3-8 and 3-9, Equation 3-7 is rewritten as

$$Q_o = \frac{NRT}{p_o} = \frac{fA}{L}\left\{0.2882\, D_{AA_o} \ln\left[\frac{1+\left(\frac{2\bar{a}}{\lambda_o}\right)\left(\frac{p_1}{p_o}\right)}{1+\left(\frac{2\bar{a}}{\lambda_o}\right)\left(\frac{p_2}{p_o}\right)}\right]\right. \qquad (3\text{-}10)$$

$$\left. + \bar{D}_{KA}\left[0.7118 + \left(0.0736\right)\left(\frac{2\bar{a}}{\lambda_o}\right)\left(\frac{p_2}{p_o}\right)\right]\frac{\Delta p}{p_o} + \bar{D}_{KA}\left(0.0368\right)\left(\frac{2\bar{a}}{\lambda_o}\right)\left(\frac{\Delta p}{p_o}\right)^2\right\}$$

where Q_o is the volumetric flow rate at the reference pressure, p_o, and D_{AA_o} is the molecular diffusivity at the reference pressure

$$D_{AA_o} = \frac{\bar{v}\lambda_o}{3} \tag{3-11}$$

It is obvious that, in most cases, the first term is negligible compared with the last two terms. With this approximation, Equation 3-10 is simplified as

$$\frac{Q_o L}{A\left(\frac{\Delta p}{p_o}\right)} = \alpha + \beta\left(\frac{\Delta p}{p_o}\right) \tag{3-12}$$

where

$$\alpha = f\bar{D}_{KA}\left[0.7118 + \left(0.0736\right)\left(\frac{2\bar{a}}{\lambda_o}\right)\left(\frac{p_2}{p_o}\right)\right]$$

$$\beta = f\bar{D}_{KA}\,(0.0368)\left(\frac{2\bar{a}}{\lambda_o}\right) \tag{3-13}$$

When the flow rates are plotted as $Q_o\ L/A\ (\Delta p/p_o)$ vs $(\Delta p/p_o)$, straight lines will result. The ratio of the intercept, α , to the slope, β , enables the calculation of the mean pore radius, $\bar{a}$, as

$$\frac{\alpha}{\beta} = 2\left(\frac{p_2}{p_o}\right) + \frac{0.7118}{0.0368\left(\frac{2\bar{a}}{\lambda_o}\right)} \tag{3-14}$$

Thus, from the values of both $\bar{a}$ and either α or β the effective area, f, is determined.

Experimental Testing

The apparatus used for permeability measurements in this work was diagrammed and explained in Part 2. Six rock samples from the Piedmont and Valley and Ridge physiographic provinces of Virginia were utilized in testing the theoretical portions of this study. Five of these rocks were taken from quarry sources which pass ASTM specifications for concrete coarse aggregates. The remaining rock, represented by

sample 6, is a slightly friable sandstone not normally used as coarse aggregate. Of the five quarried aggregates, rock 22-2 is a fine- to medium-grained dolomite; rock P-1 is a granite gneiss, or more correctly a quartz monzonite gneiss consisting of orthoclase, quartz, oligoclase and biotite; rock 26-5 is a medium-grained dense dolomite; rock H-1 is a coarse-grained, high-calcium limestone; and rock 13-1 is a fine-grained dolomite that contains 26 percent acid insoluble or non-carbonate minerals. Selected physical properties of these rocks are given in Table 9.

Table 9

Properties of Rock Samples

Sample Designation	Bulk Density (g/cm^3)	Void Fraction	Rock Type
22-2	2.80	0.00635	Dolomite
P-1	2.79	0.0187	Granite Gneiss
6	2.59	0.0539	Sandstone
26-5	2.83	0.00325	Dolomite
H-1	2.69	0.00731	Limestone
13-1	2.67	0.0259	Impure Dolomite

Data Treatment

Mean Pore Radii Measurement by Permeability

Substituting $p_2 = p_o = 1$ atmosphere and, $\lambda_o = 0.0657 \times 10^{-4}$ cm, the mean free path of nitrogen at 24° C and 1 atmosphere, Equations 3-13 and 3-14 reduce to

$$\beta = 3.54 \times 10^8 f \bar{a}^2 \tag{3-15}$$

and

$$\frac{\alpha}{\beta} = 2 + \frac{0.635 \times 10^{-4}}{\bar{a}} \tag{3-16}$$

where $\bar{a}$ is the mean pore radius in cm. In deriving Equation 3-7, it was assumed that the viscosity of fluid is constant and independent of pressure as predicted from the kinetic theory of gases. Actually the viscosity increases slightly with an increase of pressure; however, the assumption of a constant viscosity is valid for pressures up to about ten atmospheres. Figures 28-33 are plots of experimental data of Q_o L/A ($\Delta p/p_o$) vs $\Delta p/p_o$. From the intercept and the slope, the mean pore radii and the effective areas for flow were calculated from Equations 3-15 and 3-16 and listed in Table 10. The calculated values for $\bar{a}$ are used for a check of the first term of Equation 3-10, and it is found that the first term is at most one percent of the last two terms. This fact provides the justification for simplifying Equation 3-10 to 3-12.

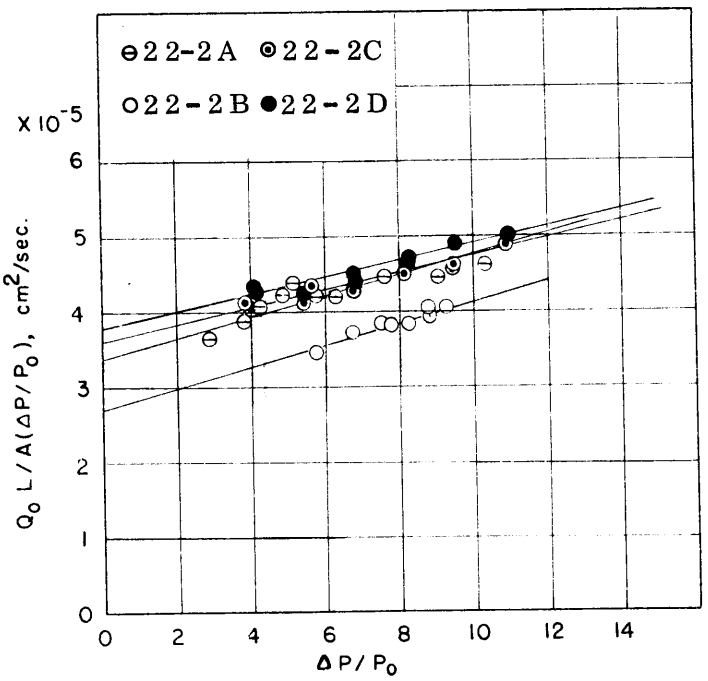

Figure 28. Permeability of sample 22-2, dolomite.

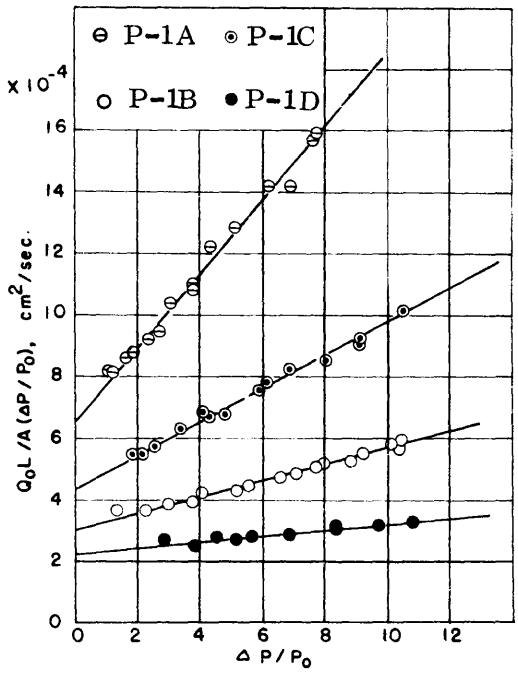

Figure 29. Permeability of sample P-1, granite gneiss.

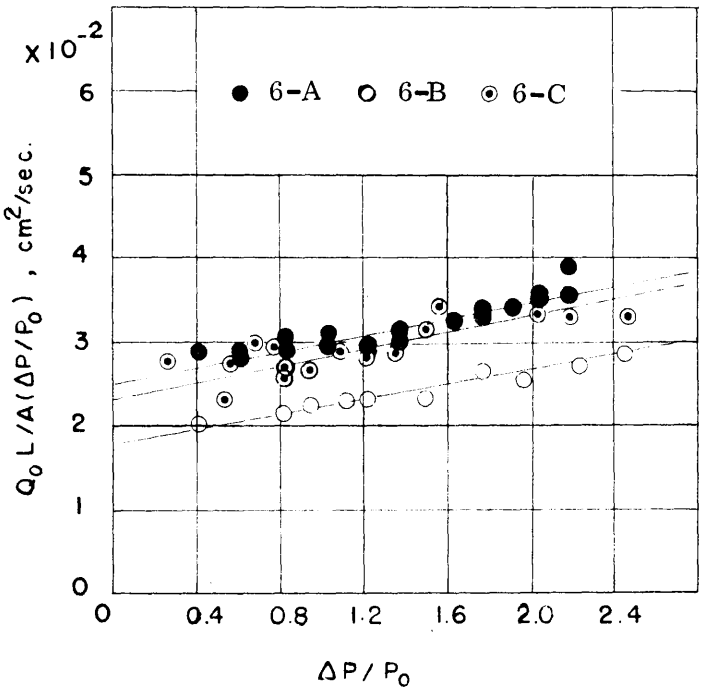

Figure 30. Permeability of sample 6, sandstone.

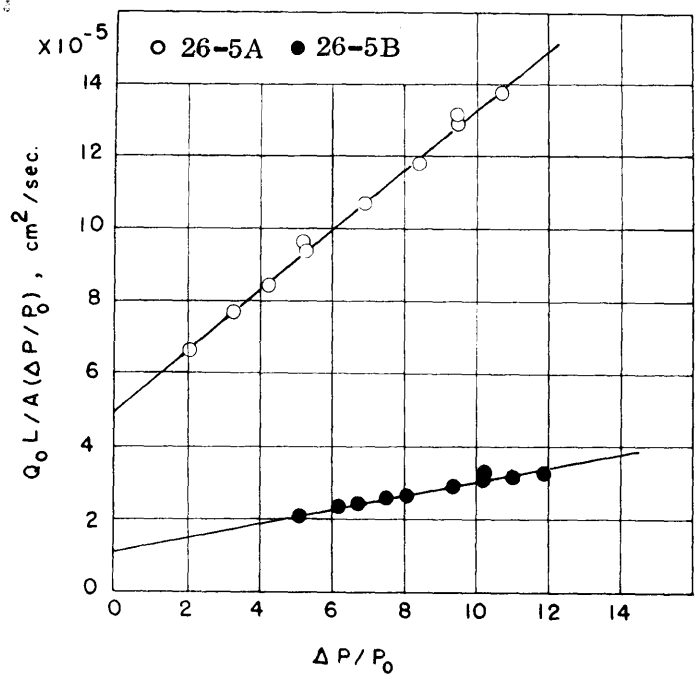

Figure 31. Permeability of sample 26-5, dolomite.

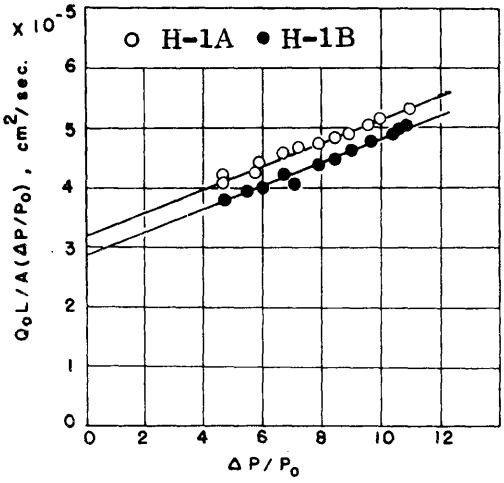

Figure 32. Permeability of sample H-1, limestone.

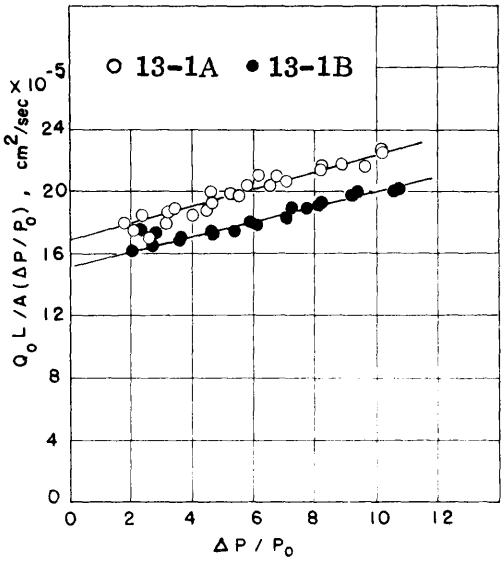

Figure 33. Permeability of sample 13-1, impure dolomite.

Table 10

Calculated Data for $\bar{a}$ and f

Sample No.	Permeability Experiments				Pore Size Distribution Curves	
	α (cm^2/sec)	β (cm^2/sec)	$\bar{a}$ (micron)	f (-)	$\bar{a}$ (micron)	V_t (cm^3 g)
22-2A	3.30×10^{-5}	0.145×10^{-5}	0.0306	4.35×10^{-4}	0.0279	0.00227
22-2B	2.65×10^{-5}	0.141×10^{-5}	0.0378	2.78×10^{-4}		
22-2C	3.60×10^{-5}	0.115×10^{-5}	0.0217	6.89×10^{-4}		
22-2D	3.77×10^{-5}	0.113×10^{-5}	0.0202	7.74×10^{-4}		
P-1A	6.50×10^{-4}	1.21×10^{-4}	0.188	9.68×10^{-4}	0.108	0.0067
P-1B	3.00×10^{-4}	0.27×10^{-4}	0.0698	15.7×10^{-4}		
P-1C	4.30×10^{-4}	0.55×10^{-4}	0.109	13.0×10^{-4}		
P-1D	2.2×10^{-4}	0.1×10^{-4}	0.0318	28.0×10^{-4}		
6A	2.50×10^{-2}	0.50×10^{-2}	0.254	2.19×10^{-2}	0.86	0.0208
6B	1.80×10^{-2}	0.425×10^{-2}	0.284	1.5×10^{-2}		
6C	2.35×10^{-2}	0.50×10^{-2}	0.235	2.56×10^{-2}		
26-6A	4.90×10^{-5}	0.84×10^{-5}	0.166	0.863×10^{-4}	0.0233	0.00115
26-5B	1.1×10^{-5}	0.197×10^{-5}	0.177	1.78×10^{-4}		
H-1A	3.17×10^{-5}	0.198×10^{-5}	0.0454	2.72×10^{-4}	0.044	0.00272
H-1B	2.85×10^{-5}	0.197×10^{-5}	0.0512	2.14×10^{-4}		
13-1A	16.8×10^{-5}	0.56×10^{-5}	0.0227	30.8×10^{-4}	0.0151	0.0097
13-1B	15.2×10^{-5}	0.53×10^{-5}	0.0238	26.4×10^{-4}		

Viscosity of nitrogen at 24 C, $\mu = 1.79 \times 10^{-4}$ poise.
Mean molecular velocity $\bar{v}$ calculated from Eq. 10 as $\bar{v} = 4.74 \times 10^4$ cm/sec.
Mean free path at 1 atm calculated from Eq. 9 as $\lambda = 657$ Å $= 0.0657$ micron.

Samples P-1-A and P-1-D are identical rock pieces, except for orientation, cut from the same hand sample. Considerable difference in the mean pore radii and the effective area fraction may be due to inhomogeniety of pore orientation in many rock types.

Mean Pore Radii Measurements by Pore Size Distribution

The cumulative pore volume-pore size curves were obtained by mercury porosimetry. The penetration was limited to pores of equivalent circular diameters larger than 0.01 micron. The pore size distribution curves were produced by differentiation of the cumulative pore volume curves and are shown in Figures 34 and 35.

Equation 3-1 is for the flow rate through a single capillary, so that the total flow rate area of porous solid is

$$N = \frac{-A}{RT} \frac{dp}{dx} \int_{a_1}^{a_2} n(a) \pi a^2 C \, da \qquad (3\text{-}17)$$

where n (a) da represents the number of pores with a radius between a and a + da, and a_1 and a_2 are the lower and upper limits of the pores, respectively. As shown in Equation 3-2, C is a function of a. However, it is assumed that C is expressed approximately as a linear function of a for the pore range between a_1 and a_2. Therefore C can be expressed as

$$C = m + m'a \tag{3-18}$$

where m and m' are constants. Consequently, the total flow rate, N, is

$$N = -\frac{A}{RT}\frac{dp}{dx}\int_{a_1}^{a_2} n(a)\,\pi a^2 (m + m'a)\,da \tag{3-19}$$

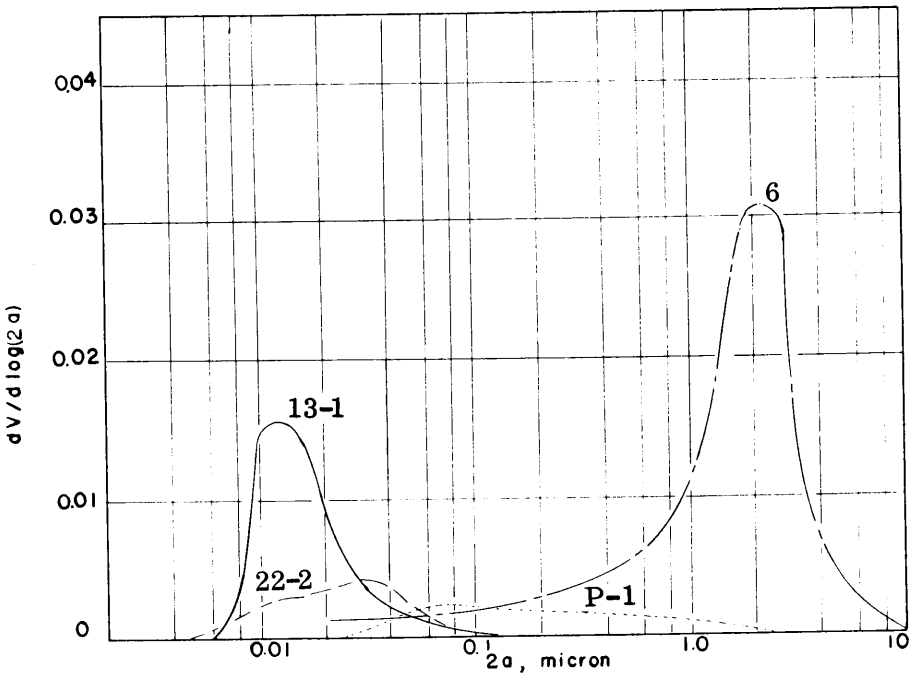

Figure 34. Pore size distribution of samples 22-2, P-1, 6, and 13-1.

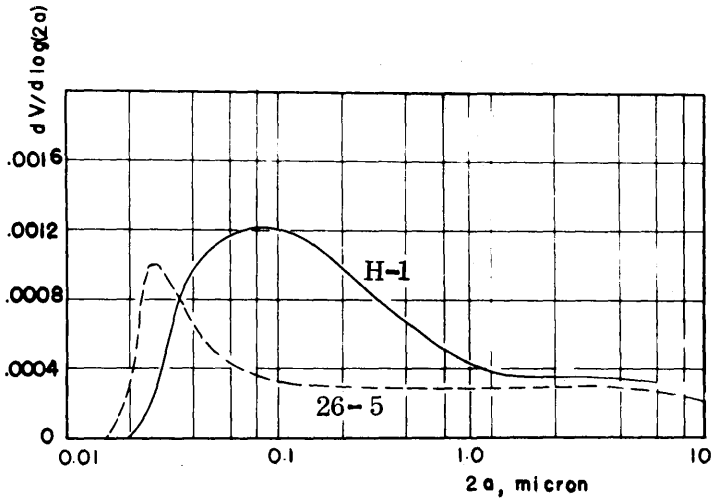

Figure 35. Pore size distribution of samples 26-5 and H-1.

On the other hand, in terms of the mean pore radius the total flow rate is expressed as

$$N = -\frac{A}{RT}\frac{dp}{dx}\overline{C}\int_{a_1}^{a_2} n(a)\,\pi\,a^2 da = -\frac{A}{RT}\frac{dp}{dx}(m + m'a)\int_{a_1}^{a_2} n(a)\,\pi\,a^2\,da \qquad (3\text{-}20)$$

Combining Equations 3-19 and 3-20, the mean pore radius is

$$\bar{a} = \frac{\int_{a_1}^{a_2} n(a)\,\pi\,a^3\,da}{\int_{a_1}^{a_2} n(a)\,\pi\,a^2\,da} \qquad (3\text{-}21)$$

The quantity $n(a)\ \pi a^2\,da$ is the void fraction of pores between a and a + da, per unit area of porous solid. This area void fraction is considered to be equal to the volume void fraction (pore volume per unit volume of porous solid). Hence, Equation 3-21 can be written in terms of the known pore volume-pore size distribution as

$$\bar{a} = \frac{\int_0^{V_t} a\,dV}{V_t} \qquad (3\text{-}22)$$

where dV is the volume of the pores between a and a + da, per unit mass of solid, and V_t the total of pores. The calculated values for $\bar{a}$ are shown in Table 10.

Results and Discussion

Surface areas were also measured for some samples using a BET apparatus (adsorption of argon at liquid nitrogen temperature). With this technique the procedure for calculating the mean pore radius, assuming cylindrical pores, is

$$\bar{a} = \frac{2V_t}{S_t} \tag{3-23}$$

where S_t is the total surface area per unit mass of solid as evaluated in the BET apparatus. However, the gas adsorption takes into account even very small irregularities in the pore wall, so that the BET method will give very large values for S_t. For instance, in sample A, the total pore volume $V_t = 0.00227$ cm^3/g and the total surface area by the BET method is $S_t = 1.76$ m^2/g. From this the mean pore radius is calculated as 0.0025 micron by Equation 3-23. This is smaller by about a factor of ten than the mean radius calculated by Equation 3-22.

Considering the dependency of the mean pore radius on the direction of flow, the agreement of the experimentally obtained mean pore radii and those calculated by Equation 3-22 using pore volume-pore size distribution curves is thought to be good for rocks with relatively small pores. Rocks having relatively large pores, such as sample 6 (Figure 30), do not appear to be as well suited for this treatment.

A comparison of $\bar{a}$ as determined by permeability experiments and $\bar{a}$ as determined by mercury porosimetry yields the following observations:

(1) The $\bar{a}$ determined by permeability is dependent on sample orientation while the $\bar{a}$ determined by mercury porosimetry represents a gross sample average;

(2) the spread of values for $\bar{a}$ for a single rock is not great compared to between-sample variation; and

(3) in general, the values of $\bar{a}$ determined by the two methods, while not uniformly excellent, might be considered good in most instances were pore sizes are small.

Table 10 shows the results of α and β calculated for each rock along with the effective pore areas determined by permeability measurements and the pore volumes (V_t) from mercury porosimetry measurements.

One final point of discussion involves the Kozeny type equation and Equation 3-2 of this work. The Kozeny equation is usually expressed in terms of the pore radius as

$$N = \frac{-A}{RT} \frac{a^2 p}{8\mu} \frac{\epsilon}{\tau} \frac{dp}{dx} \tag{3-24}$$

where ϵ is the void fraction and τ the tortuosity. The differences between the approach taken in this work and that by Kozeny are as follows:

This Study	Kozeny
(1) C = Eq.	$C = \frac{a^2 p}{8\mu}$ As discussed in a previous section, Kozeny's C holds for large pores but not for very small pores. The Kozeny equation was developed for packed beds where the extraparticle space is so large that this expression for C is valid.
(2) f is called the effective area fraction but the concept is the same as Kozeny's $f = \epsilon/\tau$.	$f = \epsilon/\tau = \epsilon/2.5$ The Kozeny-Carman equation recommends the tortuosity as $\tau = 2.5$ for packed beds (which is the ratio of flow path length to sample length).

Concerning f in this work, the correlation with, or direct relationship to, the void fraction, ϵ, has purposely been omitted. Actually, this was found inappropriate because of the inhomogeneous pore orientation. Wakao and Smith (1962) state that $f = \epsilon^2$ for homogeneous porous media.

Equation 3-2 is arrived at on a purely theoretical basis so no assumptions are necessary. It is valid for the flow of gas through a circular capillary. In applying this equation to the flow through porous media the only assumption inherent is that the pores are circular. The roughness and shape of the pores (i.e., deviation from circular capillaries) undoubtedly have some effect on the Poiseuille flow term, so the following equation would probably be more accurate:

$$C = \bar{D}_{KA} \frac{1 + \left(\frac{\pi}{4}\right)\left(\frac{2\bar{a}}{\lambda}\right)}{1 + \left(\frac{2\bar{a}}{\lambda}\right)} + \frac{w \frac{\bar{a}^2 p}{8\mu}}{1 + \left(\frac{\lambda}{2\bar{a}}\right)} \tag{3-25}$$

where w is dependent on the degree of deviation from circularity. This quantity, w, is under study but has not been accurately evaluated. Consequently, the assumption is made in this report that the pores are approximately circular, and it should be pointed out that mercury porosimetry is also based on this assumption.

Conclusions

While a great deal is known concerning the properties of permeability and porosity as separate parameters, the fundamental relationships between the two are not so well understood. The prediction of mean pore radii by treatment of gas permeability data has been attempted. This involved development of a mathematical model based on the kinetic theory of gases. The resulting equations were tested using six different mineral aggregates and comparing the results against those obtained by mercury porosimetry and BET methods. The following conclusions have resulted from the study.

(1) The pore structure in several types of mineral aggregates is inhomogeneous, varying with orientation.

(2) The mean pore radii determined by the BET method were found to be smaller than those determined on the same samples by mercury porosimetry. This finding is interpreted to be caused by the highly irregular nature of the pore walls yielding large surface area measurements by BET.

(3) In the case of mineral aggregates containing small pores, the mean pore radii obtained by treatment of permeability data in accordance with the model developed in this work compare favorably with radii obtained by mercury porosimetry.

Although the agreement of the results as stated in conclusion three is promising, the directional inhomogeneities inherent in most mineral aggregates present complications which future studies involving aggregate permeability must consider.

PART 4

CORRELATION BETWEEN POROSITY AS MEASURED BY MERCURY POROSIMETRY AND BY WATER ABSORPTION

Background

In attempts to relate the role of water absorption of included aggregates to concrete durability, the 24-hour water soak test has gained widespread acceptance. This is largely due to the simplicity and inexpensiveness of the procedure, and to the short time required for testing. However, the 24-hour water soak test has not, in many cases, correlated well with field performance data (Sweet 1948; Wray and Lichtefeld 1940).

Additional research has been performed by allowing the aggregate to soak in water until it has become saturated. Absorption to saturation has produced fair to good correlations with concrete durability (Buth and Ledbetter 1968; Walker and Hsieh 1968; Sweet 1948). However, many rocks require long periods of soaking until saturation is complete, which makes the test procedure quite time consuming (Buth and Ledbetter 1968).

It has been pointed out in the literature that the pore structure and pore characteristics of a rock influence its water absorption characteristics (Lewis, Dolch, and Woods 1953; Verbeck and Landgren 1960; Dolch 1966). With the advent of the mercury porosimeter, it has become possible to measure the porosity and pore size distribution of rocks in a relatively short time. Using mercury porosimetry it was hoped that a good correlation would be found between the porosity or pore size distribution and the long-term water absorption characteristics of the rock. In this way, the porosity or pore size distribution, as measured by the relatively quick mercury porosimetry method, could be used in place of the long-term water absorption method in predicting concrete durability.

Purpose and Scope

The primary purpose of this portion of the project was to investigate the degree of correlation between porosity as measured by mercury porosimetry and porosity as measured by long-term water absorption, for selected clastic (sandstones and siltstones) and carbonate (limestones and dolomites) rocks from Virginia. Following extensive preliminary testing, 13 rocks were selected and large slabs prepared for detailed studies. From each of these 13 slabs, several samples were taken at regularly spaced intervals for mercury porosimeter analysis. Between these samples, other samples were taken for long-term water absorption

analysis. Correlation statistics were used to investigate possible significant relationships between porosity as measured by mercury porosimetry and porosity as measured by water absorption. This statistical investigation proceeded on 4 levels; (1) for the samples taken from each slab, (2) for the clastic group, (3) for the carbonate group, and (4) for all slabs.

Several additional parameters were included to see if these could be used to improve the initial correlations observed between mercury porosimetry measurements and water absorption. These parameters included the pore size distribution as determined by mercury injection, the rate of water absorption, and the grain size as determined with the petrographic microscope.

Theory

Mercury Porosimetry Theory

A description of the Aminco mercury porosimeter, as well as the theory involved in the mercury injection technique, has already been discussed in Part 1 of this report.

Water Absorption Theory

The absorption of water by a rock takes place because the molecular attraction between the rock and water is greater than the internal molecular attraction or surface tension of the water. The water consequently wets the rock and is drawn into the pores. The water moves through a pore because of the attraction of the water molecules for the rock molecules inside the pore. The capacity of a pore to draw a liquid through the pore is called capillary potential. Absorption ceases when the energy required to move the water through the pore is greater than the capillary potential of the pore. The capillary potential tends to increase as the pore diameter decreases. Therefore, the smaller pores in a rock tend to absorb water before the larger pores do and also reach a higher degree of saturation than the larger pores (Rhoades and Mielenz 1946; Verbeck and Landgren 1960).

Experimental Procedure

The preliminary rock selection was designed to allow observation of the water absorption characteristics for a large group of representative rock types occurring in Virginia. In this way, the final rock selection could be made so that each rock exhibited a particular water absorption characteristic. In the preliminary selection, hand specimen samples were taken from 38 different lithologies at outcrops of known formations. Different formations were sampled in order to ensure variability in the rocks selected. The samples do not, however, necessarily represent the typical lithology of the formations in this study.

The samples, weighing roughly 50 grams each, were immersed in water for 150 hours, with the weight of water uptake noted at regular time intervals. This information yielded graphs of cumulative weight of water uptake versus time. From these curves, 13 rocks were selected for detailed studies on the basis of their distinctive water absorption characteristics.

Following this procedure, another trip was made to the 13 selected outcrops where specimens weighing about 70 pounds each were collected. A description of each of these 13 rocks is given in Table 11. The approximate location of each is shown in Figure 1. Each rock was taken from the same position as the original hand specimen. In the laboratory, each large piece was slabbed parallel to the bedding to a thickness of 2 1/4 inches, which resulted in a slab about 1 foot square. Rock cylinders 5/8 inch in diameter were drilled from each slab according to a grid pattern in which each cylinder was 1 1/2 inches away from the nearest other one. These rock cylinders were used for the water absorption part of this study. Between the cylinders, rock chips of approximately 2 grams were taken for mercury porosimeter analysis. A typical rock slab with the relative positions of cylinders and chips is shown in Figure 36.

Table 11

Description of Samples

Sample Designation	Description	Formation and Age
1-8	Fine-grained, Argillaceous, Calcitic Dolomite	Beekmantown, Ordovician
1-18	Dense, Medium-grained Dolomite	Beekmantown, Ordovician
13-1	Fine-grained, Argillaceous Dolomite	Newman Seam, Mississippian
Sta	Medium-grained, Limestone	Tonoloway, Silurian
Stb	Dense, Fine-grained Limestone	Tonoloway, Silurian
Oln	Dense, Fine-grained Limestone	Lincolnshire, Ordovician
6	Coarse-grained, Slightly Friable Sandstone	Erwin, Cambrian
49-1	Coarse-grained, Arkosic Sandstone	Wise, Pennsylvania
P-5 A	Dense, Fine-grained, Red Siltstone	Manassas, Triassic
P-5 B	Dense, Fine-grained, Black Siltstone	Manassas, Triassic
Mp	Medium-grained, Arkosic Sandstone	Pocono, Mississippian
Omb	Fine-grained, Ferruginous Sandstone	Martinsburg, Ordovician
Scl	Medium-grained, Ferruginous Sandstone	Clinton, Silurian

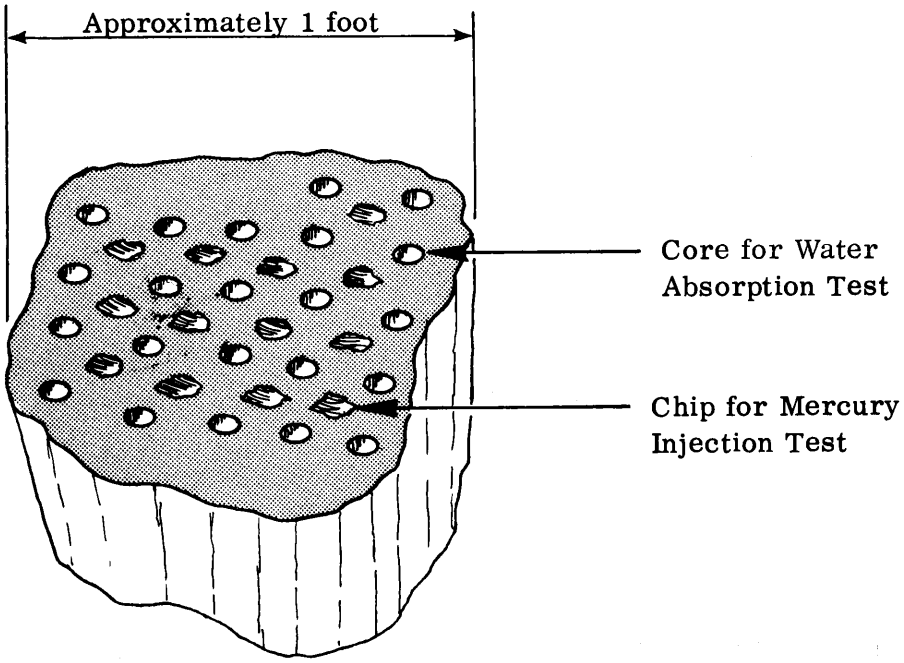

Figure 36. Diagram of a rock slab showing relative positions of rock cylinders and chips.

All of the rock cylinders were allowed to soak for 450 hours. At this point water absorption had ceased. A cumulative weight of water uptake versus time curve was plotted for each rock cylinder.

The mercury porosimeter was used to determine cumulative pore volume versus pore diameter for each rock chip. The mercury-derived cumulative pore volume data included pore diameters between .01 μ and 80 μ. An additional technique described in the Aminco porosimeter literature (1963) was used to determine the pore volume for pores greater than 80 μ in diameter. This technique determines the difference between the displacement volume of the rock sample, when immersed in mercury under a given vacuum, and the actual volume of the rock sample as determined by the Jolly balance method. This difference in volume is interpreted as pore volume for pores $>$ 80 u diameter. Based on this procedure, the carbonates did not yield measurable pore volumes for pores $>$ 80 u. The clastics, however, did have measurable pore volumes for this pore size range.

The mean grain size was determined by microscopic examination of thin sections. Using a petrographic microscope with a calibrated, graduated eyepiece, the average grain diameter for each rock slab was obtained by averaging approximately 40 representative grain cross sections from 2 thin sections.

Treatment of Data

Porosimetry Data

When the porosimetry analyses were completed a cumulative curve of pore size versus percent porosity (see Figure 37) was plotted for each rock slab. This curve was constructed by using the average volume of mercury injected into each chip at progressively higher preselected pressures.

These cumulative porosity curves show pore volume for pore diameters between .01 μ and 80 μ. Pressures greater than 13,000 psi, corresponding to diameters less than .01 μ, were not possible on the mercury porosimeter used. The pore volumes for pore diameters greater than 80 μ were not included in the cumulative porosity curves, but do appear in the computations of total porosity for each sample. Average pore size distribution curves derived by differentiation (plotting slope values) of the cumulative porosity curves (see Figure 38) were constructed for the rock slabs in order to better visualize the relative volume of each pore size.

The pore size distribution curves of many of the rocks were not easily interpreted due to the complexity of the peaked curves. Consequently, it was decided to use the ratio of pore volume of pores greater than 80 μ in diameter over pore volume of pores less than 80 μ in diameter and determine if any correlation existed between this ratio and the other measured parameters.

The total porosity for each rock chip was calculated by the equation

$$\epsilon = \frac{V_t}{V_B} \times 100$$

where ϵ is the porosity, in percent, V_t is the total pore volume of pores greater than .01 μ including those greater than 80 μ, and V_B is the bulk volume for each rock chip as measured by the Jolly balance.

Water Absorption Data

In soaking the rock cylinders the cumulative weight of water uptake in grams was assumed to be equivalent to the volume of water uptake in cm^3. This volume, divided by the bulk volume of the rock cylinder and multiplied by 100, was converted to water absorption porosity, in percent. Water absorption porosity versus time was plotted for each slab, based upon the average values for rock cylinders from that slab. Selected water absorption curves showing the range of rates and amounts of water uptake are shown in Figure 39.

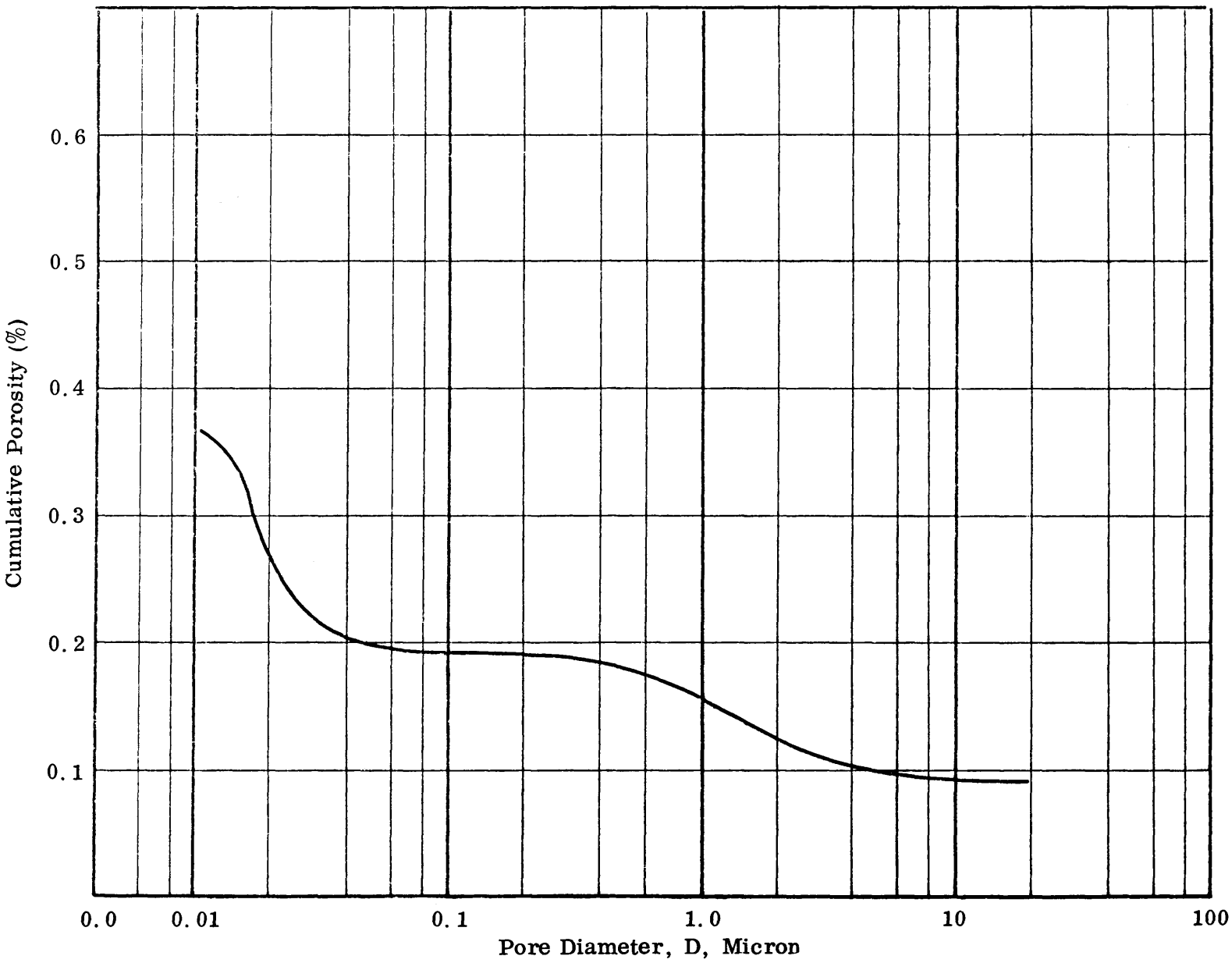

Figure 37. A cumulative porosity curve showing pore size vs. cumulative percent porosity.

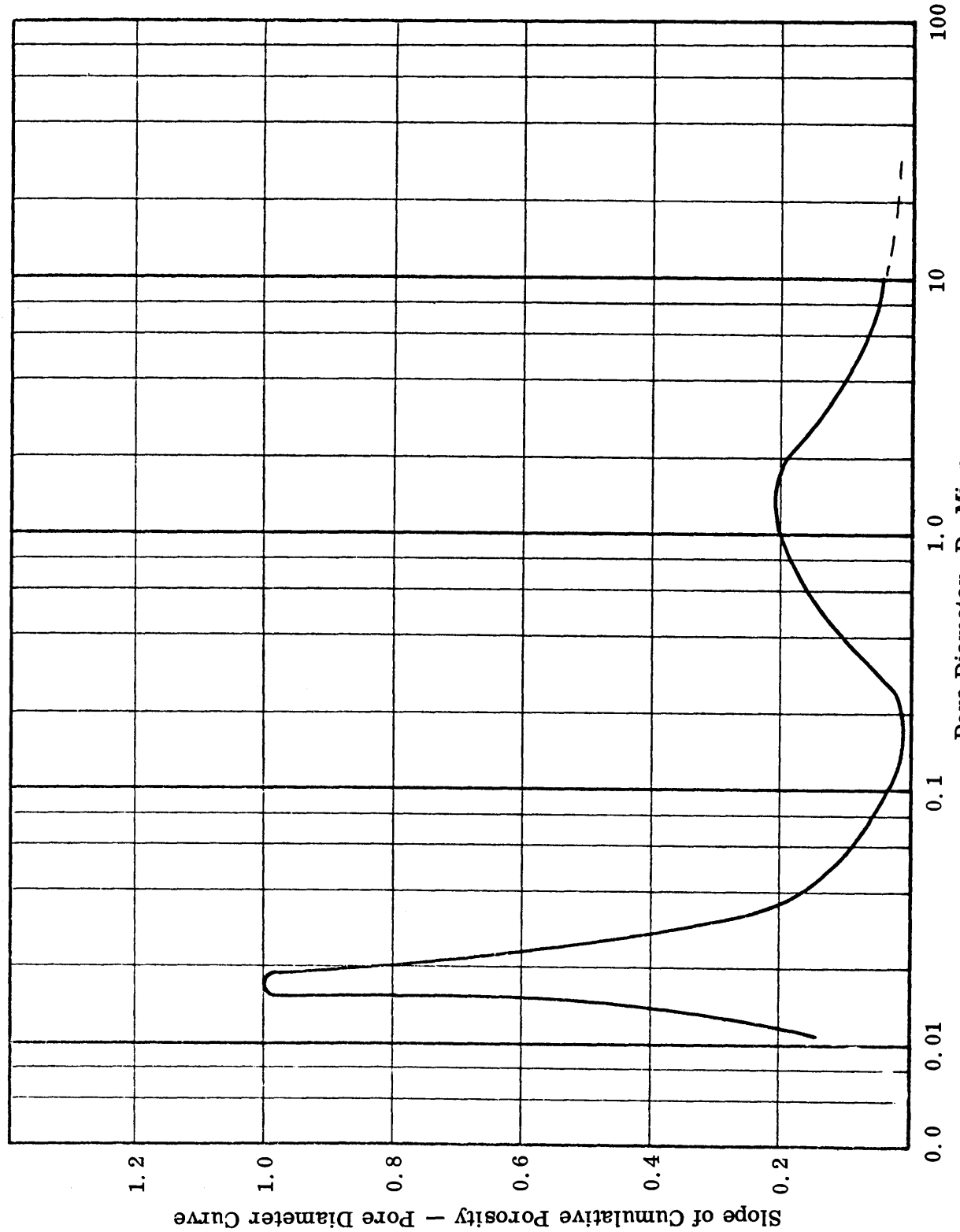

Figure 38. Pore size distribution curve constructed from the cumulative porosity curve shown in Figure 37.

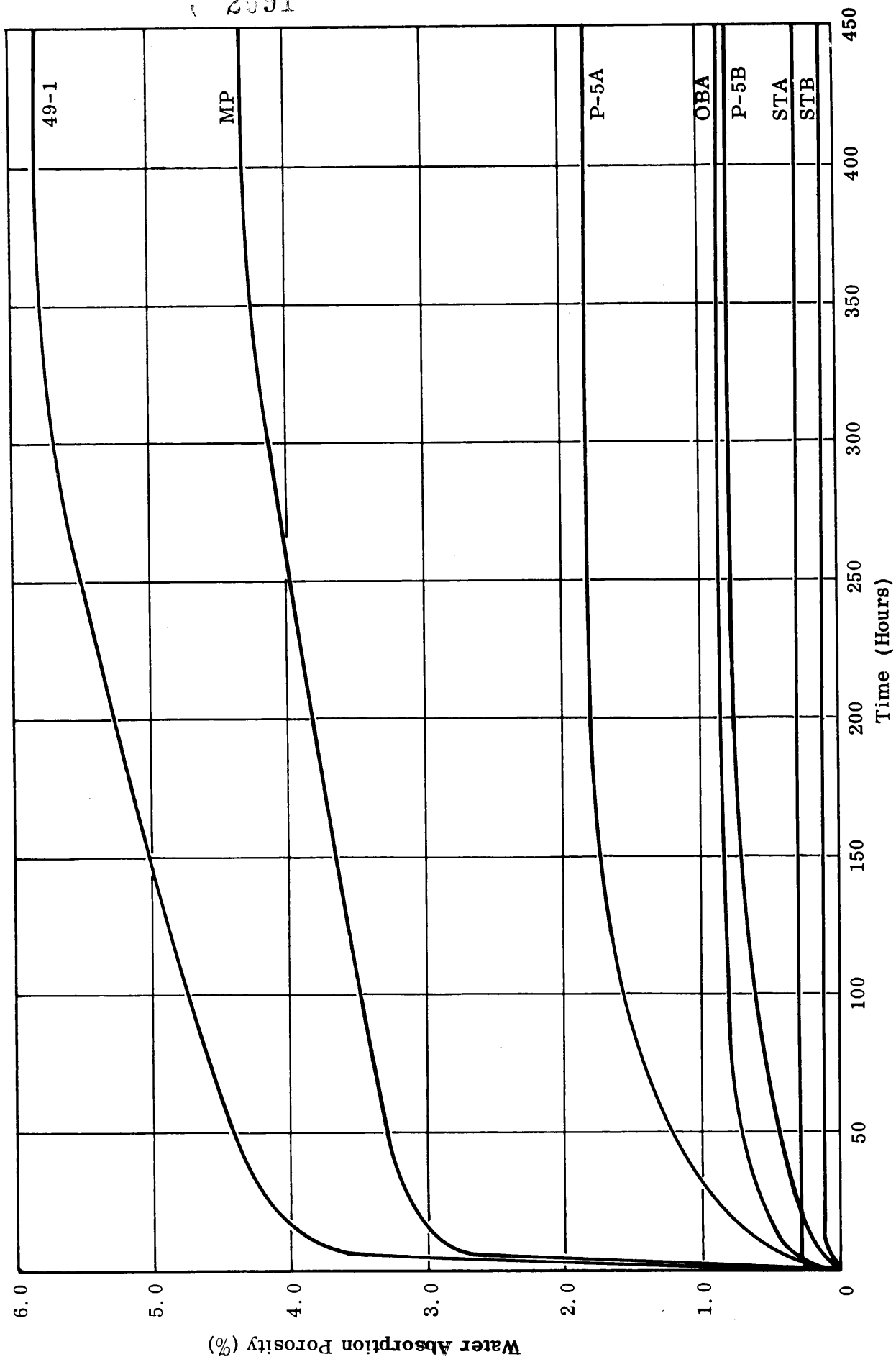

Figure 39. Selected water absorption curves.

The cumulative water absorption curve for each slab was also used to determine the rate of water absorption. The volume percent of water absorbed for the periods of 5 hours, 24 hours, 100 hours, and 200 hours was divided by the ultimate water absorption porosity and multiplied by 100. In this way, the percentage of the ultimate water absorption porosity of a slab at each of the preselected time periods was determined. The average of these four percentages gave a figure indicative of the rate of water absorption. As an example, a slab which picked up over 90 percent of its ultimate water absorption porosity in the first 3 hours of soaking would also have values over 90 percent for each of the four time periods of 5, 24, 100, and 200 hours. An average of these 4 values would also yield a value over 90 percent. On the other hand, a slab which picked up water slowly might have values of 30, 50, 70, and 90 percent for the time periods of 5, 24, 100, and 200 hours respectively. An average of these 4 values yields a rate of water absorption of 60 percent. An ordering of these values gives a simple ordering of the rate of water uptake for the individual slabs.

Correlation Tests

A correlation of porosity determined by mercury injection with porosity determined by water absorption was attempted in the following manner. The water absorption porosity for each rock cylinder was paired with the average of the mercury injection porosities for the rock chips immediately surrounding the cylinder. The number of rock chips surrounding a cylinder varied from two to four depending on where the rock cylinder was situated within the slab. Then a regression line and a correlation coefficient were computed for the following cases: (1) for samples from a single slab, (2) for samples from all slabs combined, (3) for all clastic rocks, and (4) for all carbonate rocks. A t-test was also employed in order to estimate the level of significance for each of the correlations made in this study. In addition, the percentage of the variation of the Y-axis measurements from their mean, which is explained by the calculated regression line, was calculated by squaring the correlation coefficient and multiplying by 100 (Croxton and Cowden 1963).

Further correlation tests involved the following parameters: (1) rate of water absorption, (2) pore size distribution, and (3) grain size. In these tests the average value for each parameter was used for each slab.

The statistical analysis for each correlation test included a calculated regression line and correlation coefficient, a t-test for the level of significance, and the percentage of the Y-axis variation explained by the regression line.

Because of the unusual water absorption characteristics of slab 13-1, it was omitted from the carbonate group in the correlation tests. It does appear on the graphs, however.

Results

Mercury Injection Porosity Versus Water Absorption Porosity

Table 12 shows the results of the regression analyses and correlation coefficient tests used to determine the correlation of the two parameters — porosity by mercury injection and porosity by water absorption. First and second degree regression lines were considered but the second degree curves yielded unreasonable trends, so they were omitted.

Figures 40 and 41 show selected graphs of mercury injection porosity versus water absorption porosity. Figures 40 and 41 show the highest degree of correlation found for a clastic rock and a carbonate rock respectively. The considerable scatter of points in these graphs illustrates well the low correlation coefficients listed in Table 12. The highest correlation coefficient, that for slab Mp in Figure 40, is only 0.4538. The percent of the variation of water absorption measurements explained by the regression line for Mp is only 20.6 percent, the best for any of the individual slabs.

For slabs 49-1 Oln, 1-8, Scl and P-5 B, the significance of the correlation coefficients is very low. In other words, the element of chance may well have entered into the determination of the position of the points on the graph for each slab. Even for Omb, Sta, 1-8, P-5 A, and 13-1, the element of chance may have been involved, since their significance intervals are not high. Only Mp, Stb, and 6 have high enough significance intervals to rule out chance.

Figure 42 shows the graph of mercury injection porosity versus water absorption porosity for all of the samples measured. This graph suggests only a fair correlation between the two methods of measuring porosity. Table 12 reveals that the correlation coefficient for all of the samples measured is 0.6763. The significance of the correlation coefficient is relatively high so it is reasonable to assume that chance was not involved in the distribution of points. Table 12 also shows that 45.74 percent of the variation of the water absorption porosity values from the mean is explained by the regression line.

Separate graphs of mercury injection porosity versus water absorption porosity for clastics and for carbonates are shown in Figures 43 and 44 respectively. As expected, the correlation coefficients are quite low for both groups. The significance interval for each group is very high, but the regression line of each group explains only a small percentage of the variation from the mean water absorption porosity.

Table 12

Statistical Data for Mercury Injection Porosity
versus Water Absorption Porosity

Individual Slab	Correlation Coefficient (R)	Variation % Explained by Regression Line	t_{OBS}	Significance
MP	0.4538	20.59	1.764	$t_{.90} < t_{OBS} < t_{.95}$
STB	0.4717	17.42	1.452	$t_{.90} < t_{OBS} < t_{.95}$
OMB	0.3347	11.20	1.230	$t_{.80} < t_{OBS} < t_{.90}$
6	0.3326	11.06	1.366	$t_{.90} < t_{OBS} < t_{.95}$
STA	0.3140	9.86	0.935	$t_{.80} < t_{OBS} < t_{.90}$
1-8	0.3056	9.34	0.963	$t_{.80} < t_{OBS} < t_{.90}$
P-5 A	0.2499	6.25	1.033	$t_{.80} < t_{OBS} < t_{.90}$
13-1	0.2018	4.07	0.714	$t_{.70} < t_{OBS} < t_{.80}$
49-1	0.1404	1.97	0.530	$t_{.60} < t_{OBS} < t_{.70}$
OLN	0.0531	0.28	0.176	$t_{OBS} < t_{.60}$
1-18	0.0392	0.15	0.155	$t_{OBS} < t_{.60}$
Scl	0.0206	0.42	0.068	$t_{OBS} < t_{.60}$
P-5 B	0.0078	0.01	0.028	$t_{OBS} < t_{.60}$
All Slabs	0.6763	45.74	12.420	$t_{.995} < t_{OBS}$
Clastics	0.4967	24.67	5.864	$t_{.995} < t_{OBS}$
Carbonates	0.3101	9.62	2.569	$t_{.990} < t_{OBS} < t_{.995}$

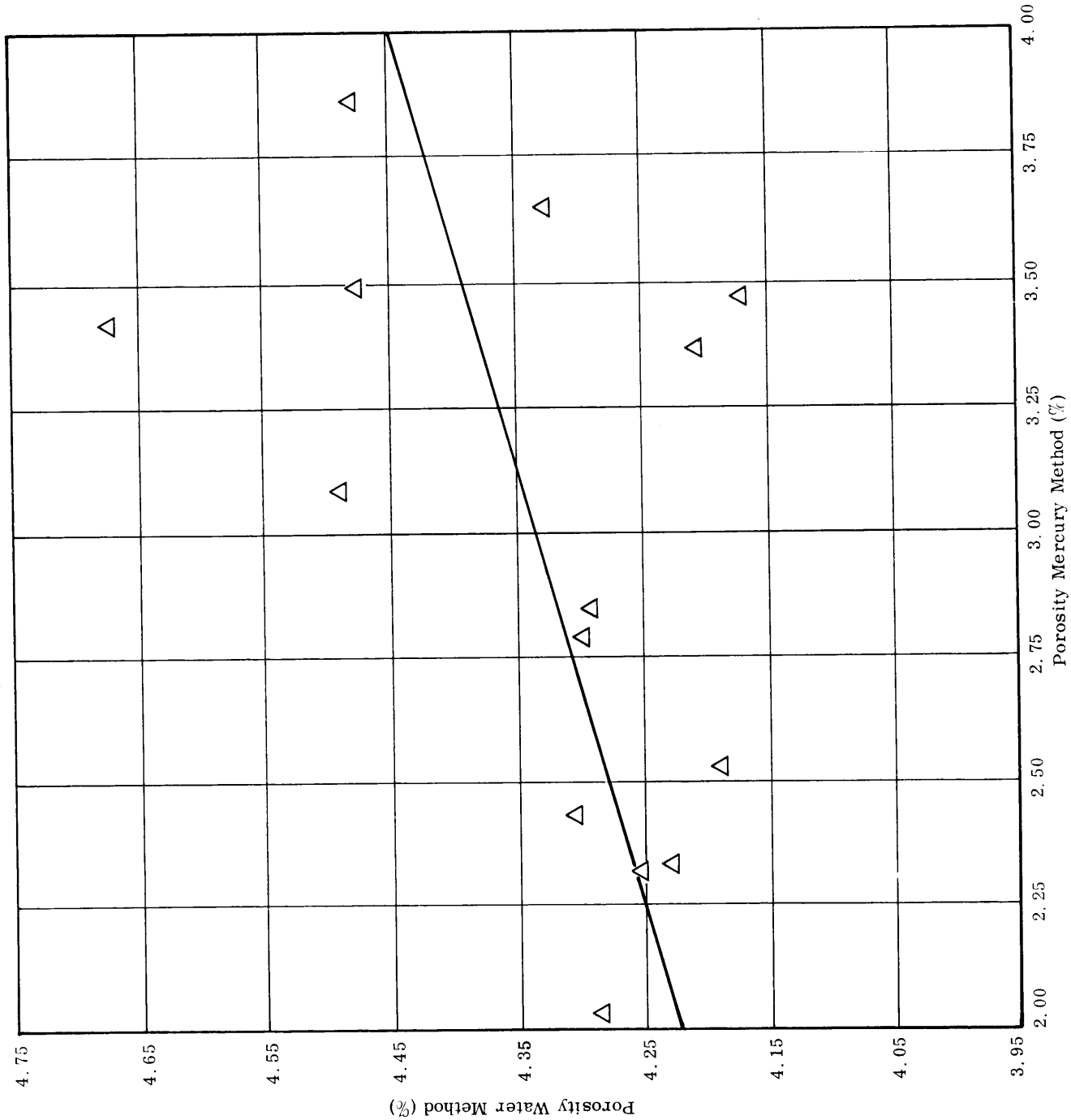

Figure 40. Mercury injection porosity versus water absorption porosity for slab MP.

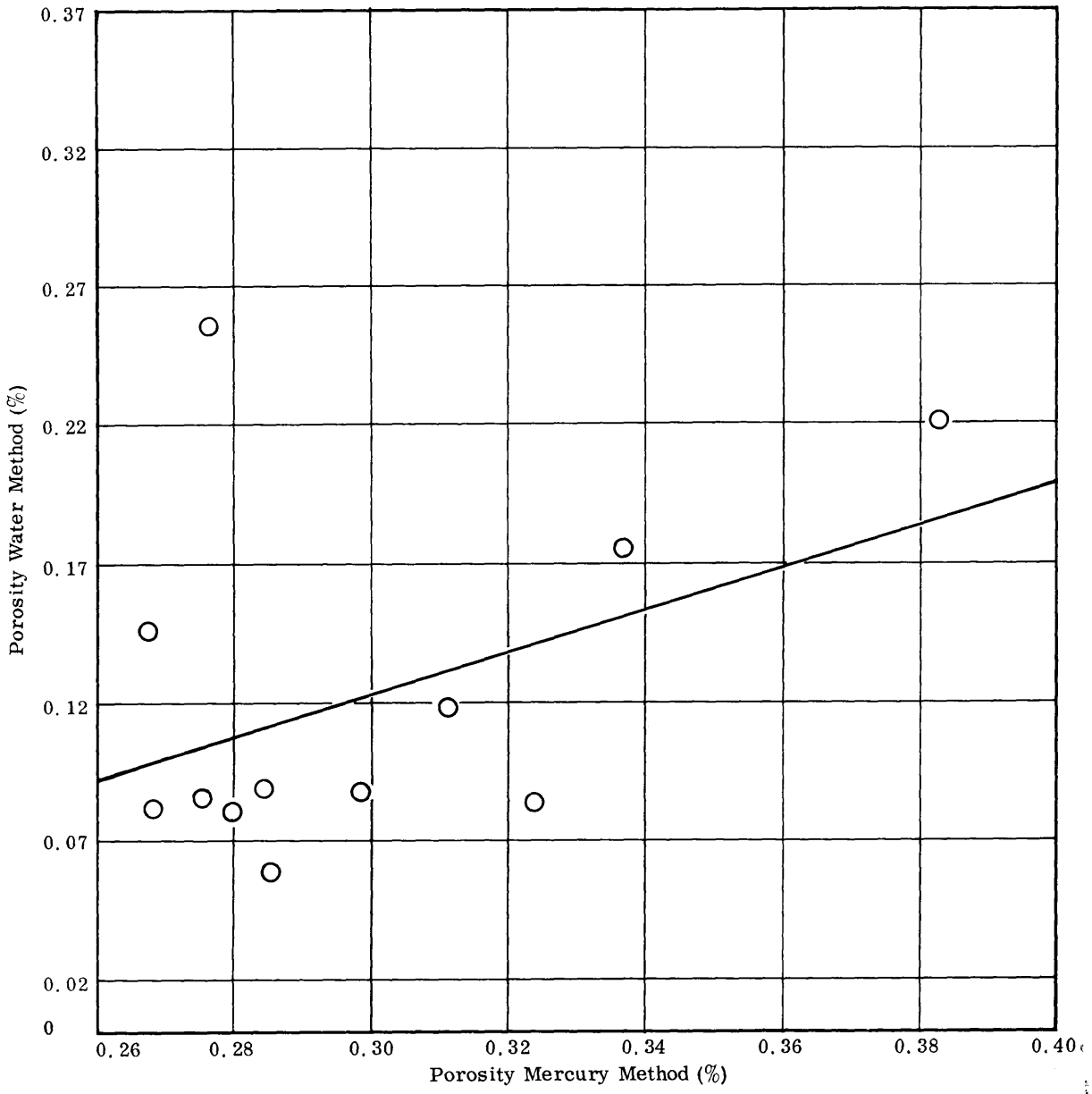

Figure 41. Mercury injection porosity versus water absorption porosity for slab STB.

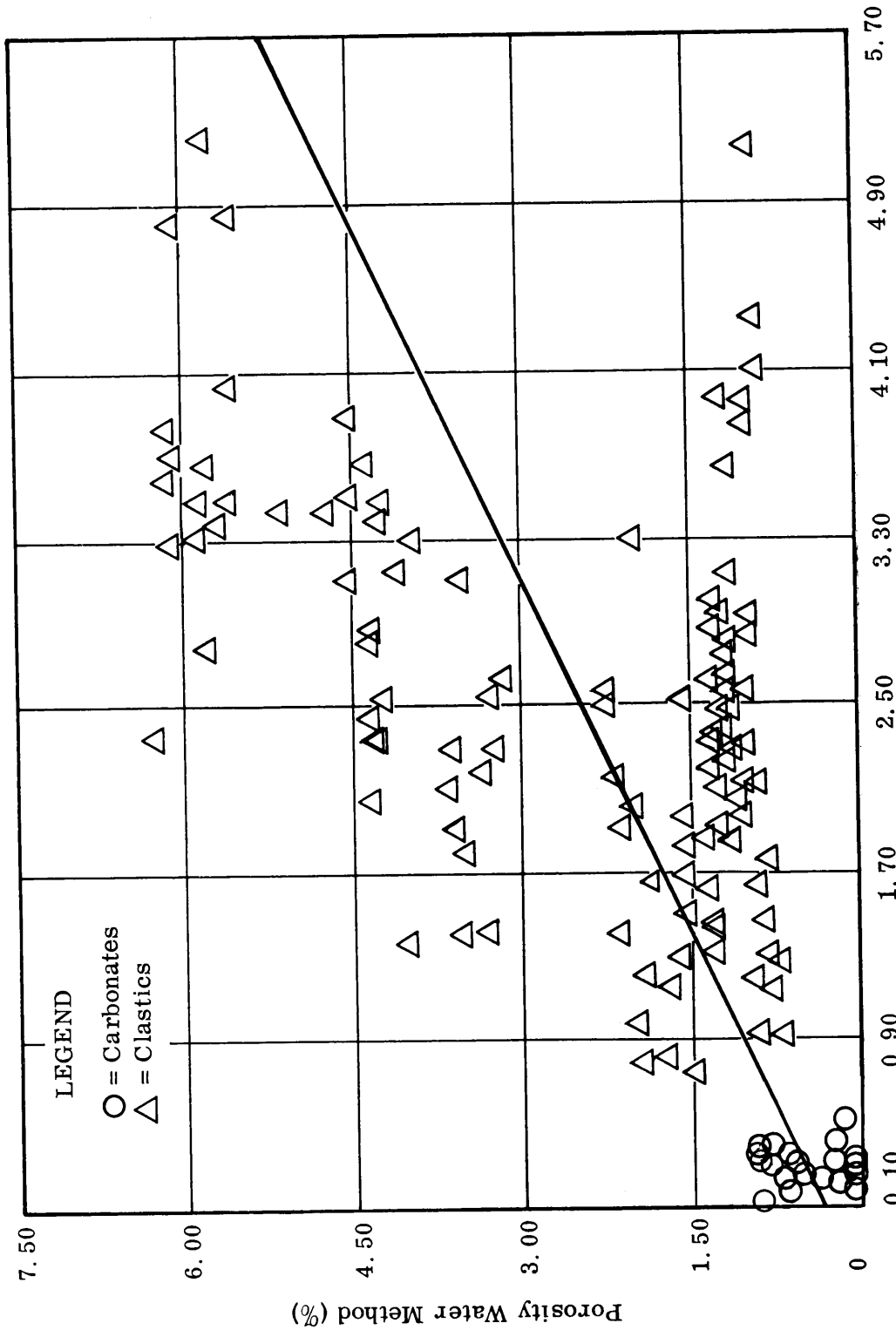

Figure 42. Mercury injection porosity versus water absorption porosity for all slabs combined.

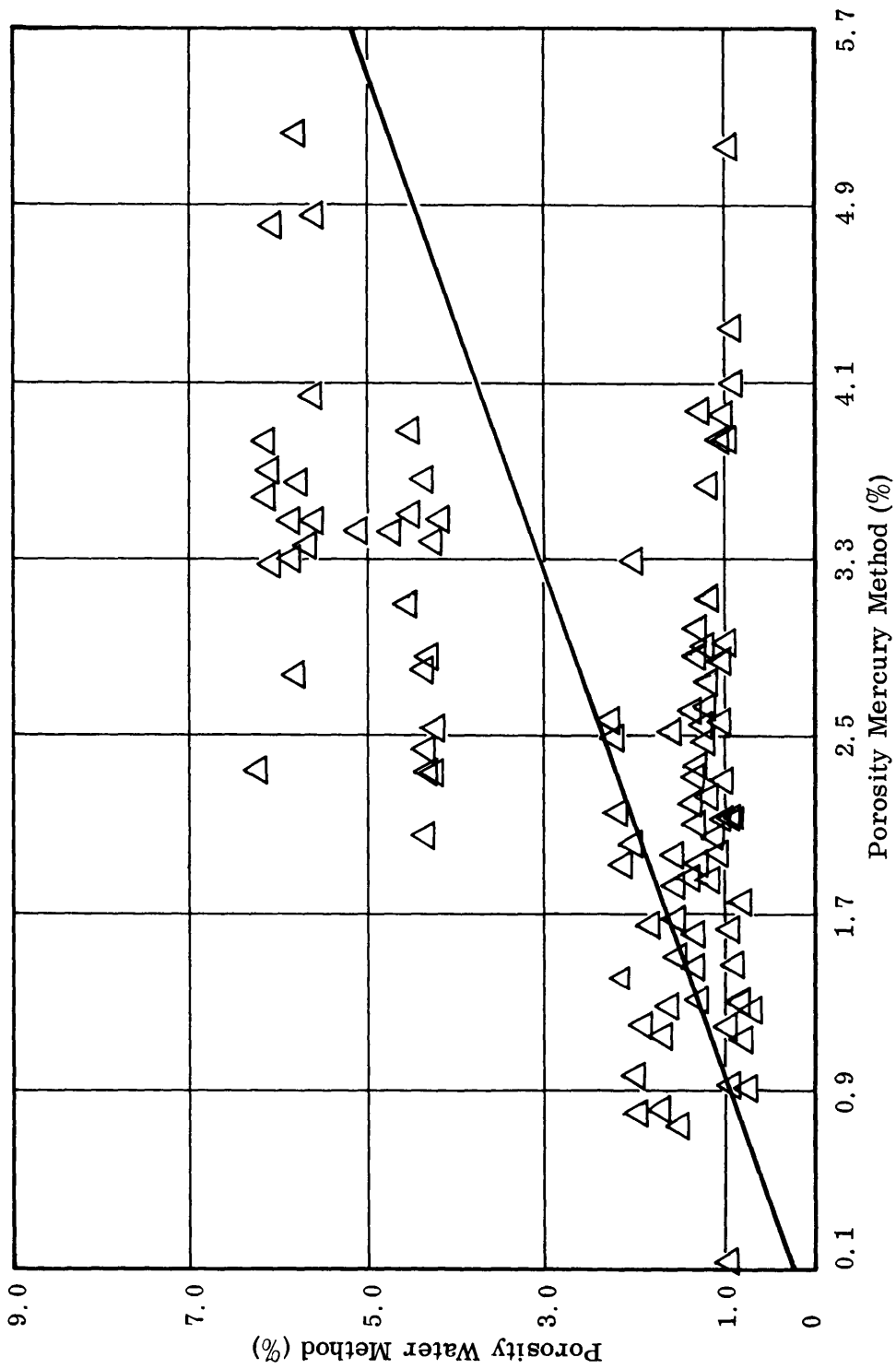

Figure 43. Mercury injection porosity versus water absorption porosity for clastic group.

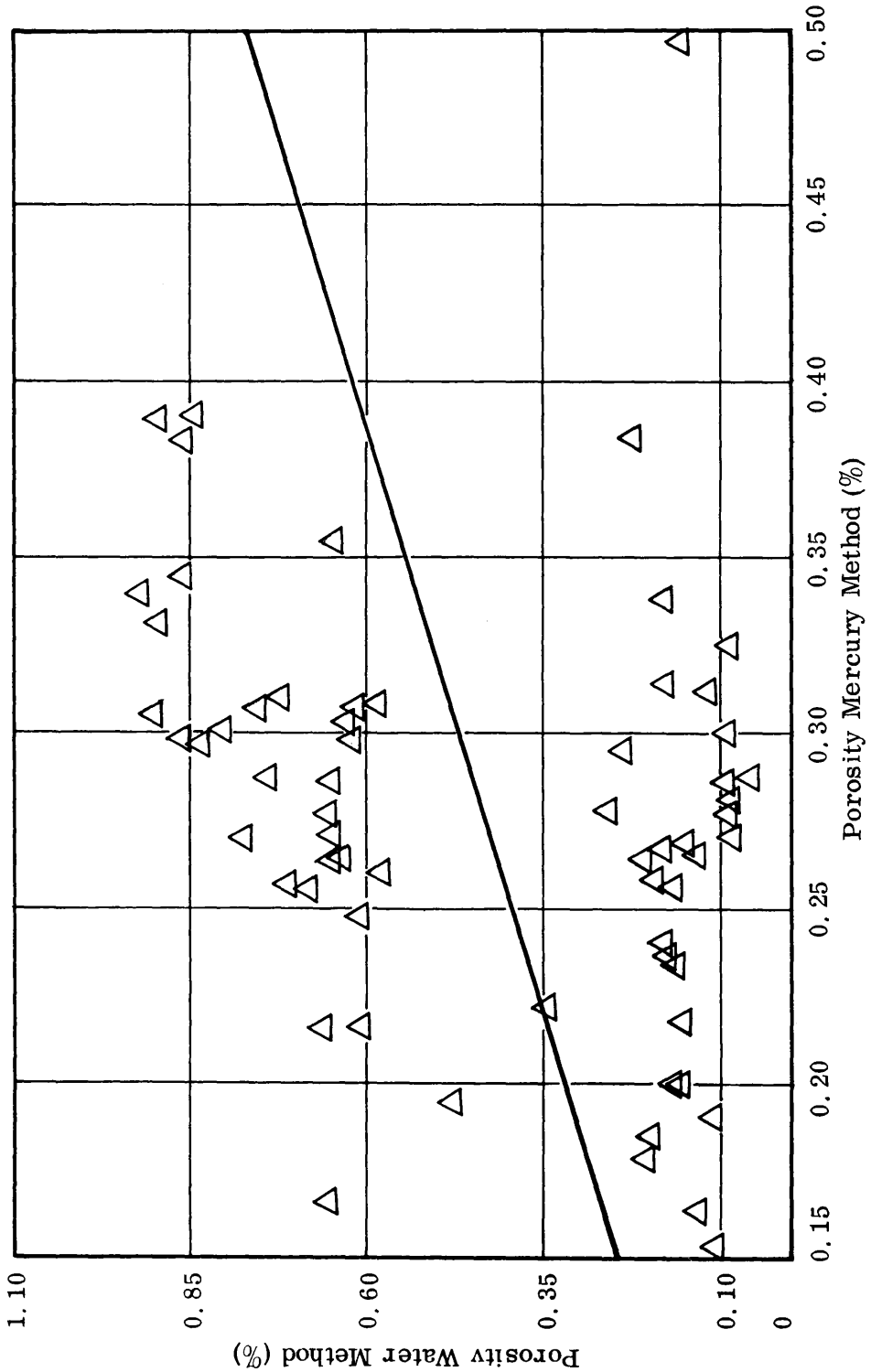

Figure 44. Mercury injection porosity versus water absorption porosity for carbonate group.

A closer look at the data plotted in Figure 43 leads one to suspect the presence of two populations showing different trends rather than a single, homogeneous group. One set of data appears to concentrate around a straight line with an approximately 40^{o} slope and an origin near zero water absorption porosity. A second trend appears to have a similar origin but runs almost horizontally across the graph. Inspection of the data indicated that most of the points in the second group belong to rock 6. In order to investigate the quality of the correlation with sample 6 omitted, slab means were plotted as shown in Figure 45. The correlation coefficient was then computed and found to be much improved at 0.898.

Inspection of the data plotted in Figure 44 also reveals two separate groups for the carbonates. However, a careful study of the properties of the rocks within the two groups yielded no obvious reason for the observed distribution. Also, no improvement in the correlation could be discerned if either group were omitted from the statistical tests.

Discussion

It was expected at the start of the study that mercury injection porosity and water absorption porosity would correlate well. However, the statistical evidence does not show this. One might think that there should be a correlation because mercury injection and water absorption both supposedly measure porosity. However, other factors obviously negate the simple relationship previously envisioned.

Because of the scope of this study, positive statements cannot be offered to explain why the mercury injection porosity does not equal the water absorption porosity. However, several points of conjecture may be presented as possible explanations. First, the water absorption porosity was obtained from rock cylinders weighing approximately 70 grams while the mercury injection porosity was obtained from rock chips weighing approximately 2 grams. The larger cylinder would provide a more representative sample. Because of its relatively small size, the rock chip would be more prone to reflect local variations in porosity than would the larger rock cylinder. The greater variation in porosity of rock chips compared to rock cylinders is illustrated by the relative dispersions of mercury injection porosity and water absorption porosity measurements from their respective mean values.

A measure of the relative dispersion of a set of values is obtained by dividing the standard deviation by the mean (Croxton and Cowden 1963). Table 13 shows the mean porosity and standard deviation for each slab, for both mercury injection porosity and water absorption porosity. The relative dispersion values for each are also given, and for every slab, except Sta, 1-8, and Stb, the dispersion of the mercury injection porosity is greater than the dispersion of the water absorption porosity. The generally greater variation for the rock chip than for the rock cylinder may have contributed to the lack of agreement between the mercury injection porosity and water absorption porosity.

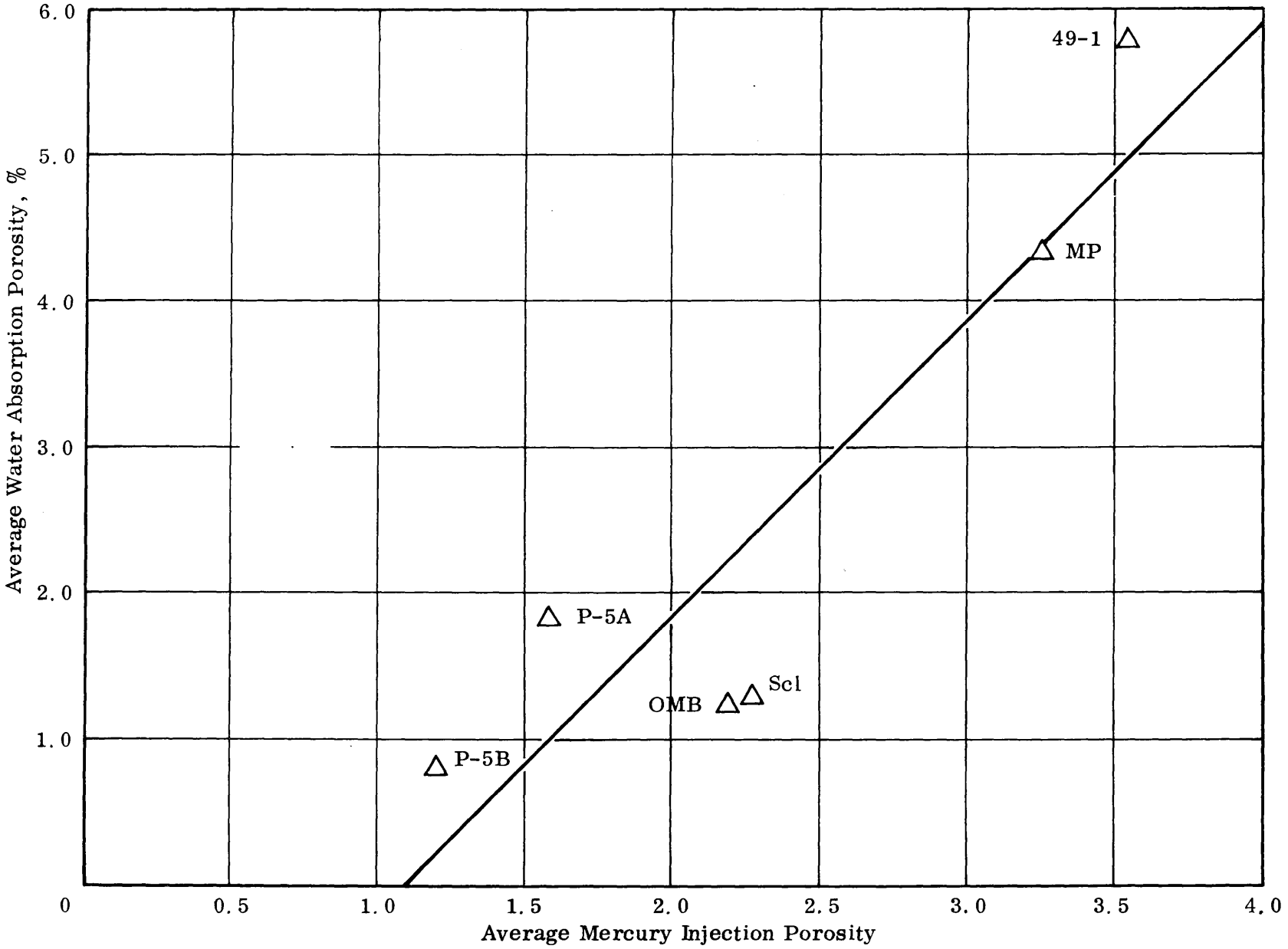

Figure 45. Average mercury injection porosity versus average water absorption porosity for all clastics except rock 6.

Table 13

Relative Dispersion Data for Mercury Injection Porosity and Water Absorption Porosity

Slab	HG Injection Mean ϵ	HG Injection Standard Deviation	Water Absorption Mean ϵ	Water Absorption Standard Deviation	HG Injection Relative Dispersion	Water Absorption Relative Dispersion
Scl	2.276	1.101	1.267	0.205	0.484	0.162
P-5 A	1.577	0.706	1.812	0.264	0.447	0.146
6	3.214	1.392	0.982	0.085	0.433	0.086
Omb	2.186	0.900	1.216	0.043	0.412	0.035
49-1	3.519	1.227	5.787	0.288	0.349	0.050
P-5 B	1.197	0.416	0.794	0.086	0.347	0.108
Mp	3.247	0.696	4.330	0.144	0.214	0.033
13-1	2.174	0.829	3.504	0.293	0.382	0.084
Sta	0.204	0.050	0.294	0.209	0.244	0.712
1-8	0.331	0.066	0.852	0.470	0.199	0.552
Oln	0.256	0.046	0.169	0 .027	0.180	0.157
1-18	0.279	0.047	0.651	0.053	0.169	0.081
Stb	0.292	0.040	0.122	0.063	0.136	0.516

Secondly, differences in the measured porosity could have resulted from differences in the penetrating liquid used. Water has the capability of being absorbed between crystal lattices of certain minerals (Searle and Grimshaw 1959). This absorption initially involves interlattice spacings below 10 Å, or less than .001 μ (Grim 1953). The mercury porosimeter can penetrate pores only as small as .01 μ in diameter. Water can also be absorbed into intraparticle fractures because of the polar water molecule and the charge imbalance at the fractured surface of the mineral (Searle and Grimshaw 1959). Because of its unique properties, water may enter into spacings which are not reachable by the mercury porosimeter used in this study. Unfortunately no discussion was found in the literature of differences in porosity by mercury injection and water absorption.

Thirdly, at least small miscalculations of porosity may have resulted from the assumption that the physical properties of water and mercury remain constant for both large pore penetrations and small pore penetrations. Grim (1953) cites several investigations which show that adsorbed water on clay minerals has a density different from 1 gram/cm^3. There is confusion, however, as to the nature and magnitude of this density change. Until this confusion is cleared, the importance of this factor of changing physical properties will remain unknown.

On the positive side, the omission of one rock (No. 6) from the graph showing only clastic samples increased the correlation coefficient significantly. Subsequent work in this section also points out that sample 6 behaves anomalously in other ways; i.e., it shows very high mercury injection porosity and low water absorption porosity. The recognition of anomalous rock material such as rock 6 perhaps could be predicted after more detailed study than was accomplished in this project.

Again, to summarize briefly, there has been no statistical evidence which could substantiate a significant relationship between porosity by mercury injection and porosity by water absorption. For the individual slabs, for all the slabs combined, and for the clastics and carbonates, the correlation coefficients are poor. The regression lines for each of these groupings fail to account for a reasonable percentage of the variation of water absorption porosity. In many cases, the distribution of points was probably influenced by chance. It would appear that, based on this work, porosity by mercury porosimetry is unable to accurately predict the water absorption porosity of mineral aggregates.

Rate of Water Absorption Versus Porosity

Correlations

A graph showing the rate of water absorption versus mercury injection porosity is shown in Figure 46. This figure suggests a possible relationship between mercury injection porosity and rate of water absorption, for both the clastic and the carbonate groups. The

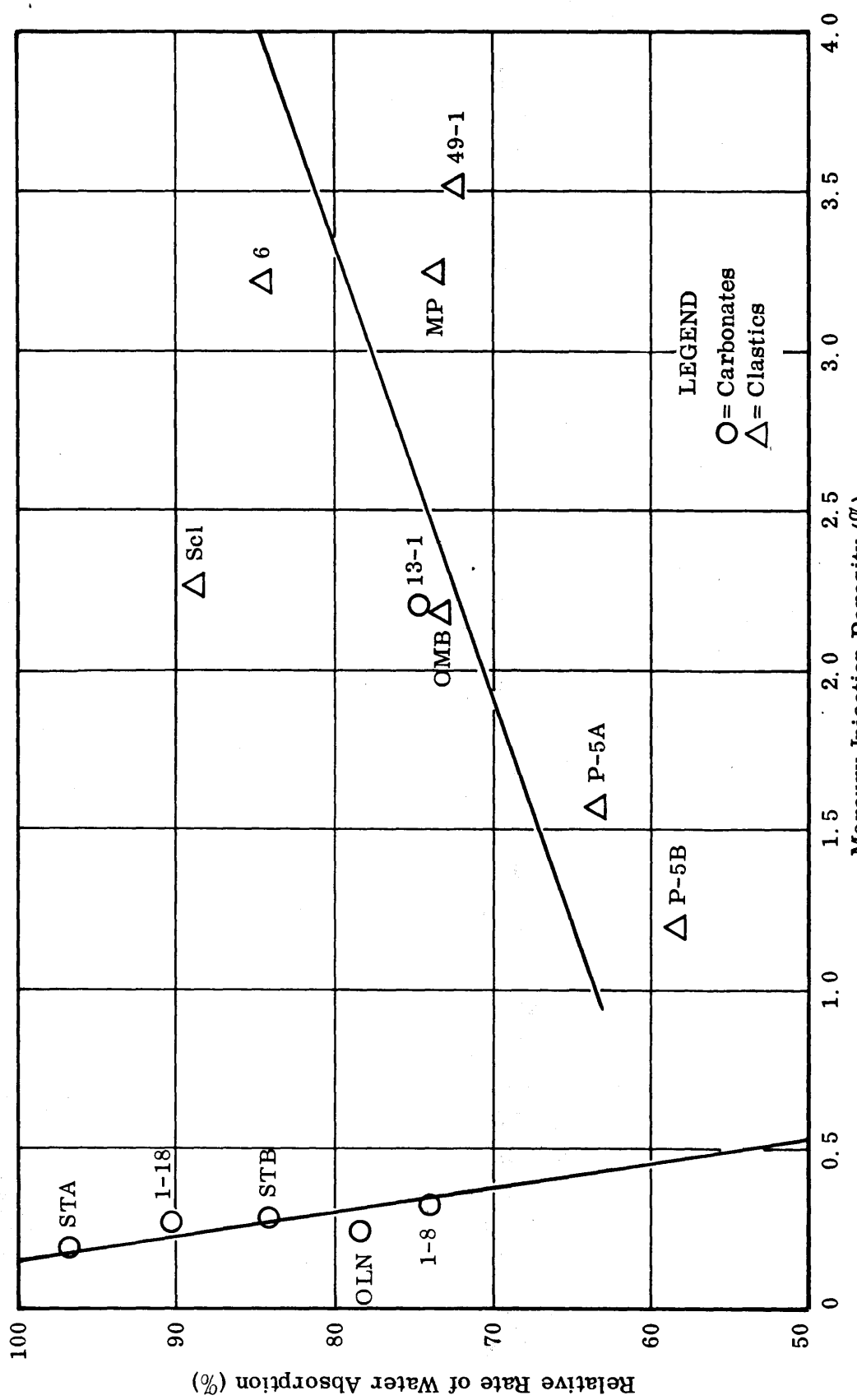

Figure 46. Mercury injection porosity versus relative rate of water absorption.

trends vary, however, in that the clastics show a positive slope and the carbonates a negative slope. Despite these seemingly fair conditions, Table 14 shows that the correlation coefficients are low for both the clastics and the carbonates. Also, both regression lines fail to account for at least 65 percent of the variation of the water absorption porosity. The operation of the element of chance, however, is doubtful because the level of significance for both clastics and carbonates is sufficiently high.

Table 14

Mercury Injection Porosity Versus Rate of Water Absorption

Type	Correlation Coefficient (R)	Variation % Explained By Regression Line	t_{OBS}	Significance
Clastics	+ 0.5827	33.95%	0.934	$t_{.80} < t_{OBS} < t_{.90}$
Carbonates	- 0.6696	44.84%	1.046	$t_{.80} < t_{OBS} < t_{.90}$

No statistical analysis was performed on the relationship for all of the slabs combined because inspection of Figure 46 showed the carbonates obviously separated from the clastics. A correlation analysis would be misleading.

Figure 47 reveals a very poor relationship for the clastics between the rate of water absorption and the amount of water absorbed. The carbonates show a fair trend. Table 15 indicates that the clastics and carbonates show very low correlation coefficients. Both regression lines fail to explain over 92 percent of the variation of water absorption porosity. Chance could well have been involved in the distribution of the points in Figure 47 because the level of significance for both clastics and carbonates is very low.

Examination of Figure 47 suggests that a statistical test for all of the slabs combined would again be misleading. The scatter of points is separated into two clusters, one for the clastics and one for the carbonates.

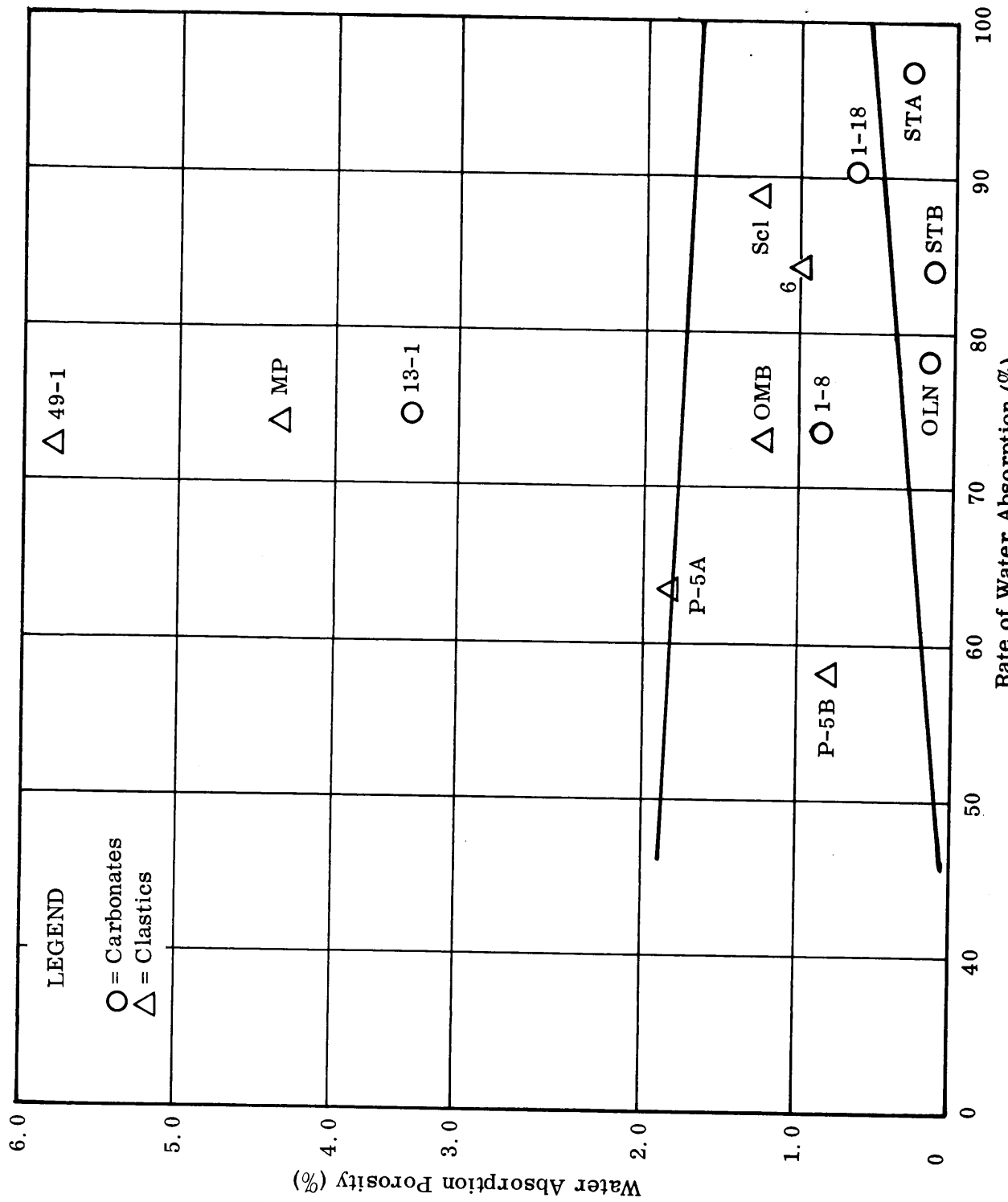

Figure 47. Relative rate of water absorption versus water absorption porosity.

Table 15

Water Absorption Porosity Versus Rate of Water Absorption

Type	Correlation Coefficient (R)	Variation % Explained By Regression Line	t_{OBS}	Significance
Clastics	+0.0283	0.08%	0	$t_{OBS} < t_{.60}$
Carbonates	+0.2820	7.95%	0.143	$t_{OBS} < t_{.60}$

Discussion

The rate of water absorption into mineral aggregates is determined partly by pore size (Lewis, Dolch, and Woods 1953). The smaller the pore size, the larger the capillary potential (Rhoades and Mielenz 1946). Also, the continuity of the pores contributes to the rate of water absorption. Total porosity, however, is not directly related to either pore size or pore continuity. So it would not necessarily be expected that the porosity be related to the rate of water absorption. This was evident in the statistical treatment and graphs presented in Figures 46 and 47.

In summary, there does not seem to be a reliable way of indirectly relating mercury injection porosity to water absorption porosity by way of the rate of water absorption. The material in this section has failed to show any statistical evidence which would suggest a significant relationship between the rate of water absorption and either mercury injection porosity or water absorption porosity.

The Role of Pore Size

Correlations

The pore size distribution curves were prepared and studied but are not included in this report. Attempts at utilizing the curves for correlation were hampered by the nature of the pore size distributions. The carbonates had very similar pore size distributions which were difficult to separate for analyses. Figure 48 shows the average pore size distribution for slab Oln. It is typical of the carbonates. The clastics also had pore size distributions which were not readily differentiated. The average pore size distribution of Scl, typical for many of the clastics, is shown in Figure 49.

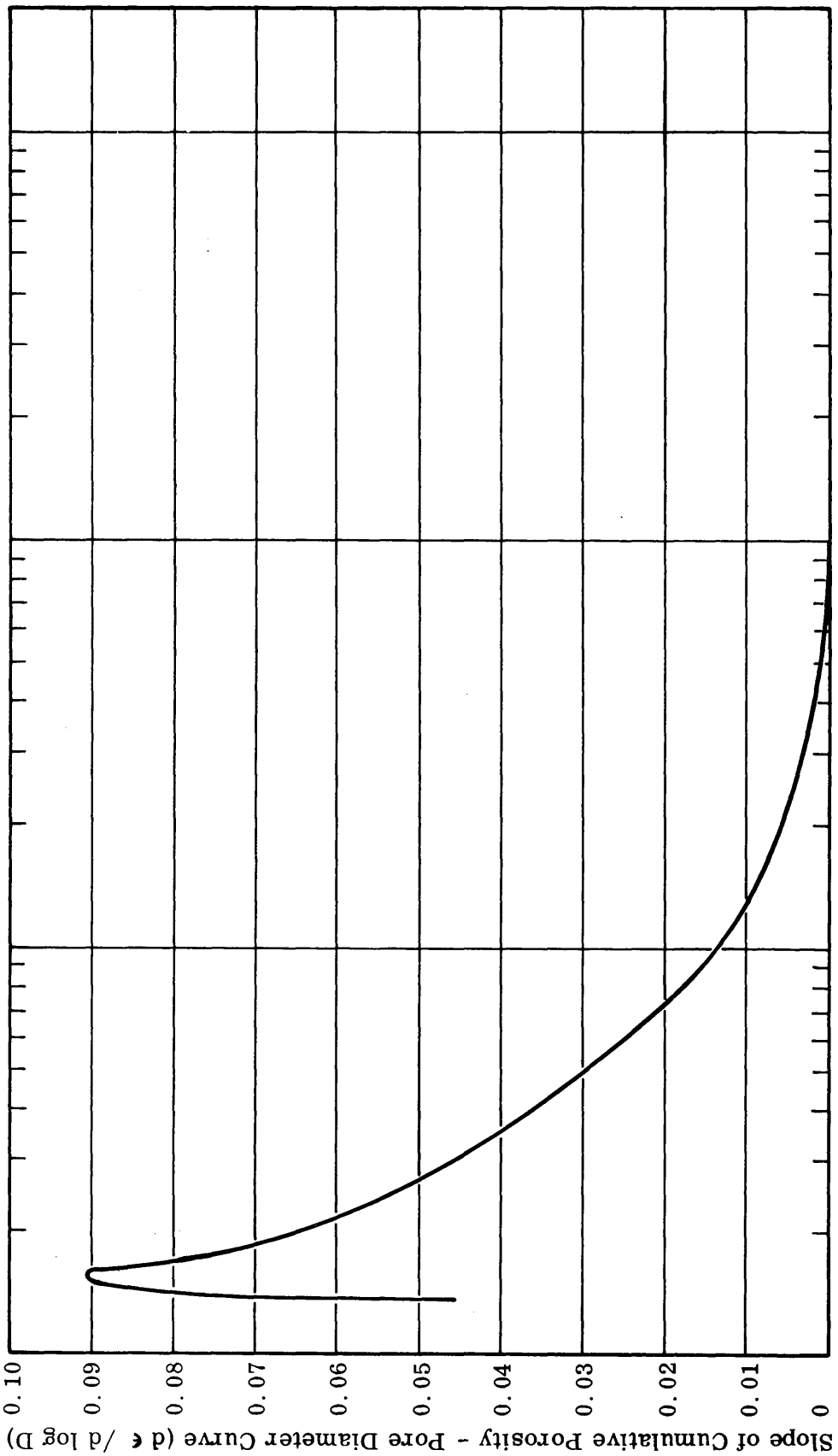

Figure 48. Average pore size distribution for slab OLN.

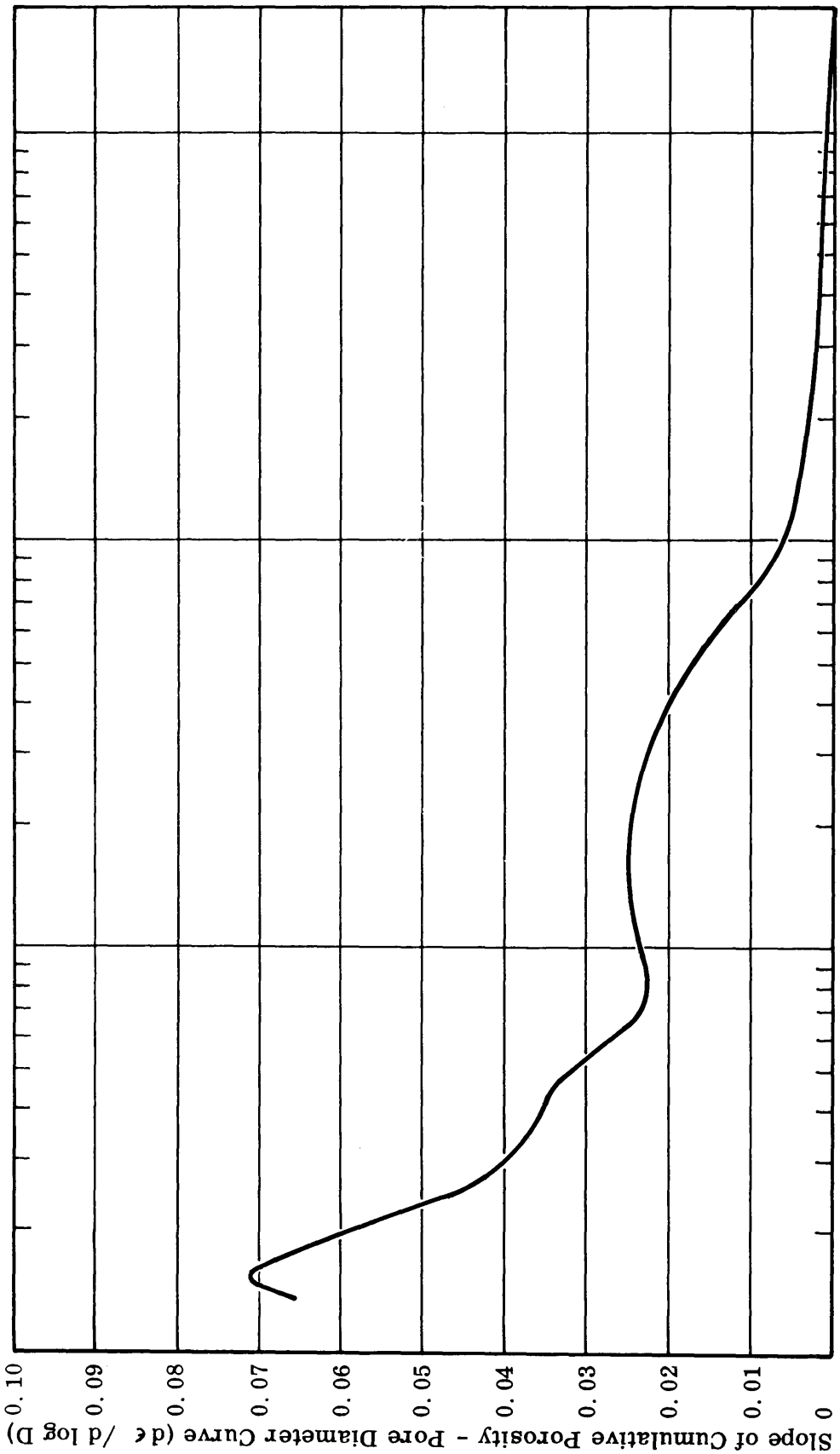

Figure 49. Average pore size distribution for slab Scl.

Despite this difficulty it was thought that some measure of pore size distribution should be included in the study to see if correlations could be found between a pore size distribution factor and other measured parameters. Consequently, the ratio of the volume for pores $> 80\ \mu$ over volume for pores $< 80\ \mu$ was accepted as a logical measure of pore size distribution and is used in this section. The notation used for this ratio is $\frac{> 80\ \mu \text{ Porosity}}{< 80\ \mu \text{ Porosity}}$. Figure 50 shows the graph of the ratio $\frac{> 80\ \mu \text{ Porosity}}{< 80\ \mu \text{ Porosity}}$ versus the water absorption porosity. The carbonates do not appear on this graph, or on Figures 51 and 52 because pore volume for pores $> 80\ \mu$ was so small that it could not be measured with the technique used.

The clastics appear to follow a trend in Figure 50. Table 16 shows a correlation coefficient of -0.7437, a fair to moderately good correlation. The regression line explains over 55 percent of the variation of water absorption porosity from the mean. The high significance interval suggests that chance was not involved in the distribution of points in Figure 50.

Table 16

$\frac{> 80\ \mu \text{ Porosity}}{< 80\ \mu \text{ Porosity}}$ Versus Water Absorption Porosity

Type	Correlation Coefficient (R)	Variation % Explained By Regression Line	t_{OBS}	Significance
Clastics	- 0.7437	55.31	1.849	$t_{.90} < t_{OBS} < t_{.95}$

Figure 51 shows the graph of $\frac{> 80\ \mu \text{ Porosity}}{< 80\ \mu \text{ Porosity}}$ versus the ratio $\frac{\text{water absorption porosity}}{\text{mercury injection porosity}}$. A definite trend is suggested for the clastics, and Table 17 indicates a good correlation coefficient of -0.7777. The regression line explains 60.5 percent of the variation of water absorption porosity. The level of significance for this relationship is quite high.

The graph of $\frac{> 80\ \mu \text{ Porosity}}{< 80\ \mu \text{ Porosity}}$ versus the rate of water absorption is shown in Figure 52. The scattered points do not suggest a good trend and Table 18 reveals that the correlation coefficient is a low 0.1884. The regression line explains less than 4 percent of the variation, and the level of significance is low.

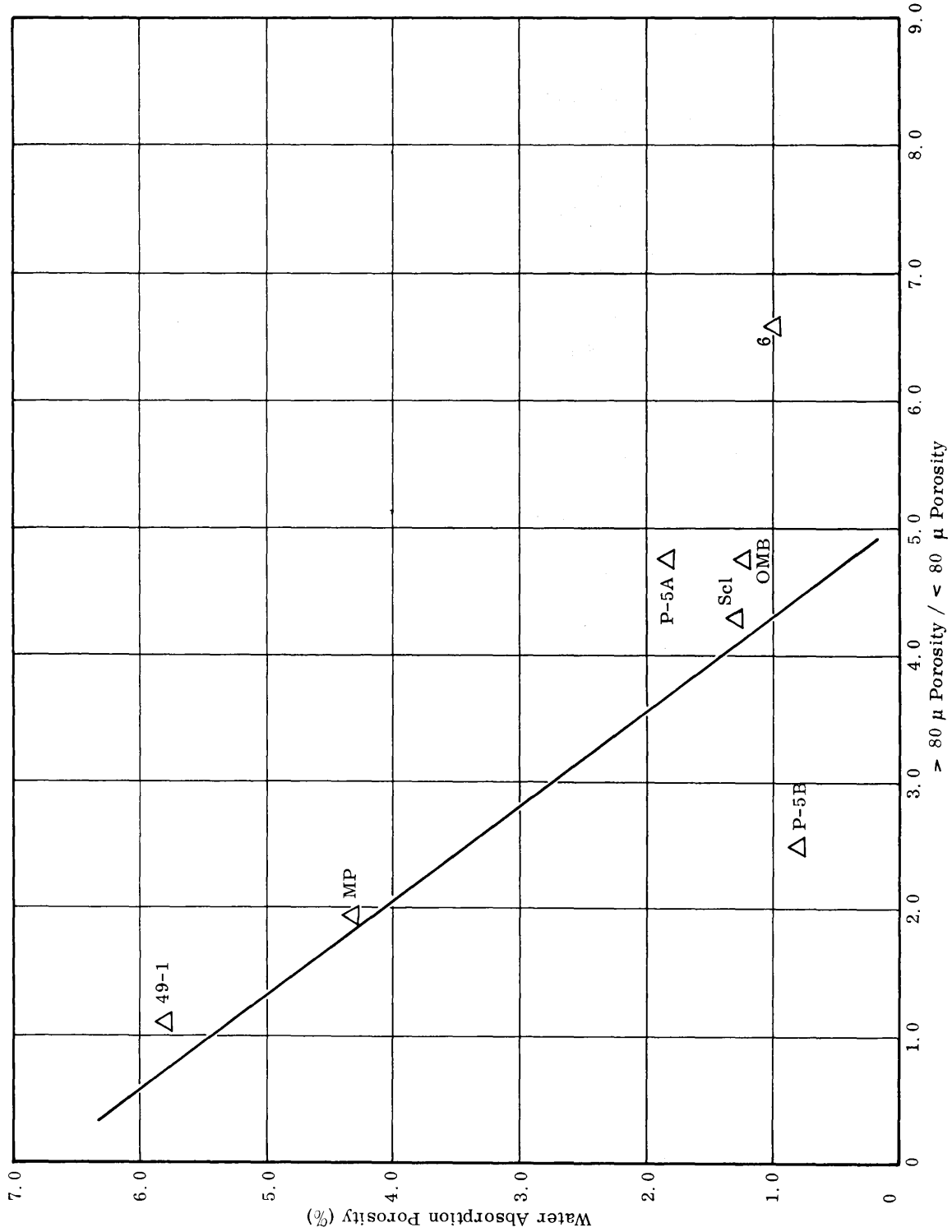

Figure 50. > 80 μ porosity/< 80 μ porosity versus water absorption porosity.

Despite this difficulty it was thought that some measure of pore size distribution should be included in the study to see if correlations could be found between a pore size distribution factor and other measured parameters. Consequently, the ratio of the volume for pores $> 80\ \mu$ over volume for pores $< 80\ \mu$ was accepted as a logical measure of pore size distribution and is used in this section. The notation used for this ratio is $\frac{>80\ \mu \text{ Porosity}}{<80\ \mu \text{ Porosity}}$. Figure 50 shows the graph of the ratio $\frac{>80\ \mu \text{ Porosity}}{<80\ \mu \text{ Porosity}}$ versus the water absorption porosity. The carbonates do not appear on this graph, or on Figures 51 and 52 because pore volume for pores $> 80\ \mu$ was so small that it could not be measured with the technique used.

The clastics appear to follow a trend in Figure 50. Table 16 shows a correlation coefficient of -0.7437, a fair to moderately good correlation. The regression line explains over 55 percent of the variation of water absorption porosity from the mean. The high significance interval suggests that chance was not involved in the distribution of points in Figure 50.

Table 16

$\frac{>80\ \mu \text{ Porosity}}{<80\ \mu \text{ Porosity}}$ Versus Water Absorption Porosity

Type	Correlation Coefficient (R)	Variation % Explained By Regression Line	t_{OBS}	Significance
Clastics	- 0.7437	55.31	1.849	$t_{.90} < t_{OBS} < t_{.95}$

Figure 51 shows the graph of $\frac{>80\ \mu \text{ Porosity}}{<80\ \mu \text{ Porosity}}$ versus the ratio $\frac{\text{water absorption porosity}}{\text{mercury injection porosity}}$. A definite trend is suggested for the clastics, and Table 17 indicates a good correlation coefficient of -0.7777. The regression line explains 60.5 percent of the variation of water absorption porosity. The level of significance for this relationship is quite high.

The graph of $\frac{>80\ \mu \text{ Porosity}}{<80\ \mu \text{ Porosity}}$ versus the rate of water absorption is shown in Figure 52. The scattered points do not suggest a good trend and Table 18 reveals that the correlation coefficient is a low 0.1884. The regression line explains less than 4 percent of the variation, and the level of significance is low.

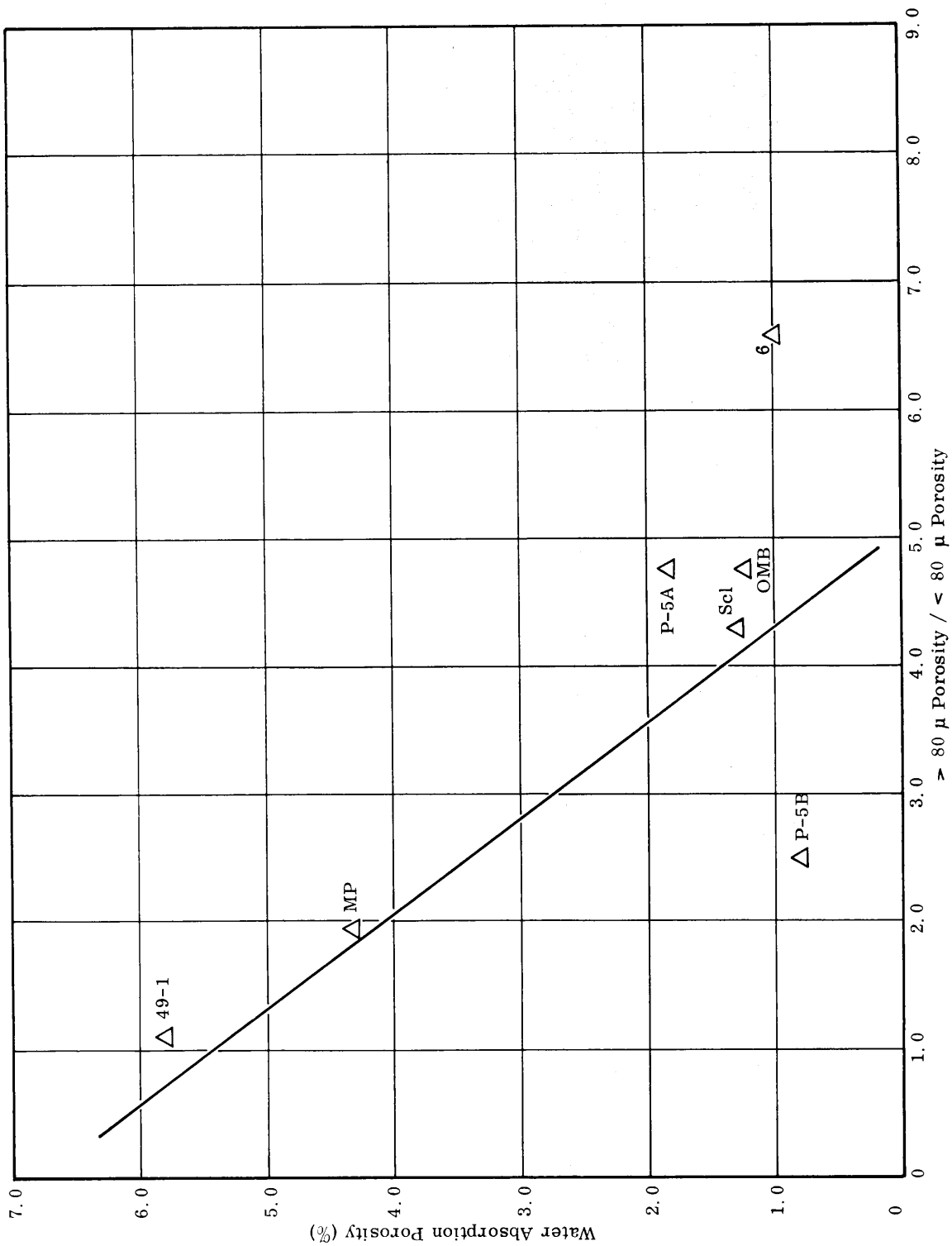

Figure 50. $>80\ \mu$ porosity/$<80\ \mu$ porosity versus water absorption porosity.

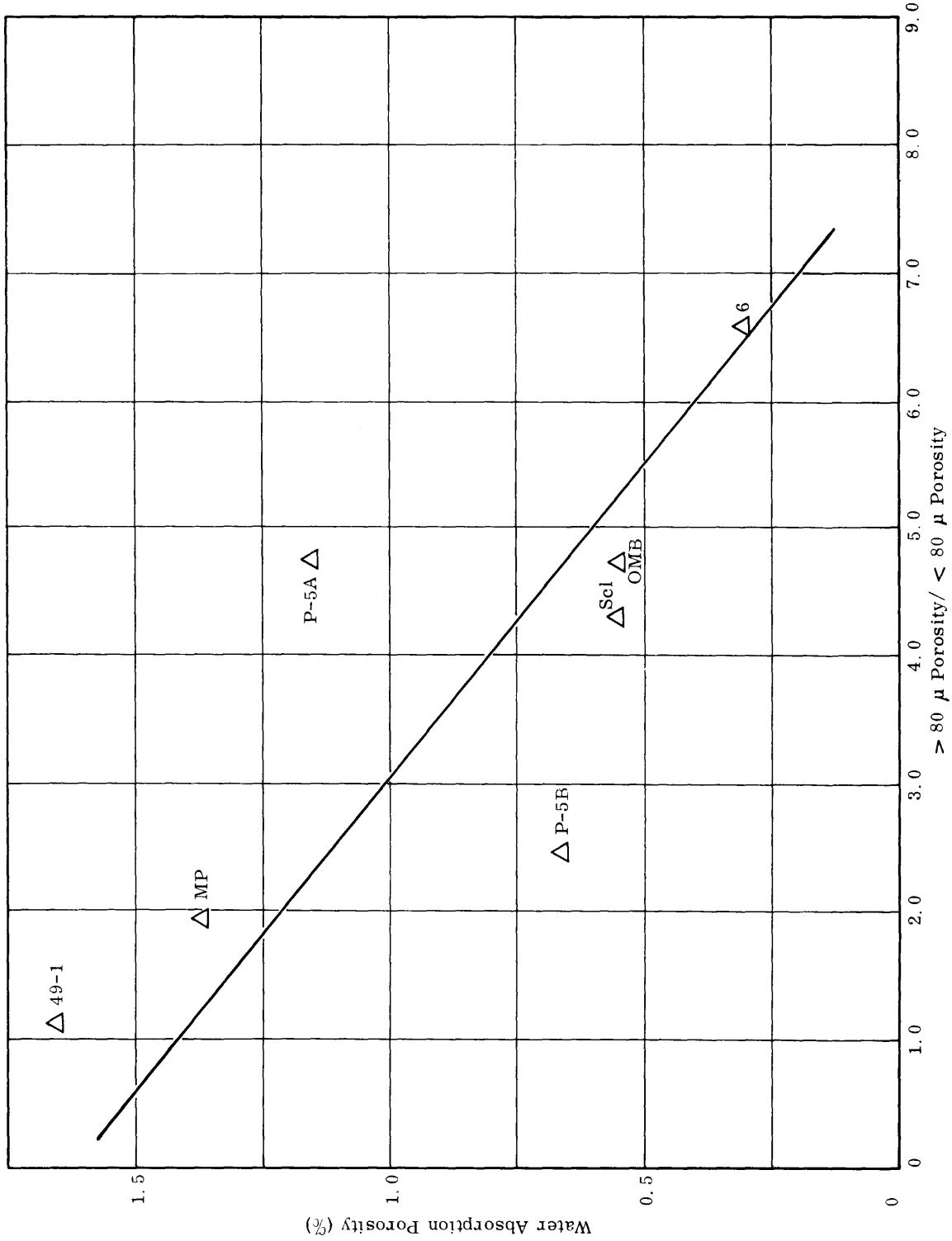

Figure 51. > 80 μ porosity/< 80 μ porosity versus water absorption porosity.

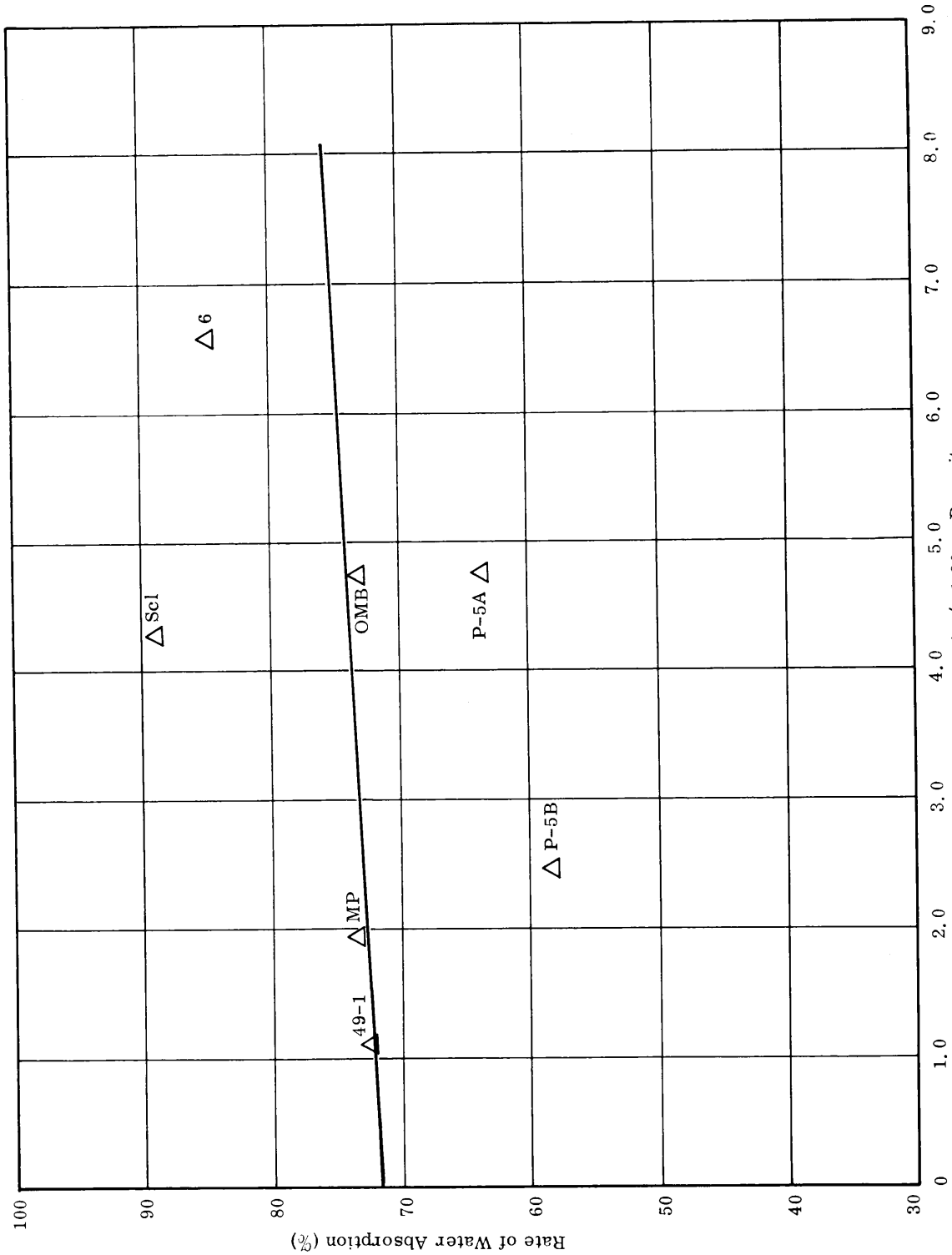

Figure 52. > 80 μ porosity/<80 μ porosity versus rate of water absorption.

Table 17

$\frac{\geq 80\,\mu \text{ Porosity}}{< 80\,\mu \text{ Porosity}}$ Versus $\frac{\text{Water Absorption Porosity}}{\text{Mercury Injection Porosity}}$

Type	Correlation Coefficient (R)	Variation % Explained By Regression Line	t_{OBS}	Significance
Clastics	- 0.7777	60.48%	2.151	$t_{.95} < t_{OBS} < t_{.975}$

Table 18

$\frac{> 80\,\mu \text{ Porosity}}{< 80\,\mu \text{ Porosity}}$ Versus Rate of Water Absorption

Type	Correlation Coefficient (R)	Variation % Explained By Regression Line	t_{OBS}	Significance
Clastics	0.1884	3.55	0.429	$t_{.60} < t_{OBS} < t_{.70}$

Discussion

The ratio $\frac{> 80\,\mu \text{ Porosity}}{< 80\,\mu \text{ Porosity}}$ is an arbitrary figure which shows one pore size relationship in a rock. As this ratio decreases, the air that is trapped within the pores becomes less of an important factor in absorption because entrapped air is more likely to affect absorption in larger pores than in smaller pores. This decrease in the effect of entrapped air would be reflected in a highe water absorption porosity. Figure 50 suggests that the relatively low ratios of $\frac{> 80\,\mu \text{ Porosity}}{< 80\,\mu \text{ Porosity}}$ for slabs 49-1 and Mp are related to the relatively high water absorption porosities for both slabs. Likewise the relatively high ratios of $\frac{> 80\,\mu \text{ Porosity}}{< 80\,\mu \text{ Porosity}}$ for slabs P-5B, Scl, Omb, P-5A, and 6 may be related to the relatively low water absorption porosities observed.

It would be expected that a rock containing a significant amount of entrapped air could not reach a high degree of saturation under normal soaking conditions. The resultant water absorption porosity would be less than the effective porosity. Because the mercury injection method forces mercury into pores, the resulting mercury injection porosity might be greater than the water absorption porosity. Figure 51 shows that as the ratio $\frac{>80\ \mu\ \text{Porosity}}{<80\ \mu\ \text{Porosity}}$ increases, the ratio of water absorption porosity to mercury injection porosity decreases. In all cases except P-5A, the rock shows greater porosity by water absorption than by mercury injection when $\frac{>80\ \mu\ \text{Porosity}}{<80\ \mu\ \text{Porosity}}$ is less than 2.0. Above 2.0, the mercury injection porosity is greater than the water absorption porosity. For rocks P-5B, Scl, Omb, and 6, the probability of high amounts of entrapped air due to the large pore size, results in a low water absorption porosity. The fact that the mercury injection porosity is larger than the water absorption porosity shows that pore volume is present which is not being penetrated by the absorbed water. It would appear for rocks 49-1 and Mp that the influence of small pores is greater than in the other rocks. Consequently, the capillary potential for the two rocks is larger. This results in a considerably larger water absorption porosity than mercury injection porosity. Apparently the water is reaching pores which cannot be reached by the mercury injection technique.

Figure 52 does not show a good relationship between the ratio $\frac{>80\ \mu\ \text{Porosity}}{<80\ \mu\ \text{Porosity}}$ and the rate of water absorption. Based on capillary principles, it might be expected that as the ratio $\frac{>80\ \mu\ \text{Porosity}}{<80\ \mu\ \text{Porosity}}$ increases, the capillary potential of the rock would decrease. A decrease in capillary potential would be expected to result in a decrease in the rate of water absorption. However, the data do not show this trend, so other factors such as the rapid inflow of water into very large pores and the difficulty of removing entrapped air in small pores might be working contrary to capillary potential.

Another factor, which was not previously taken into consideration, is the increase in viscous drag as the pore sizes become smaller (Dolch 1966). So as $\frac{>80\ \mu\ \text{Porosity}}{<80\ \mu\ \text{Porosity}}$ increases, the capillary potential would decrease, but the viscous drag would decrease as well. The rate of water absorption would be reduced by the lower capillary potential, but would be increased by the lower viscous drag. The lack of a signficiant trend in Figure 52 does not give a quantitative insight into these two opposing relationships.

In summary, the ratio $\frac{80\ \mu\ \text{Porosity}}{80\ \mu\ \text{Porosity}}$ appears to be a fairly worthwhile measure in predicting the water absorption porosity for the clastic rocks used in this study. However, the correlation coefficient is only moderately good so the predictive potential is not an excellent one. The method also suffers because the carbonates failed to show a measurable porosity for pores >80 μ in diameter. Thus, they could not be included in this phase of the study.

The ratio also correlated fairly well with the ratio of water absorption porosity over mercury injection porosity for the clastics. The correlation coefficient is fairly high but the regression line failed to account for nearly 40 percent of the variation of $\frac{\text{water absorption porosity}}{\text{mercury injection porosity}}$. Again, this method of prediction suffers because carbonates could not be included in the study.

There appeared to be no significant relationship between the ratio $\frac{\geq 80\,\mu \text{ Porosity}}{< 80\,\mu \text{ Porosity}}$ and the rate of water absorption.

The Role of Grain Size

Correlations

Figure 53 is a graph of the average grain size versus mercury injection porosity for both clastics and carbonates. Each group shows a separate trend. Table 19 reveals that the clastics have a good correlation coefficient of +0.8317. The regression line for the clastics explains nearly 70 percent of the variation of the mercury injection porosity. The high level of significance suggests that chance was not involved in the distribution of points.

Table 19

Average Grain Size Versus Mercury Injection Porosity

Type	Correlation Coefficient (R)	Variation % Explained By Regression Line	t_{OBS}	Significance
Clastics	+0.8317	69.17	2.785	$t_{.975} < t_{OBS} < t_{.99}$
Carbonates	+0.6000	36.00	0.799	$t_{.70} < t_{OBS} < t_{.80}$

The carbonates have a relatively poor correlation of -0.6000 and an explained variation of only 36 percent. The moderate level of significance implies that chance may have been a factor in the distribution of the points shown in Figure 53.

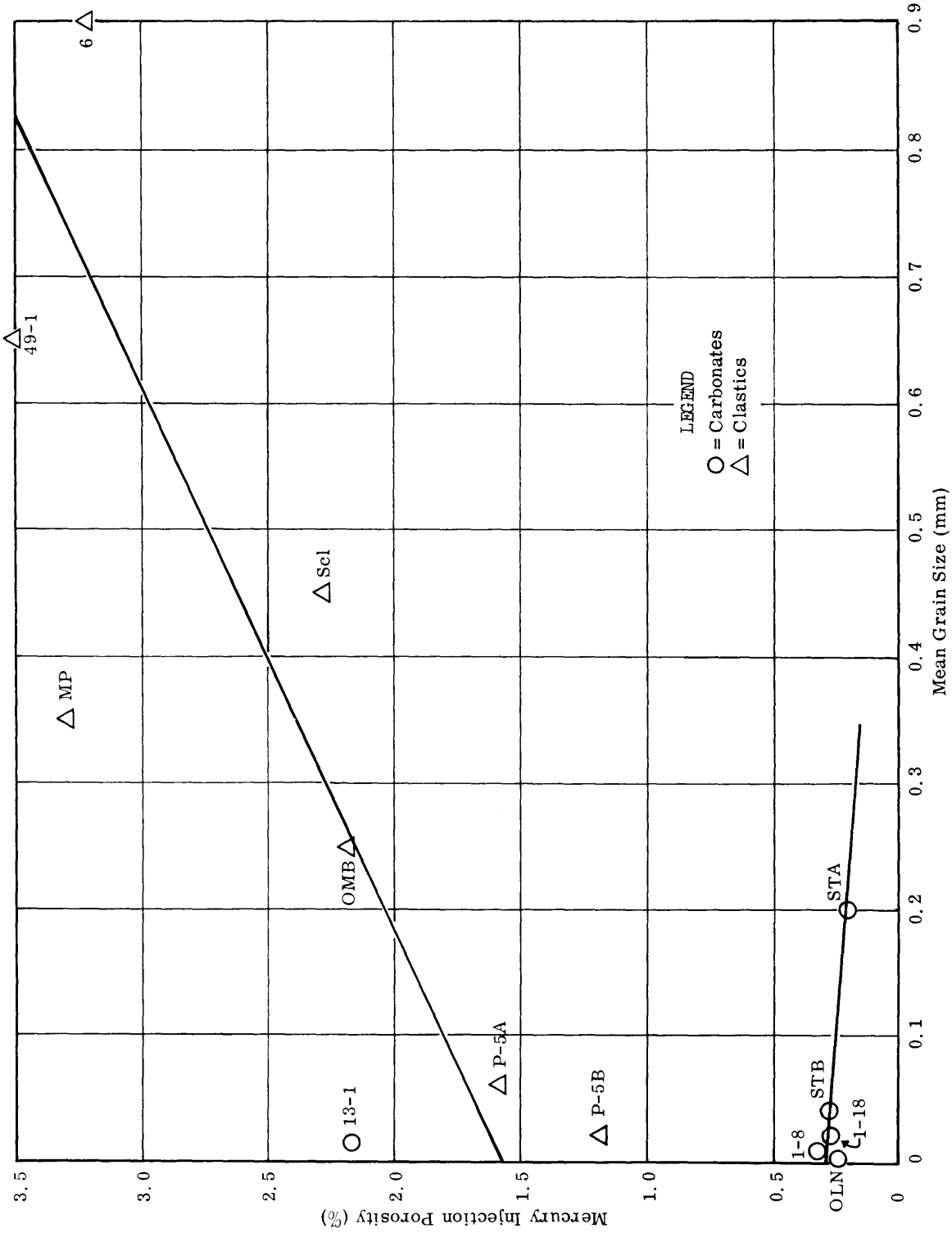

Figure 53. Mean grain size versus mercury injection porosity.

Based on the distributions of average grain size (see Figures 53, 54, and 55) no statistical analyses were made for all of the slabs combined. The scatter of points in each of the three graphs shows two distinct clusters, one for clastics and one for carbonates. Correlation coefficients would be misleading under these circumstances.

The graph of average grain size versus water absorption porosity for clastics and carbonates is shown in Figure 54. Generally, the dispersion of points is great. Table 20 shows that the correlation coefficients for each rock type are very low. The regression lines fail to account for over 90 percent of the variation of the water absorption porosity. A factor of chance is suggested for the plot of points for both clastics and carbonates because of the moderate level of significance for each group.

Table 20

Average Grain Size Versus Water Absorption Porosity

Type	Correlation Coefficient (R)	Variation % Explained By Regression Line	t_{OBS}	Significance
Clastics	+ 0.2619	6.86	0.159	$t_{OBS} < t_{.60}$
Carbonates	+ 0.2254	5.08	0.091	$t_{OBS} < t_{.60}$

Figure 55 shows the graph of average grain size versus the rate of water absorption for clastics and carbonates. A definite trend exists for the clastics, while a trend for the carbonates is only moderately suggested. Table 21 shows that the clastics have a fairly good correlation of + 0.7513 with an explained variation of 56.5 percent. The high level of significance suggests that chance was not a factor in the distribution of the clastics in Figure 55.

Table 21 indicates that grain size correlates poorly with the rate of water absorption in the case of the carbonates. The explained variation is only 40 percent and the level of significance is low enough to suggest a possible involvement of chance in the distribution of the data points.

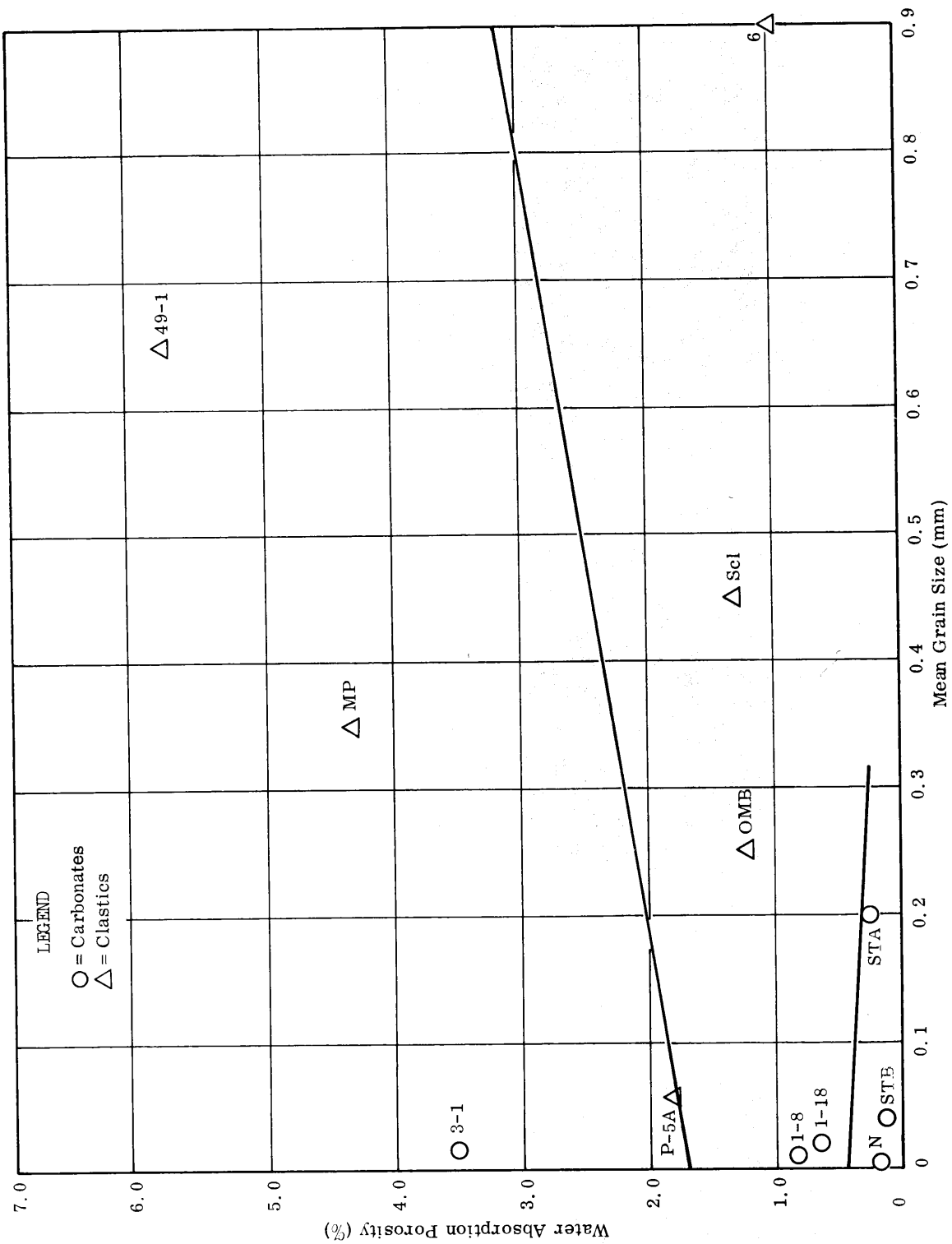

Figure 54. Mean grain size versus water absorption porosity.

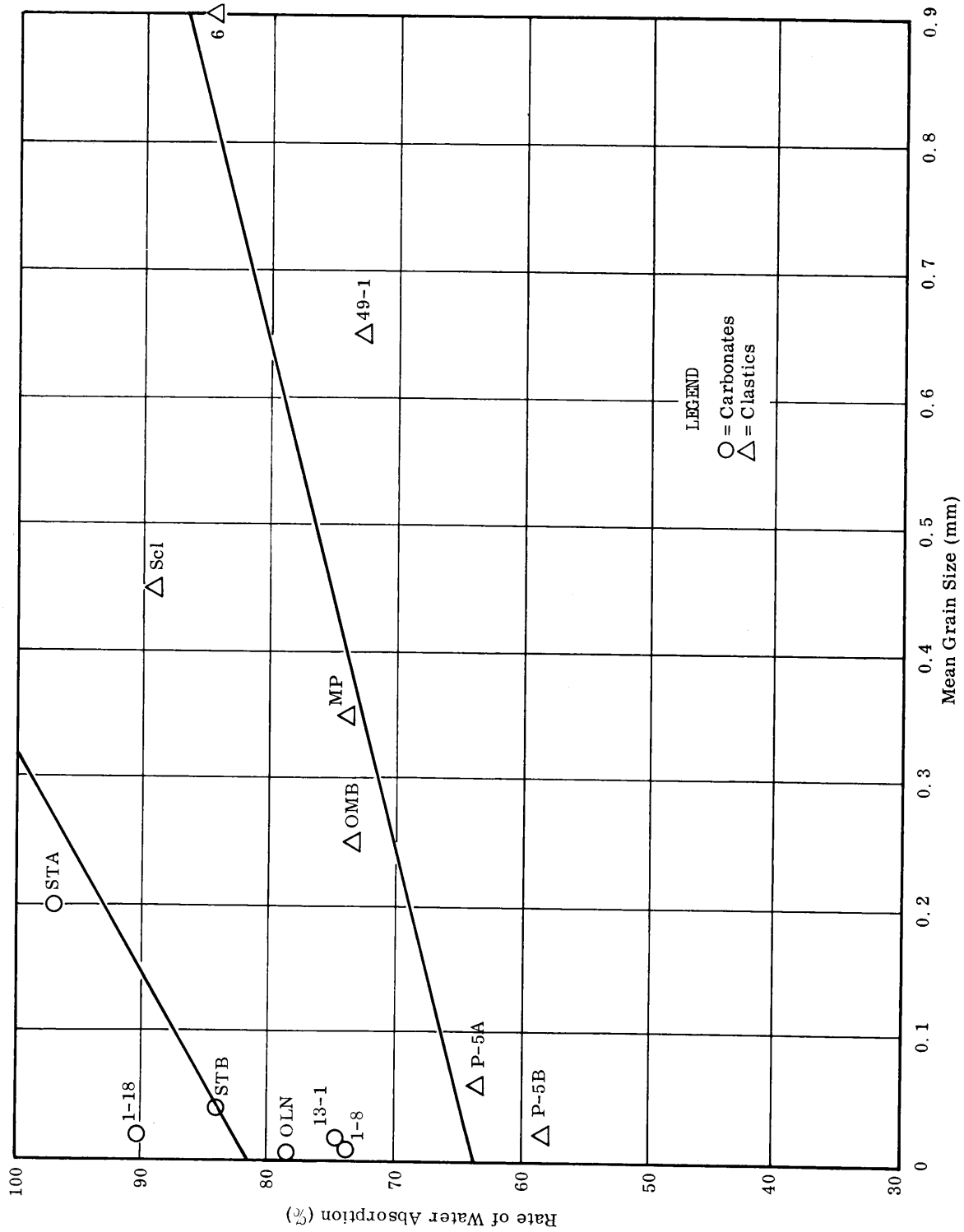

Figure 55. Mean grain size versus rate of water absorption.

Table 21

Average Grain Size Versus Rate of Water Absorption

Type	Correlation Coefficient (R)	Variation % Explained By Regression Line	t_{OBS}	Significance
Clastic	+ 0.7513	56.45	1.913	$t_{.90} < t_{OBS} < t_{.95}$
Carbonate	+ 0.6325	40.00	0.894	$t_{.70} < t_{OBS} < t_{.80}$

Discussion

According to theory, the grain size or crystal size of a rock does not influence the amount of its void space or its porosity (Russell and Dickey 1950). However in nature, as the grain size increases, the interparticle void size generally increases as well, but an increase in the grain size may not be accompanied by an increase in the porosity as measured by water absorption due to the probable increase in entrapped air contained in the larger pore sizes. This is indicated in Figure 54.

Mercury injection is not affected as much by entrapped air as is water absorption. As long as the pore sizes are greater than .01 μ, the mercury will be injected into the pores. So, if the interparticle void size increases as the grain size increases, the mercury injection technique can measure the increased pore volume. This appears to be the case with the distributions shown in Figure 53, where grain size and porosity as determined by mercury injection tend to increase together.

For the clastics, Figure 55 has shown a fair correlation between average grain size and the rate of water absorption. As grain size increases, the rate of water absorption increases. Provided other factors such as sorting and cementation do not interfere, interparticle voids increase in size as grain size increases (Choquette and Pray 1970). As a consequence, the capillary potential decreases and the viscous drag decreases. Figure 55 suggests that as grain size increases the decrease in viscous drag may be more of a factor than the decrease in capillary potential. This would explain the increased rate of water uptake as the size of the constituent grains of a rock become larger.

Because secondary cementation and solution play important roles in determining the nature of pores in carbonates, it would not necessarily be expected that crystal size would affect the pore size and pore continuity, and thereby influence the rate of water absorption.

In summary, grain size does not appear to be a reliable parameter for indirectly relating mercury injection porosity to water absorption porosity. Although the clastics have a good correlation between grain size and mercury injection porosity, they have a very poor correlation between grain size and water absorption porosity. The carbonates fail to show a significant correlation for either relationship.

A fairly good relationship is suggested for the clastics in the case of grain size versus rate of water absorption. The carbonates, however, again show a poor correlation between these two parameters.

Total Porosity and Effective Porosity

One final point that should be made in this report is that concerning effective porosity versus total porosity. The porosity of a rock as measured by long-term water absorption or by mercury porosimetry may not give an indication of its non-connected void space. The total porosity of a rock for interconnected and unconnected voids can be determined by the following equation (Hiltrop and Lemish 1960),

$$\text{Total porosity } (\%) = 100 \left(1 - \frac{\gamma_B}{\gamma_p}\right)$$

where γ_B is the bulk density measured with the Jolly balance and γ_p is the powder density measured with a pycnometer.

In order to gain some insight into the relationship between the effective porosity and total porosity in Virginia aggregates the following procedure was utilized for selected rocks. From each slab, one rock cylinder was chosen which had a water absorption porosity similar to the average porosity for the entire slab. An approximately 10 gram portion of each cylinder was used for the bulk density determination and then powdered for the powder density determination. Table 22 shows the calculated total porosities for the 13 rock cylinders. Also given is the water absorption porosity for each rock cylinder and the average mercury injection porosity for the rock chips immediately surrounding each rock cylinder. The last two columns show the percent ratios of effective porosity to total porosity for the water absorption method and mercury porosimetry method.

For the clastics, the total porosity is better approximated by the mercury injection method than by the water absorption method, by a factor of 78.7 percent to 63.0 percent. For the carbonates, this relationship is reversed by a factor of 58.1 percent to 44.5 percent.

Table 22

Effective and Total Porosities

Clastics

Rock Cylinder	Total Porosity	Water Absorption Porosity	Mercury Injection Porosity	100 ($\frac{H_2O}{Total}$)	100 ($\frac{H_2O}{Total}$)
49-1 8	5.90	5.80	3.28	98.3	55.6
MP 14	4.57	4.32	3.64	94.5	79.6
Scl 11	2.98	1.26	2.84	42.3	95.3
6 5	2.63	.98	2.55	37.3	97.0
P-5A 11	2.54	1.86	1.18	73.2	46.5
P-5B 5	2.11	.76	1.74	36.0	82.5
OMB 19	2.03	1.21	1.91	59.6	94.1
			Average	63.0	78.7

Carbonates

13-1 6	4.26	3.52	1.90	82.6	44.6
1-18 7	1.40	.65	.26	46.4	18.6
1-8 1	1.10	.85	.38	77.3	34.5
STA 13	.55	.34	.22	61.8	40.0
STB 12	.48	.14	.27	29.2	56.3
OLN 9	.33	.17	.24	51.5	72.7
			Average	58.1	44.5

The implications of the values in Table 22, while by no means crystal clear, do give rise to some interesting speculations. The carbonates apparently have a large volume of either very small pores (<.01 μ) or of pores inaccessible to water or mercury. Probably the latter is the case because even very small pores should be available to water under long-term water absorption conditions if they are interconnected.

The fact that the water and mercury percentages for the clastics are higher than those for the carbonates is not too surprising since it is logical to think of the clastics as composed of more discrete grains than the carbonates. It is interesting that for the clastics many of the mercury percentages were significantly higher than those for water. In the case of rock 6, a coarse open sandstone, it would appear that the large openings between grains had little capillary pull on water but were readily accessible to mercury.

Many anomalies occur in the table which appear to defy any rational explanation. For instance, clastic samples P-5A and P-5B were collected from the same quarry source from similar strata yet they react in exactly opposite fashions. P-5A seems to be open to water absorption, while P-5B shows a high percentage of its pores available to mercury. The same pattern seems to be true of STA and STB.

One final speculation will dwell on the possible effects of high volumes of pores apparently inaccessible to either water or mercury. An example would be rock 1-18. Would these inaccessible pores react in a fashion analogous to entrained air in concrete? If so then the freeze-thaw durability of such aggregates may be expected to be quite high. This possibility might well bear looking into in future research.

Conclusions

The primary purpose of this portion of the project was to investigate the possible correlation between porosity as measured by mercury porosimetry and porosity as measured by the water absorption method. If an essentially strong correlation had been found then this could have been the basis for developing a test method wherein rapid mercury injection could be used to predict long-term water absorption. In addition, the factors of pore size distribution, rate of water absorption, and texture were investigated in hopes of indirectly relating mercury injection porosity to water absorption porosity. The results of these studies are as follows:

1. Aggregate porosity as measured by mercury porosimetry was found to show only a weak correlation at best with long-term water absorption.

2. No significant success was attained for relating mercury injection porosity to water absorption porosity indirectly by use of the rate of water absorption.

3. The ratio $\frac{>80\text{ u Porosity}}{<80\text{ u Porosity}}$ correlates fairly well with water absorption porosity for the clastic rocks. The prediction of water absorption porosity by this ratio is not recommended, however, because the level of variability is unacceptable and because the carbonates considered in this study showed no significant volume of pores larger than 80 μ.

4. No significant relationship was found between the ratio $\frac{>80\text{ u Porosity}}{<80\text{ u Porosity}}$ and the rate of water absorption.

5. Grain size was found not to correlate significantly with either mercury injection porosity, water absorption porosity, or rate of water absorption.

6. An exception to the trend noted in conclusion No. 1 was found when aggregate No. 6, a coarse, open sandstone, was excluded from the clastic group. This improved the correlation coefficient from a low 0.497 to a moderately good 0.898. However, the variability remained high.

7. Clastic and carbonate rocks exhibited different behavioral trends when effective porosities determined by mercury injection and water absorption were compared to total porosities determined by the powder-pycnometer method. The possiblity that inaccessible pores might favorably affect aggregate durability was suggested and is offered as an interesting area for future research.

8. Due to: 1) the poor correlations and high variability obtained between mercury porosity and long-term water absorption for both the carbonate and clastic rock groups, 2) the lack of improvement in the correlation when various other parameters are interjected, and 3) the difficulty of predicting the exclusion of an aggregate such as No. 6, little optimism can be generated for a rapid test by mercury porosimetry at this time.

IMPLEMENTATION

The purpose and expected results of this project as spelled out in the working plan (Sherwood 1963) indicated that the study would concentrate on developing fundamental information on the nature of aggregate pore characteristics. This would, in turn, serve as background for possible future studies where aggregate durability would be emphasized and related to aggregate pore structure.

The obvious implementation of the research presented in this report would then be to serve as background for durability studies using aggregates from the same or similar sources. This has not been attempted as a comprehensive study to date. However, some research along these lines has been performed in the Concrete Section of the Virginia Highway Research Council, and additional efforts are contemplated.

A second use envisioned for the research performed for this report was that of relating aggregate porosity as determined by mercury injection to water absorption. The hope for correlation of the rapid mercury injection test for porosity with long-term water absorption yielded disappointing results. Even when other properties such as absorption rate, texture, and size of pores were introduced, the correlations remained weak at best.

Unless other related parameters can be discovered and incorporated in such a way as to improve this correlation, then the rapid mercury injection test appears to correlate too imprecisely with water absorption to allow satisfactory prediction of aggregate water uptake.

In summary, it would appear that the principal value of the work reported here will be to further the fundamental knowledge of aggregate pore structure and, hopefully, act as an intermediate step in the complex and difficult area of laboratory testing of mineral aggregates to predict their field performance.

ACKNOWLEDGEMENTS

This study was financed by Highway Planning and Research Funds administered by the Federal Highway Administration.

Appreciation is expressed to John C. Stulting, instrument maker, who fabricated the specialized equipment used.

The research was carried out under the general supervision of the late Tilton E. Shelburne and Jack H. Dillard, his successor in the position of Virginia State Highway Research Engineer.

REFERENCES

Aminco-Winslow Porosimeter, 1963, Catalog Number 5-7109, Instruction Number 598-A.

Baptist, O. C., 1966, "Permeability and Capillarity in Petroleum Reservoir Engineering," Symposium on Permeability and Capillarity, 69th Annual Meeting, ASTM.

Blanks, R. F., 1949, "Modern Concepts Applied to Concrete Aggregates," Am. Soc. Civil Engineers, Proceedings V. 75, pp. 441-468.

Bondarenko, N., and Nerpin, S., 1965, "Rheological Properties of Water in Porous Media," Rilem Bulletin No. 29.

Buth, E., and Ledbetter, W. B., 1968, "The Importance of Moisture Absorption Characteristics of Lightweight Coarse Aggregate," Highway Research Record No. 226, Highway Research Board, pp. 35-40.

Carll, J. F., 1880, "The Geology of the Oil Regions of Warren, Venango, Clarion, and Butler Counties," 2nd Geological Survey of Pennsylvania, V. 3, p. 482.

Carman, P. C., 1956, Flow of Gases Through Porous Media, Academic Press, New York.

Chilingar, G. V., 1956, "Use of Ca/MG Ratio in Porosity Studies," Am. Assoc. Petroleum Geologists, Bull., V. 40, pp. 2489-2493.

Choquette, P. W. and Pray, L. C., 1970, "Geologic Nomenclature and Classification of Porosity in Sedimentary Carbonates," AAPG, V. 54, No. 2

Croxton and Cowden, 1963, Applied General Statistics, Prentice Hall, Inc.

Dolch, 1966, "Porosity", Special Technical Publication 149-A, ASTM p., 443.

Fancher, G. H., 1950, "The Porosity and Permeability of Clastic Sediments and Rocks," Subsurface Geologic Methods — A Symposium, L. W. Lerow, ed., Colorado School of Mines, pp. 685-713.

Griffiths, J. D., 1950 Producers Monthly, No. 8, p. 26.

Grim, R. E., 1953 Clay Mineralogy, McGraw-Hill, New York, N.Y.

Hassler, G. L., and Brunner, E., 1945, "Measurement of Capillary Pressures in Small Core Samples," Am. Inst. Mining Metall. Engineers Trains., V. 160, pp. 114-123.

Hiltrop, C.L., and Lemish, J., 1960, "Relationship of Pore-Size Distribution and Other Rock Properties to Serviceability of Some Carbonate Aggregates," HRB Bull. 239, Highway Research Board, p. 1-23.

Hobbs, C. R. B., 1957, "Petrography and Origin of Dolomitic-Bearing Carbonate Rocks of Ordovician Age in Virginia, " Virginia Polytechnic Inst. Bull.,Eng. Expt. Sta. Ser. 116 p. 128.

Johnson, W. E., and Breston, J. N., 1951, Producers Monthly, V. 15, No. 4.

King, F. H., 1898, "Principles and Conditions of the Movements of Groundwater," U.S.G.S., 19th Ann. Report, Pt. 2, pp. 59-294.

Kozeny, J., B. S., 1927, Akad, Wiss Wien, V. 136, Part II a, p. 271.

Lemish, J., Rush, F. E., and Hiltrop, C. L., 1958, "Relationship of Physical Properties of some Iowa Carbonate Aggregates to Durability of Concrete," HRB Bull. 196, Highway Research Board, pp. 1-16.

Lewis, D. W., Dolch, W. L., and Woods, K. B., 1953, "Porosity Determinations and the Significance of Pore Characteristics of Aggregates," Proceedings, ASTM, V. 53, pp. 949-958.

Melcher, A. F., 1921, "Determination of Pore Space of Oil and Gas Sands," Am. Inst. Mining Engineers, Trans. V. 65, p. 469-497.

Mitchell, J. K., and Younger, J. S., 1966, "Abnormalities in Hydraulic Flow Through Fine-Grained Soils," Symposium on Permeability and Capillarity of Soils, ASTM, 69th Annual Meeting.

Muskat, M., 1937, The Flow of Homogenous Fluids Through Porous Media, McGraw-Hill, New York, N.Y.

Pressler, E. D., 1947, "Geology and Occurrence of Oil in Florida," Bull. 31, AAPG, p. 1851.

Purcell, W. R., 1949, Capillary Pressures — Their Measurements Using Mercury and the Calculation of Permeability Therefrom," Jour. Petroleum Tech., V.I., No. 2 pp. 39-46.

Rhoades, R. F., and Mielenz, R. C., 1946, "Petrographic and Mineralogic Characteristics of Aggregates," Symposium on Mineral Aggregates, ASTM,Spec. Tech. Publ. 83, pp. 20-48

Ritter, H. L., and Drake, L. C., 1945, "Pressure Porosimeter and Determination of Complete Macro-Pore Size Distributions," Industrial and Engineering Chemistry, Analytical Edition, V.17, pp. 782-786.

Ritter, H. L. and Erich, L. C., 1948, "Pore Size Distribution in Porous Materials," Anal. Chemistry, V. 20, pp. 665-670.

Russell, C. F., and Dickey, P. A., 1950, "Porosity, Permeability, and Capillary Properties of Petroleum Reservoirs," Applied Sedimentation, P. D. Trask, Ed., New York, John Wiley, pp. 579-615.

Schaffer, R. J., 1932, "The Weathering of Natural Building Stones," London, Dept. Sci. and Industrial Research, Spec. Rept. No. 18, p. 53.

Searle, A. B., and Grimshaw, R. W., 1959, The Chemistry and Physics of Clays and Other Ceramic Materials, Interscience Publishers, Inc.

Sherwood, W. C., 1963, "Working Plan — Porosity and Permeability Studies of Virginia Aggregates," Virginia Highway Research Council.

Slichter, C. S., 1898, "Theoretical Investigation of the Motion of Ground Waters," U.S.G.S., 19th Ann. Rept. Pt. 2, pp. 295-384.

Stanton, T. E., 1940, "Expansion of Concrete Through Reaction Between Cement and Aggregate," Proceedings, American Society of Civil Engineers, V. 66, p. 1781.

Sullivan, R. R., 1941, "Further Study of the Flow of Air Through Porous Media," Journal of Applied Physics, V. 12, p. 503.

Sweet, H. S., 1948, "Research on Concrete Durability as Affected by Coarse Aggregate," Proceedings, ASTM, V. 48, pp. 988-1016.

Verbeck, G., and Landgren, R., 1960, "Influence of Physical Characteristics of Aggregates on Frost Resistance of Concrete," Proceedings, ASTM 60, p. 1063.

Wakao, N., Otani, S., and Smith, J. M., 1965, "Significance of Pressure Gradients in Porous Materials," Part I. Diffusion and Flow in Fine Capillaries. AIChE Jour., Vol. 11, p. 435.

Wakao, N., and Smith, J.M., 1962, "Diffusion in Catalyst Pellets," Chemical Engineering Science, V. 17, p. 825.

Waldschmidt, W. A., Fitzgerald, P.E., and Lunsford, C.L., 1956, "Classification of Porosity and Fractures in Reservoir Rocks," AAPG Bull., V. 40, pp. 953-974.

Walker, R. D., and Hsieh, T. C., 1968, "Relationship Between Aggregate Pore Characteristics and Durability of Concrete Exposed to Freezing and Thawing," Highway Research Record No. 226, Highway Research Board, pp. 41-49.

Washburn, E. W., 1921, "Porosity and the Mechanism of Absorption," Am. Ceramic Soc. Jour., V. 4, pp. 916-922.

Washburn, E. W., and Bunting, E. N., 1922, "Porosity VI. Determination of Porosity by the Method of Gas Expansion," Am. Ceramic So. Jour., V. 5, pp. 112-129.

Weyl, P. K., 1960, "Porosity Through Dolomitization: Conservation-of-Mass Requirements," Jour. Sed. Petrology, V. 30, pp. 85-90.

Wray, F.N., and Lichtefeld, H. J., 1940, "Influence of Test Methods on Moisture Absorption and Resistance of Coarse Aggregate to Freeze-Thaw," Proceedings, ASTM V. 40, pp. 1007-1020.